Master thesis : Modeling and dynamical analysis of dopaminergic neuron activity and its role in reward quantification

Auteur : Garcia Garcia, Pauline
Promoteur(s) : Drion, Guillaume
Faculté : Faculté des Sciences appliquées
Diplôme : Master en ingénieur civil biomédical, à finalité spécialisée
Année académique : 2021-2022
URI/URL : http://hdl.handle.net/2268.2/14511

Modeling and dynamical analysis of dopaminergic neuron activity and its role in reward quantification

Master's thesis completed in order to obtain the degree of Master of Science in Biomedical Engineering by

Pauline Garcia Garcia

Promotor:
Guillaume Drion

Jury members:
Guillaume Drion
Christophe Philips
Vincent Seutin
Pierre Sacré
Davide Ruffoni

University of Liège - School of Engineering and Computer Science
Academic year 2021 - 2022

Modeling and dynamical analysis of dopaminergic neuron activity and its role in reward quantification

Pauline Garcia Garcia

Supervisor: G. Drion
Master in Biomedical Engineering, University of Liège
Academic year 2021-2022

Abstract

Dopamine is a chemical released by the brain which has long been associated with the pleasant feeling that accompanies a reward. The neurons that release such chemical, called dopaminergic neurons, have therefore been the subject of research and study for years. In fact, understanding the behaviour of the neurons that drive the regulation of dopamine levels and their interactions with the other entities that compose the brain is necessary for the understanding of a larger entity called the reward circuit. This circuitry which drives multiple phenomenona such as motivation, emotions, etc. Impairment and alterations in the circuitry is also known to lead to psychiatric disorders and addiction.

Dopaminergic neurons present a specific behaviour as they actually fire in different modes which are imbricated together. On one hand, when unsolicited, they fire at a slow and robust rate. On the other hand, when they are triggered, their frequency of firing increases which also increases the dopamine release. This variability allows to regulate the dopamine in the brain.

This thesis focuses on the study of a model developed by G. Drion on the dynamics of dopaminergic activity.

The first part of this thesis aims to reproduce experimental results that were obtained to validate the model. Using engineering tools such as model reduction and phase plane analysis, a deeper study of the dynamics of the model is performed in order to understand the mechanisms that drive the behaviour of the model.

As a second part, the aim is to use the model in order to develop a hypothesis on the regulation of the firing frequency of dopaminergic neurons according to physiological properties of the neurons and linking it to the quantification of reward in the brain.

Acknowledgements

Firstly, I would like to express my sincere gratitude to my supervisor, Pr. Guillaume Drion, for his expertise and time spent on the development of this work.

Secondly, I am also very grateful for both of his PhDs, Kathleen Jacquerie and Caroline Minne, for their availability, their supervision and their devotion to the completion of the project. I would not have been able to complete this work without their insightful feedbacks. I am also grateful the rest of the lab team, Nora S., Nora B. and Juliette for their company during the semester.

Finally, I am thankful for the wonderful friendships created during my studies, Florence, Caroline, Şeyda and Julie, and my family for always believing my abilities, especially my mother for her support, my father for his enthusiasm in my studies and my brothers for countless coffee breaks. And Floriane, for her unlimited trust, love and support.

Liège, June 8^{th}, 2022

Pauline Garcia Garcia

Contents

Chapter 1

Introduction

1.1 Motivation : Modeling dopaminergic neurons and their link to reward quantification

In 1954, [Olds and Milner, 1954] performed an experiment in which rats were stimulated with the help of intracranial electrodes placed in several parts of the brain to observe the changes in the rats' behaviour. The electrical stimulation was delivered by a lever that the rats were allowed to activate as they wished. During the experiment, the rats would stimulate themselves regularly when the electrodes were placed in specific regions of the brain. This highlighted a region of the brain they called the septal area which was found to be the most responsive, as the rats would volontarly pull the lever multiple times. Thanks to this preliminary experiment, the presence of a *reward phenomenon* was found to be localized in specific regions of the brain.

The concept of reward was later described by [Schultz, 1997] as "the positive value that is acribed to an object, a behavioral act, or an internal physical state" and the role of dopamine and dopaminergic neurons linked to this phenomenon was also theorized. The activity of specific neurons has been identified to vary depending on the *context*. This behaviour was described as *reward prediction errors* where they fire at different frequencies according to the reward and the expectation.

At the cellular level, an interplay between specific membrane mechanisms which allow to reproduce the specific firing pattern of dopaminergic neurons and reproduce their activity has been identified in several studies.

The aim of this thesis is therefore to study and quantify the reward according to the context by linking it to the dopaminergic activity in a computational way. In order to do so, this thesis aims to answer and study the following points

- *What is the role of dopaminergic neurons and their implications in reward?*
- *What are the mechanisms underlying the behaviour of dopaminergic neurons and how can they be studied ?*
- *What are the mathematical dynamics that interplay in the dynamics of dopaminergic neurons ?*
- *Can experimental results of dopaminergic neurons be reproduced ?*

- *What are the effects of afferent inputs on the dopaminergic neuron ?*
- *How can they be linked to reward prediction errors ?*

1.2 Structure

In order to answer those questions, this thesis will be divided into several parts and chapters.

Part 1 Part 1 aims to describe the basics that are required to understand neurons and dopamine. The focus is firstly set in the second chapter (Chapter 2) on the mesolimbic dopaminergic pathway, also called reward pathway, where its main components are described as well as its main roles and involvements. The third chapter (Chapter 3) then focuses on the electrophysiology of dopaminergic neurons found in the pathway. It investigates the firing modes and the ionic currents that drive the activity in order to describe a model using conductance-based modeling in the following chapter (Chapter 4).

Part 2 The second part of this thesis is focused on the validation of the model on experimental data. In the seventh chapter (Chapter 7), five experiments which highlight the specific behaviour of dopaminergic neurons are reproduced using the model. Preliminarly, the model is reduced (Chapter 6) in order to allow phase plane analysis alongside the reproduction of the experiments, allowing to understand the dynamics of the model.

Part 3 The third part of this thesis focuses on the implication of the excitatory input of NMDA. Experimental effects are firstly reproduced to validate the model and then the model is taken further to theorise its effects and develop an hypothesis for reward quantification.

Part 4 The fourth and final part focuses on summarising the results and drawing conclusions from them. It is then followed up by a discussion of ideas to take the model further and deepen the analysis of the dynamics.

1.3 Additional note

In this work, several animations are available (Figure 7.6, Figure 7.16, Figure 8.2, Figure 8.9). They are available in the additional files joined to this manuscript in case the animation does not work for the reader.

Stucture and motivations

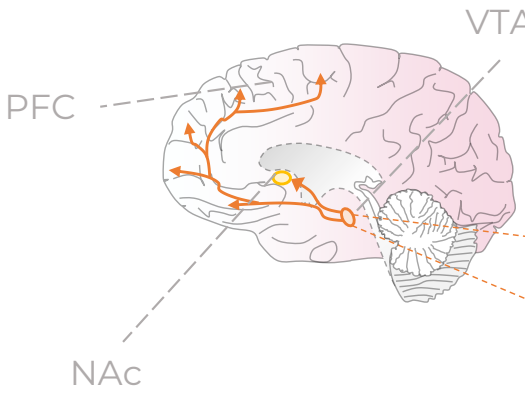

Understanding the dynamics of dopaminergic neurons in reward

Part 1 : Backgound

→ *Reward dopaminergic pathway*

Nucleus accumbens (NAc), Prefrontal cortex (PFC) and Ventral Tengmental Area (VTA)

Components

Addiction, depression,...

Implications

→ Focus on *Slow pacemakers* DA neurons

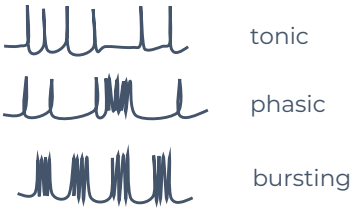

Firing patterns

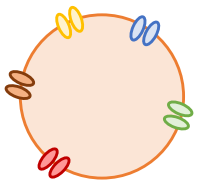

Identifying main ionic currents

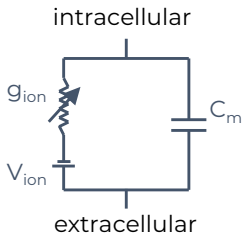

Modeling with conductance-based model

Part 2 : Experiments and reproduction of results

→ Focus on the role of SK channels and L-type calcium channels

Experiments

↳ Computational reproduction

↳ Dynamical analysis

→ Model validation

Part 3 : Effect of NMDA

→ NMDA is known to drive changes in firing for DA neurons. Effect of adding it to experiments of Part 2 ?

Computational simulation

↳ Dynamical analysis

→ NMDA hypothesis of reward quantification

Part I

Background

Chapter 2

Reward circuit

As it was already introduced, the phenomenon of processing of the *reward* is found to be localised in specific regions of the human brain [Olds and Milner, 1954]. This section aims to describe the reward circuit by introducing the main regions of the brain that are involved in the phenomenon as well as implications of this circuitry situations.

2.1 Dopamine and dopaminergic pathways

Dopaminergic pathways are connections within the brain involving the transmission of a chemical called *dopamine* in order to convey information between neurons and regions of the brain. The levels of dopamine in the brain have been proven to be associated with positively-valenced emotions, i.e. the pleasantness of a stimulus [Kauschke et al., 2019].

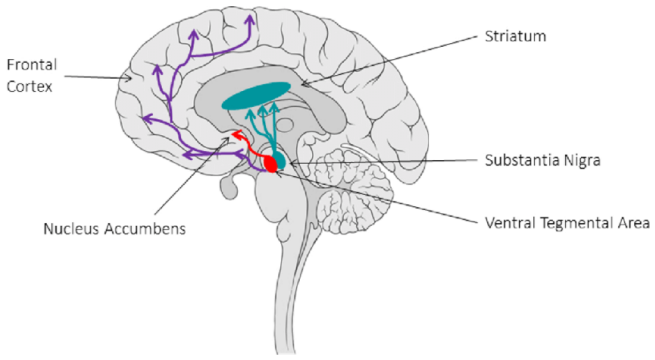

Figure 2.1: **Dopaminergic pathways** - Representation of the different dopaminergic pathways in the brain. Purple = mesocortical dopaminergic pathway ; red = mesolimbic dopaminergic pathway ; blue = nigrostriatal dopaminergic pathway. Figure from [Reneman et al., 2021]

In the brain, multiple dopaminergic pathways have been identified and are represented in Figure 2.1 :

- *Mesolimbic* dopaminergic pathway (in purple) which is involved in the signalling of positive errors in reward prediction [Schultz, 1997].
- *Mesocortical* dopaminergic pathway (in red) which is related to the mesolimbic dopaminergic pathway [Luo and Huang, 2016].
- *Nigrostriatal* dopaminergic pathway (in blue) involved in the control of motor actions [Luo and Huang, 2016].

This work focuses on the mesolimbic pathway, also referred as the *reward pathway*, which is the circuit that mediates the consumption of reward [Ranaldi, 2014].

2.2 Mesolimbic dopaminergic pathway

It is a known and established dopaminergic pathway that finds its centre in the ventral tegmental area and has projections into the ventral striatum (especially the nucleus accumbens and the olfactory tubercle). It also innervates the prefrontal cortex [Bear et al., 2016], as can be seen in Figure 2.1.

2.2.1 Ventral tegmental area

The first component of the mesolimbic dopaminergic pathway is the ventral tegmental area (VTA), an organ located in the midbrain represented in red on Figure 2.1. This organ plays a significant role in reward-related behaviours [Bouarab et al., 2019].

The VTA is composed of 65% of dopaminergic neurons. Dopaminergic neurons are cells that release dopamine into the regions where they project. The regulation of the release of dopamine is mediated by the influence of other neurons which project to the VTA. [Bouarab et al., 2019]

However, the VTA also releases other types of neurotransmitters. In fact, the other non-dopaminergic cells are primarly GABAergic neurons, i.e. neurons which release the chemical *GABA* (see section 3.3.3) [Nair-Roberts et al., 2008]. GABAergic and DA neurons work together to regulate the dopamine release. [Bouarab et al., 2019]

The VTA receives projections from several parts of the brain [Morikawa and Paladini, 2011]. The multiplicity of those inputs shows that the reward circuit integrates a set of complex stimuli.

2.2.2 Prefrontal cortex

The prefrontal cortex is a region of the brain located at the front of the brain. It is a heterogeneous structure that finds three main substructures that play distinct roles in the reward processes

- dorsal anterior cingulate cortex (dACC) : strongly connected to the striatum as well as subcortical regions that are related to the encoding of the reward. It is also connected to regions of brain related to motor areas which creates a *bridge* from reward to action. It is thought that the dACC encodes the *history* of rewards. It also plays two different roles in the assessment of motivation (by performing a cost-benefit analysis) and in adaptive decision making. [Chau et al., 2018]

- ventromedial prefrontal cortex (vmPFC) : It is thought that the vmPFC is important in reward based decisions. In fact, the vmPFC encodes *subjective* values of reward and is able to compare between multiple available options in order to establish the most rewarding. [Chau et al., 2018]

- orbitofrontal cortex (OFC) : Similarly to the dACC and the vmPFC, the OFC is also able to encode reward value. In this case, it encodes the value of the stimulus based on past encounters with it. It is also involved in *flexible decision making* when a stimulus value changes with time. [Chau et al., 2018]

2.2.3 Nucleus accumbens

The central processing element of the reward is the organ called nucleus accumbens. It is part of the ventral striatum and it is thought to play a major role in several psychological disorders, among others, mood disorders. It receives dopaminergic inputs from the VTA and it has been proven that altering the quality of those connections can lead to depression [Salgado and Kaplitt, 2015].

2.3 Roles and involvement

The reward circuit motivates the individual to reproduce a behaviour by creating a feeling of *pleasure* associated. The circuit plays a significant role in multiple other behaviours that are related to this feeling, such as the phenomenon of addiction, depression and conditioning, among others. [Schultz, 1997, Nestler, 2015, MacNicol, 2017]

2.3.1 Conditioning

As it was described by [Schultz, 1997], dopaminergic neurons of the VTA play a significant role in reward-based learning, in *classical conditioning*. Classical conditioning is a type of learning that is well known for its experiment that was performed by Pavlov on dogs. The dogs were conditionned to associate a *neutral* , such as a bell, to a *reward* like seeing food. They would always be exposed to the sound of the bell before seeing the food. The dog initially react to the sight of the food but, as the experiment goes on, the dogs start to react to the neutral stimulus as an expectation of the reward, i.e. *reward prediction*.

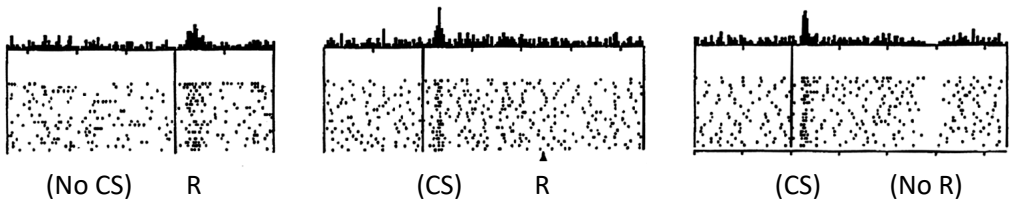

Figure 2.2: **Reward prediction errors** - Changes in the dopaminergic activity according to presentation of conditioned stimulus and reward **(left)** No conditioned stimulus is presented so when a reward is presented, the dopaminergic activity of neurons increases **(middle)** A conditioned stimulus is shown which shifts the increase in dopaminergic activity to the CS instead of the expected reward **(right)** A conditioned stimulus is presented but no reward which first increases the dopaminergic activity at (CS) and then drops it at (no R). Figure adapted from [Schultz, 1997]

[Schultz, 1997] then showed that dopaminergic neurons activity plays a role in *reward prediction error* (see Figure 2.2). It can be visualised that when a reward is shown but no conditioned stimulus (no CS) is presented beforehand, the activity of dopaminergic neurons increases at the time of the reward (R). If conditioning was done and a reward is presented, the activity of dopaminergic neurons is actually going to increase when the neutral stimulus (CS) is presented and the reward isn't going to generate the same change in activity. Finally, if there was conditioning and the CS is shown but no reward is

presented afterwards then the activity of dopaminergic neurons initially increases then decreases. It computes the difference between what is expected and what is obtained.

2.3.2 Addiction

Several drugs act on the reward pathway by altering the release of dopamine in the system.

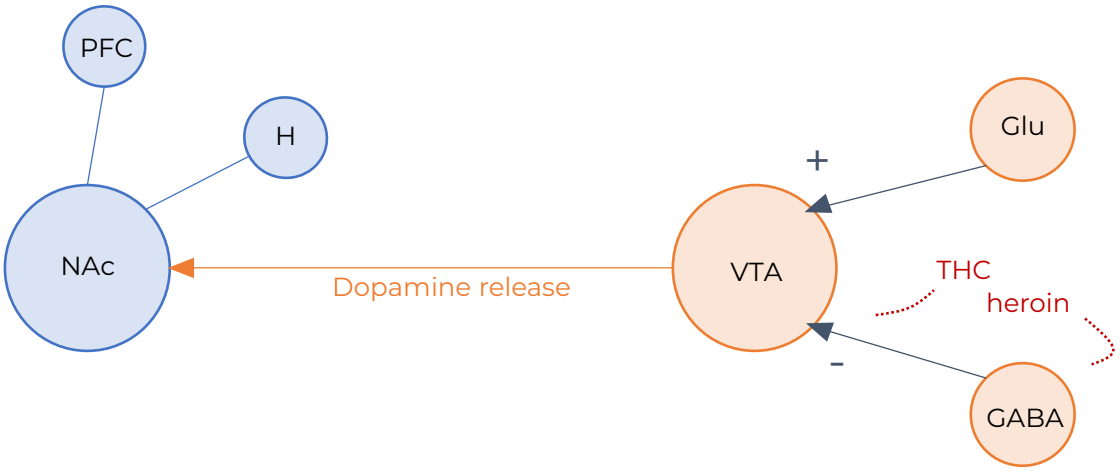

Figure 2.3: Simplified model of the main actors in the development of an addiction. Glu = glutamatergic neuron (excitatory) ; GABA = GABAergic neuron (inhibitory) ; VTA = Ventral tegmental area ; NAc = Nucleus accumbens ; PFC = Prefrontal cortex ; H = Hypothalamus. Figure from V. Seutin

In Figure 2.3 is represented a simplified reward circuit and the effects of multiple drugs on the reward circuit. Heroin increases the dopamine release by bonding to μ-opioid receptors which inhibits the activity of GABAergic neurons. Since GABA activity *inhibits* dopaminergic neurons, the release of dopamine is increased. [MacNicol, 2017]

The use of THC has similar effects as it binds to cannabinoid receptors and inhibits the activity of GABAergic neurons which enhances the release of dopamine by the VTA. [Zhang et al., 2017]

2.3.3 Depression

Depression, or Major Depressive Disorder, is a disease which that leads to loss of motivation. It is thought that some symptoms of depression might be explained by faults in the signalling of dopaminergic activity. In fact, low levels of dopamine in the nucleus accumbens correlate with lack of motivation for rodents to seek for rewards. [Dunlop and Nemeroff, 2007]

In order to treat depression, most treatments are slow and they target serotonin and norepinephrine. In [Gould et al., 2019], a new faster treatment is described, the molecule *(R,S)-ketamine*, which has a much faster effect and is thought to act on the NMDA receptors of the reward circuit in multiple possible ways. (R,S)-ketamine is believed to inhibit NMDAr of inhibitory neurons which will make them less effective, promoting glutamate release which would promote dopaminergic activity.

Chapter 3

Dopaminergic neuron physiology

This chapter aims to describe the physiology and electrophysiology of dopaminergic neurons as well as how they are modeled.

3.1 Elements of physiology

Dopaminergic neurons are a subcategory of the main component of the neural system, a cell called the *neuron*. This section aims to describe the physiology as well as the specific behaviour of these cells.

3.1.1 Biology of a typical neuron

Neurons are the basic building block of the central nervous system. A typical neuron is a type of cell composed of a cellular body, dendrites and an axon.

- the cellular body or periarkion is the region that contains the nucleus and other organelles where the proteins are synthesised [Bear et al., 2016]
- The dendrites are tree-like structures which form projections to other neurons and receive inputs. They convey the information received to the cellular body [Bear et al., 2016]
- The axon which allows the neuron to send information to other neurons by allowing the propagation of a signal called the *action potential*. [Bear et al., 2016]

The axon and dendrites allow the communication between neurons at specific sites called *synapses* as shown in 3.1 [Leprince, 2019a]. This concept will be developed in further sections.

3.1.2 Excitability

What makes neuron differ from typical cells is their electrical behaviour. In fact, they enjoy the propriety of *excitability*. The neuron can either be *at rest* or it can be *excited* and generate an action potential.

Resting state

The neuron's resting membrane potential is determined by the counterbalance of the two types of current generated by the ions gradient between the membrane's both sides. In fact, at equilibrium, the conducting currents and diffusing currents counterbalance which leads to the cancelling of net ion

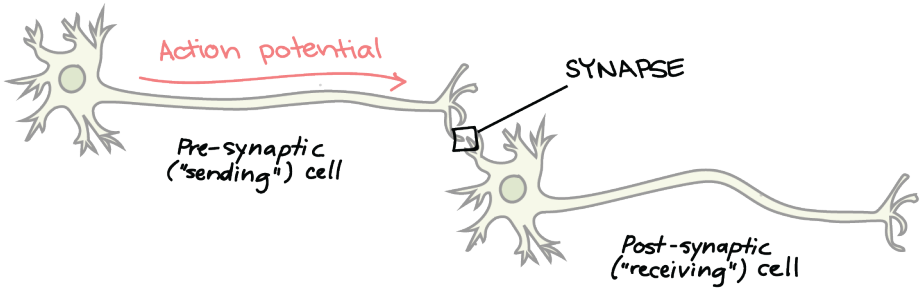

Figure 3.1: **Representation of the connection between two neurons** - The presynaptic neuron fires an action potential which is transmitted through the synapse to the post-synaptic cell. Figure from [noa, 2022]

current through the membrane [Sepulchre, 2008]. A deeper description of such potential is available in the appendix (Section 11.1).

Excited state

By applying an electrical stimulus, the neuron can switch from a resting state to the excited state. In fact, the chemical equilibrium is altered and the stimulus rearranges the ions concentrations locally on both sides of the membrane thanks to channels. The potential of the membrane depends on the gradient of ions which are *permeable* to the membrane. This permeability depends on transmembrane proteins called *ions channels*. They allow ions to diffuse passively in and out of the cell according to their gradient. There also exists another type of transmembrane proteins related to the motion of ions, *ion transporters*, which actively transport ions against their gradient to actually create the gradients. [Bear et al., 2016]

When a depolarising stimulus is applied, two behaviours are possible.

- If the stimulus is not large enough, it leads to a change in the resting potential of the membrane as long as the stimulus is applied but no significant change in the behaviour membrane potential is observed.
- If a large enough depolarising stimulus is applied, then it can alter the resting potential above a *threshold* that is going to generate an *action potential* (AP).

This AP is generated by the successive activation and deactivation of *voltage-gated* ion channels, i.e. ion channels whose permeability depends on the membrane potential, which will allow successive flux of ions to cross the membrane and therefore altering its electrochemical potential as described in Figure 11.1 available in the appendix.

3.1.3 Transmission of information

The transmission of information between two neurons is done in a region called the *synapse*. A synapse is the junction between the axon of a neuron (called the *presynaptic neuron*) and the dendrites of another (the *post-synaptic neuron*). [Leprince, 2019b]

Human synapses are called chemical synapse because the information is conveyed thanks to neuromodulatory chemicals called *neurotransmitters* and *neuromodulators*.

As one can visualise in Figure 3.2, the neurotransmitters are stored in *synaptic vesicles* in the terminal of the axon and their release is triggered by the AP. The action potential activates the opening of voltage-gated Ca^{2+} channels which allows a flux of Ca^{2+} in the axon. This influx triggers the release of the vesicles into the synapse. Finally, the neurotransmitters bind to receptors on the post-synaptic end which causes a flow of ions and generates either an *excitatory post-synaptic potential* (EPSP) or an *inhibitory post-synaptic potential* (IPSP) that will lead to respectively either enhanced or inhibited likelihood of firing an AP for the post-synaptic neuron. [Leprince, 2019b]

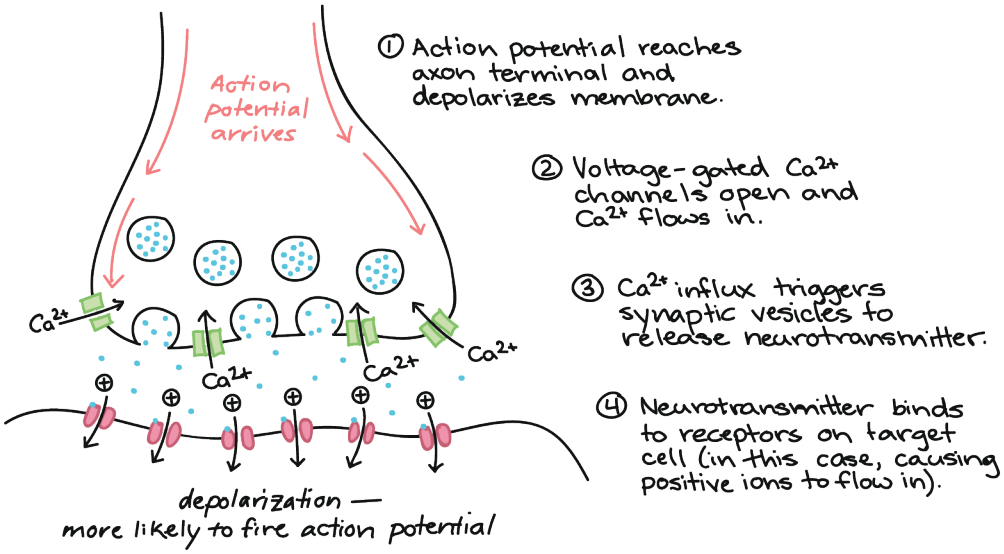

Figure 3.2: Description of the mechanisms that cause the release of neurotransmitters into the synaptic cleft by the action potential. Figure from [noa, 2022]

There are several types of molecules that are identified as neurotransmitters and neuromodulators. The majority are amino acids (AA) or derivatives, such as *glutamate*, *glycine*, *γ-amino-butyric acid* (GABA); or monoamine neurotransmitters, such as *dopamine*, *serotonin*, and *norepinephrine*... [Hampel and Lau, 2

3.2 Dopaminergic neurons

Dopaminergic neurons are a type of neuron that synthesises and releases dopamine in the central nervous system. They are found in the substantia nigra pars compacta, the ventral tegmental area, and the retrorubral field [Luo and Huang, 2016]. They present a specific electrical behaviour because they display multiple modes of firing. This section aims to describe and identify the firing modes and to identify the ion currents which drive this behaviour as well as the neuromodulators that influence these ion currents.

3.2.1 Firing modes

In the VTA, there are two types of dopaminergic neurons. In this work, the focus is on the *slow pace-makers*. [Seutin, 2022] There are three main modes of firing that have been identified in dopaminergic activity of those neurons.

Tonic firing DA neurons are pacemaker cells, meaning they fire at a regular pace when they are unsolicited, at an exceptionally regular pace ranging from 0.5 to 5 Hz [Khaliq and Bean, 2010]. This type of firing is called *tonic firing*. It has been observed that this pacemaking is robust to perturbations [Guzman et al., 2009].

Phasic firing However, when they are triggered, dopaminergic neurons have the characteristics of switching from tonic firing to phasic firing. Both types of firing are shown in Figure 3.3. An input of glutamate increases the dopaminergic neuron firing frequency during the time of the stimulus increases. This change in tonic frequency is correlated to an increase in dopamine release in the synaptic cleft.

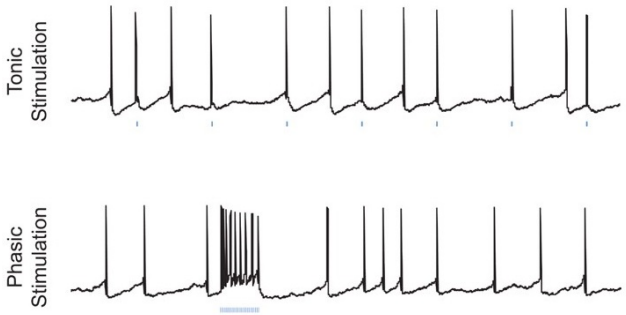

Figure 3.3: **Types of firing of the dopaminergic neuron (top)** Tonic firing. The neurons fires at a regular pace at around 1 Hz **(bottom)** Phasic firing. Increased frequency of firing rate. Figure adapted from [Tsai et al., 2009]

Bursting The third type of firing is observed under special conditions. When a specific type of ion channels called *SK channels* (see later) is blocked and they are triggered by an excitatory input, dopaminergic neurons may switch to bursting [Philippart et al., 2016] [Johnson et al., 1992]. As a reminder, bursts are "groups of high frequency spikes followed by quiescent periods" [Constantinou et al., 2016]. In [Johnson et al., 1992], they showed that after SK channels blockade, DA neurons switch to a bursting behaviour when solicited by NMDA. To observe such behaviour in vitro, it also requires a hyperpolarising current to counterbalance the excitatory NMDA input. Otherwise, the neurons reach a state of *depolarisation block* where they are overly stimulated and stop firing.

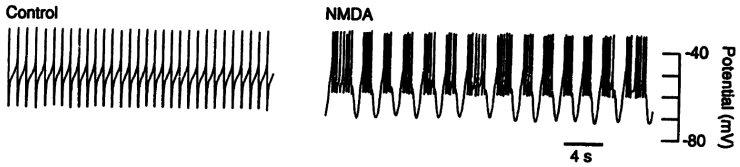

Figure 3.4: **Bursting** - Experimental results from [Johnson et al., 1992] that highlights the switch to bursting with NMDA stimulation in apamin solution

In order to mathematically characterise the type rhythm of the neurons in further experiments, a *coefficient of variability* (CV) is obtained by extracting the interspike intervals t_i (the time between each spike) and then computing statistics

$$CV = \frac{std(t_i)}{mean(t_i)} \tag{3.1}$$

where std is the standard deviation. Low values of CV indicate that the standard deviation is low and the mean high, i.e. the firing pattern is regular and slow while higher values hint irregularities in the firing pattern leading to higher values of standard deviation and smaller interspike intervals.

3.3 Neurotransmitters and neuromodulators

In the scope of this work, only three neurotransmitters and neuromodulators are of interest, namely dopamine, glutamate and GABA. The effect of other neurotransmitters and neuromodulators on dopaminergic neurons will not be included.

3.3.1 Dopamine

Dopaminergic neurons are called this way because their firing triggers the release of *dopamine*. Dopamine (*3,4-dihydroxyphenethylamine*) is a macromolecule which is synthesised in the cytoplasm of dopaminergic neurons [Dunlop and Nemeroff, 2007]. The release of dopamine in the synapse by the presynaptic neuron is going to bind to *dopaminergic receptors* of the post-synaptic neuron.

Dopaminergic receptors are *G-protein coupled* receptors meaning that their activation, thanks to the release of dopamine in the synapse and binding of dopamine to the receptors, is going to activate a cascade of chemical reactions in the post-synaptic neuron. There are at least 5 types of dopaminergic receptors, grouped into two families, which lead to different cascades as summarised in Table 3.1.

- The first family is *D1-like receptors*, which gathers D1 and D5 receptors. They are grouped together because their triggering activates $G_{s\alpha}$-coupled protein which subsequently activates the adenylate-cyclase second messenger system. [Dunlop and Nemeroff, 2007]
- The second family, composed of D2, D3 and D4, is called the *D2-like receptors*. They are linked to the protein $G_{i\alpha}$ and their activation results in an antagonist effect to D1-like as they reduce the adenylate-cyclase activity. [Dunlop and Nemeroff, 2007]

An increase (resp. decrease) in adenylate cyclase activity leads to an increase (resp. decrease) in cyclic adenosine 3'5'-monophosphate (cAMP). This increase (resp. decrease) leads to more (resp. less) activation of cAMP-dependent protein kinase (PKA). The activation of the PKA leads to more gene expression on the post-synaptic end so more receptors are expressed. This phenomenon, called *long term potentiation* (LTP), leads to the strengthening of the connection between the presynaptic and postsynaptic neurons. The opposite effect is called *long term depression* (LTD) [Beninger and Miller, 1998, Vaughn et al., 2017]

It is thought that the two modes of dopamine release (phasic or tonic) are necessary to trigger the two types of dopaminergic receptors. Phasic firing is thought to activate D1-like receptors while the tonic firing activates D2-like receptors [Zweifel et al., 2009].

3.3.2 Glutamate

Glutamate is the neurotransmitter released by glutamatergic neurons. It is the most abundant excitatory neurotransmitter. It binds to postsynaptic receptors called AMPAr (α-amino-3-hydroxy-5-methyl-4-isoxazolepropionic acid receptor) and NMDAr (N-methyl-D-aspartate receptor). The switch from tonic to phasic firing is actually mediated by the input of glutamate [Wang et al., 2021]. It is

Receptor	Family	G-protein	Effect
D1 D5	D1-like receptors	Coupled to protein $G_{s\alpha}$	facilitate LTP
D2 D3 D4	D2-like receptors	Coupled to protein $G_{i\alpha}$	Facilitate LTD

Table 3.1: **Dopamine receptors** - Summary of the different dopaminergic receptors [Bhatia et al., 2021, Zweifel et al., 2009]. G-protein refers to the G-protein to which the receptor is coupled to.

released by excitatory synapses and it binds to NMDAr and allows a flux of cations (Ca^{2+}, K^+ and Na^+) that will facilitate the firing of an AP for the post-synaptic neuron [Leprince, 2019a].

3.3.3 GABA

Inhibitory neurons release the neurotransmitter GABA (aminobutyric acid) which binds to $GABA_A$ and $GABA_B$ postsynaptic receptors and is going to inhibit the activity of the post-synaptic neuron.

3.3.4 Summary

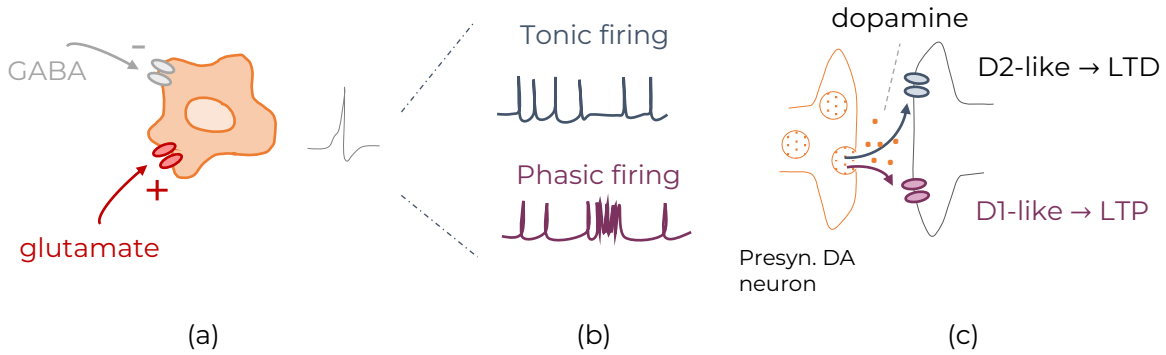

Figure 3.5: **Summary** - Summary of the different types of firing that are observed in vitro for slow pacemakers dopaminergic neurons found in the VTA **(a)** Dopaminergic neurons of interest are slow pacemakers from the VTA which are inhibited (-) by GABA or excited (+) by glutamate **(b)** Dopaminergic neurons fire in different ways, either tonic (low frequency and steady) (grey) or phasic (high frequency for short amount of time) (purple) **(c)** Both firings activate different dopaminergic receptors which have different effects (either LTP or LTD)

3.4 Ionic currents

The specific electrophysiological behaviour of dopaminergic neurons can be explained by studying the currents generated by the flux of ions across the neuron membrane. In the scope of this work, it will be assumed that the mechanisms and ion currents responsible for the behaviour of dopaminergic neurons

are the same for SNc and VTA dopaminergic neurons. As it is shown in [Seutin, 2022], their firing patterns are very similar.

The currents that have been identified to be the most relevant to reproduce the firing types observed in DA neurons activity are the followings :

- Calcium current through L-type calcium channels
- Calcium current through N-type calcium channels
- Sodium current through sodium channels
- Delayed rectifier potassium current
- The excitatory input generated by the activation of NMDAr
- The potassium current related to ether-a-go-go gene
- The potassium current induced by SK channels

Each of their implications in the behaviour of dopaminergic neuron's firing are going to be described in further sections.

3.4.1 Pharmacology

In order to understand what are the implications of the ionic currents that drive the evolution of dopaminergic neurons membrane potential and subsequently, their firing pattern, drugs called *channel blockers* are used to alter the state of ionic channels and stop the flux ions to observe the physiological response of the cell to this blockade. A simplified mechanism of action is represented in Figure 3.6.

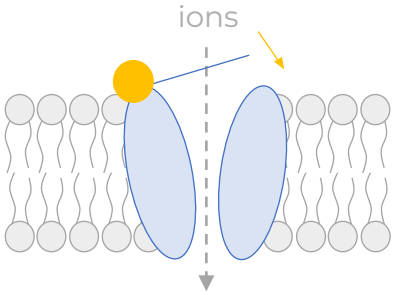

Figure 3.6: **Ion channel blockers** - General mechanism of action of ion channel blockers (yellow). The ion channel blocker binds to the channel (blue) which causes the closing of the channel (yellow arrow) and stops the ion flux. [Bear et al., 2016]

Typically, the blocker binds to a region of the channel and the interaction generates in reaction the closing or inactivation of the channel. In the case of dopaminergic neurons, the main ion channels whose blockade are induced to understand the dynamics are L-type calcium channels, N-type calcium channels, SK channels and ERG channels as it will be developed in the following section.

The main ion channel blockers that were used in the scope of this work and their effect on ion channels are the following

- **Nifedipine** is a calcium channel blocker of the family dihydropyridine whose activity is exclusive to **L-type calcium channels**. In this work, it is administered in concentrations from 5 to 20 µM which allows to fully block the channels [de Vrind et al., 2016]

- **Apamin** is a compound that is believed to bind to residues in the pore region (inside the channel) of potassium **SK channels**. Typically, it is administered in saturating conditions from 50 to 300 nM. [Kirkpatrick and Bourque, 1996]

- **ω-Conotoxin** is a drug that is known to exclusively block **N-type calcium channels** without affecting the L-type calcium channels of the central nervous system (CNS). In fact, L-type calcium channels are present in the cardiomyocites as well as in the CNS. However, they present differences in the dihydropyridine receptors which makes that ω-conotoxin binds to both L-type calcium channels and N-type calcium channels in muscles. [Takemura, 1992] It is administered in 1µM concentration. [de Vrind et al., 2016]

- **E-4031** is a selective blocker of the **ERG potassium channels**. In [Ji et al., 2012], it is administered in 10µM concentrations to observe the effect on the firing of dopaminergic neurons.

- Additionally, several calcium channel blockers, namely **TTA** 3µM, **ω-agatoxin** 1µM and **SNX** 100nM are used to block respectively **T-type**, **P/Q-type** and **R-type calcium** channels.

3.4.2 Role of L-type calcium channels

Calcium enters the cell thanks to ion channels of several types that have different properties, for example their speed of activation etc. [Wright et al., 2009]. They are voltage activated channels, i.e. their state of activation depends on the membrane potential. [Ortner, 2021]

Reference	Origin of the DA neuron	Effect on pacemaking
[Nedergaard et al., 1993]	SNc	Lost
[Mercuri et al., 1994]	SNc and VTA	Sustained
[Puopolo et al., 2007]	SNc	Lost
[Chan et al., 2007]	SNc-SNc	Sustained-Lost
[Guzman et al., 2009]	SNc	Sustained
[Putzier et al., 2009]	SNc	Lost
[Khaliq and Bean, 2010]	VTA	Sustained
Seutin et al, unpublished	SNc	Sustained

SNc: substantia nigra pars compacta ; VTA: Ventral tegmental area

Table 3.2: **Effect of L-type channel blockade on the pacemaking** - Summary of experiments to block voltage dependant Ca^{2+} channels, effects on the pacemaking of midbrain DA neurons. Adapted from [Drion et al., 2011]

During pacemaking, the main source of calcium comes from the slow inactivating L-type channels so it is one of the targets of studies to understand the firing pattern of dopaminergic neurons. To do so, channel blockade has been induced in vitro in several studies and the subsequent impact on the pacemaking was monitored. A summary of the studies done by [Drion et al., 2011] is available in Table 3.2. It shows discrepancies in the results. Some studies conclude that the pacemaking is kept by the neuron while others obtain the opposite result.

The heterogeneous conclusions of the results are interesting because the pacemaking behaviour of the DA neurons is observed to be homogeneous and robust, but the heterogeneous results show that the mechanisms behind are not [de Vrind et al., 2016, Scuvée-Moreau et al., 2004].

3.4.3 SK calcium activated channels

Small-conductances Ca^{2+}-activated K^+ (SK) channels are channels whose activation relies on low concentrations of calcium (100 nM - 1 µM). They are not voltage dependent, meaning that their state does not depend on the membrane potential but rather on the calcium concentration in the cytosol. They work as a way to regulate the excitability of the neurons and they actually are the mechanism responsible for the homogeneous pacemaking in spite of heterogeneous calcium channels [Scuvée-Moreau et al., 2004].

3.4.4 Ether-a-go-go related gene channels

Ether-a-go-go-related gene channels (ERG) are voltage dependant potassium channels that are found in pacemaking cells, e.g. cardiomyocites and midbrain dopaminergic neurons, and that regulate the excitability of the cell by mediating the repolarisation stage. [Shepard et al., 2007]

They are closed when the membrane is hyperpolarised and open during depolarisation. However, their opening leads to an almost instantaneous inactivation so there is little to no potassium current during the peak of the AP. During repolarisation, the channels activate again and allow a strong inward potassium current. The main effect of this current is therefore on the duration of a pause that follows bursting, i.e. it mediates the depolarisation block. [Shepard et al., 2007] [Yu and Canavier, 2015]

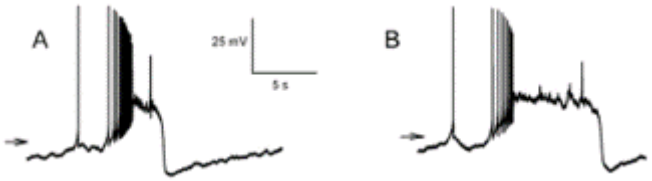

Figure 3.7: **Effect of ERG blockade on the shape of bursting in DA neurons (A)** Control conditions **(B)** Under ERG blockade, the duration of depolarisation block that follows a burst is elongated. figure from [Ji et al., 2012]

3.5 Summary

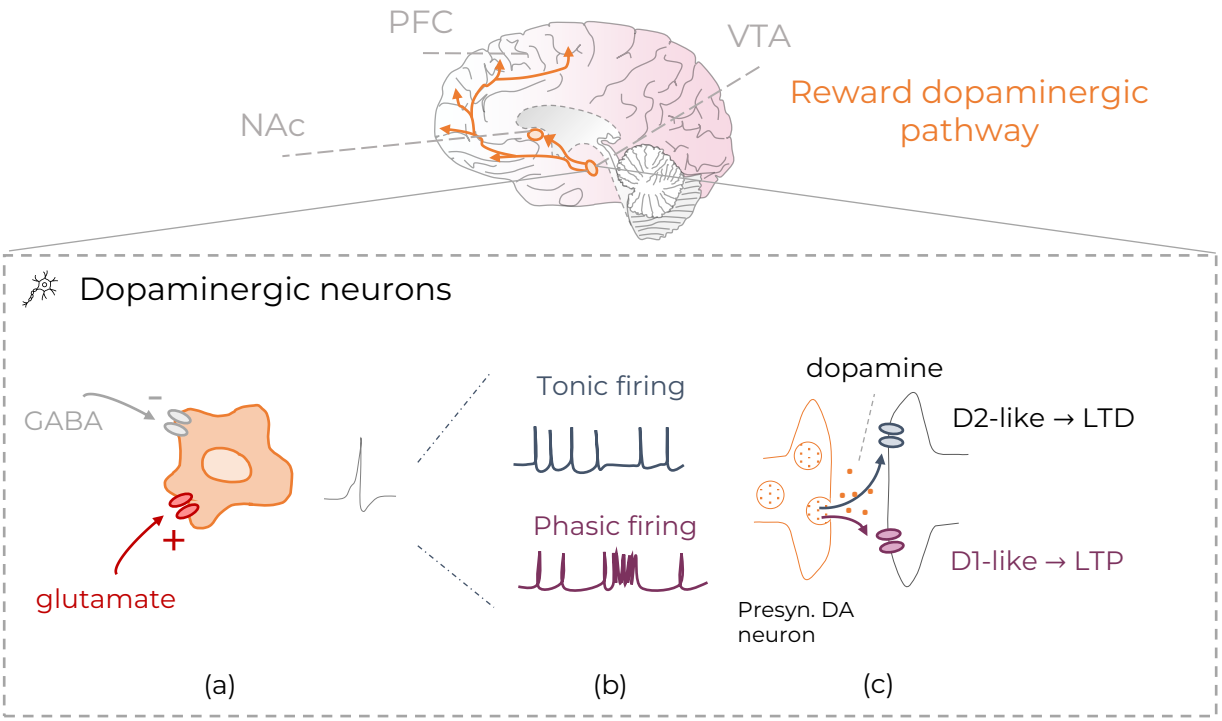

(a) Dopaminergic neurons of interest are slow pacemakers from the VTA

(b) Dopaminergic neurons fire in different ways, either tonic (low frequency and steady) or phasic (high frequency for short amount of time)

(c) Both firing cause dopamine release but activate different dopaminergic receptors which have different effects (either LTP or LTD)

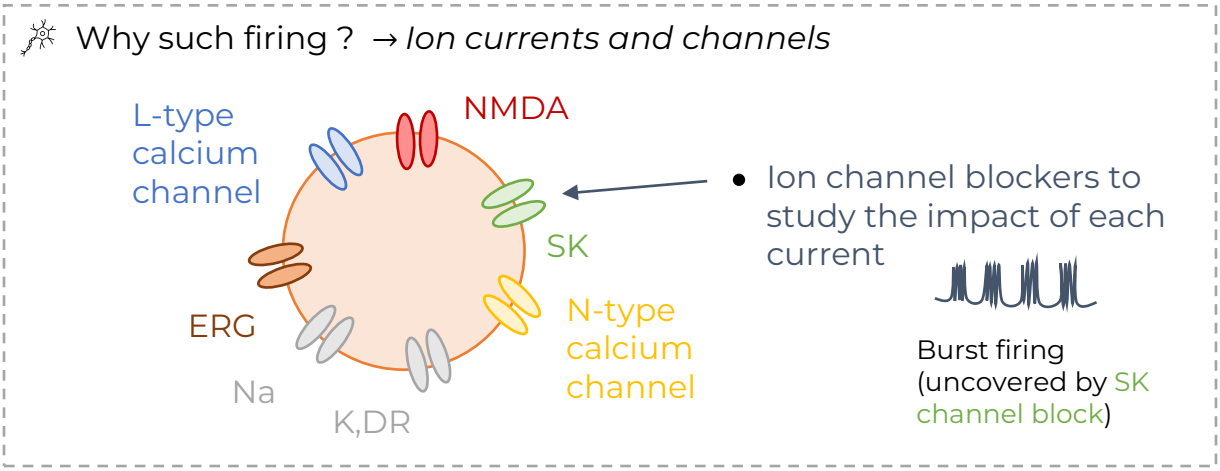

Chapter 4

Modeling

In order to be able to reproduce and study the behaviour of dopaminergic neurons, one must be able to model them. This chapter aims to describe the basic modeling that is used to describe the behaviour of neurons, the model that is used and finally the tools that are used to study the dynamics of the model.

4.1 Modeling of the dopaminergic neuron

4.1.1 Conductance-based modeling

In 1952, [Hodgkin and Huxley, 1952] introduced the concept of *conductance-based models* as a way to mathematically study the excitability of the neuron's membrane. They described an analogy of an electrical circuit in which the membrane's bilipidic layer can be seen as a capacitance and the ion specific channels are modeled as non-linear conductances as represented in Figure 4.1.

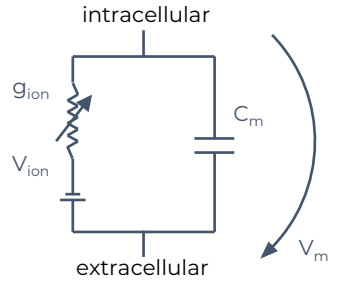

Figure 4.1: **Analogy** - Electrical analogy of a neuron's membrane. Adapted from [Sepulchre, 2008]

This analogy allows to use Kirchhoff's law of currents, i.e. that *the sum of the currents at a node must be equal to 0, combined with the use of Ohm's law.* This leads to equation (4.1).

$$\sum_i I_i + C_m \frac{dV_m}{dt} = I_{app} \tag{4.1}$$

where I_i refers to the current of each ion i through the membrane, C_m is the capacitance of the membrane and I_{app} is the applied current.

The conductance of each ion through the channels depends on the state of the channels. In fact, a

channel can either be *open*, *closed* or *inactivated*. [Hodgkin and Huxley, 1952] defined the conductances as the following expression, equation (4.2).

$$g_i = \bar{g}_i m_i^{p_i}(V_m) h_i^{q_i}(V_m) \tag{4.2}$$

where m_i (resp. h_i) is the variable that represents the activation (resp. inactivation) gate for each ion i.

In their initial model, [Hodgkin and Huxley, 1952] identified that the ions necessary for the creation of a potential are the ions sodium Na^+ and potassium K^+. Equation (4.2) can therefore be rewritten for those ions and the expressions of p_{ion} and q_{ion} for each of the gating variables were found by curve fitting of experimental data. Finally, one can obtain the mathematical expression of the variation of state for the gating variables by applying the mass action law. The equations of the variables can therefore be written as

$$\frac{dm_{ion}(V)}{dt} = \frac{m_{\infty,ion}(V) - m_{ion}(V)}{\tau_m(V)} \tag{4.3}$$

$$\frac{dh_{ion}(V)}{dt} = \frac{h_{\infty,ion}(V) - h_{ion}(V)}{\tau_h(V)} \tag{4.4}$$

where τ_m (resp. τ_h) represents the time constant it takes for the gate m_{ion} (resp. h_{ion}) to reach its steady state value, $m_{\infty,ion}$ (resp. $h_{\infty,ion}$).

In conclusion, this type of modeling offers a lot of versatility as the ionic currents and the channels considered can be easily tuned. Moreover, they offer a lot of interpretability because the currents considered in the model are actually physiological.

4.1.2 Dopaminergic neuron model

The aim of this model is to describe the specificity of the behaviour of DA neurons. It must be able to reproduce the different firing patterns (tonic, phasic and burst firing - see section 3.2.1) Moreover, the interplay of the calcium ion channels and the role of the SK channels in regulating the firing of the neurons must be translated in the model.

Taking into account the specificity of the behaviour of DA neurons, the evolution of the membrane potential is written by [Drion, 2015] as the following sum of currents

$$C_m \frac{dV_m}{dt} = -I_{Na} - I_{K,DR} - I_{CaL} - I_{CaN} - I_{SK} - I_{ERG} - I_{NMDA} - I_{leak} + I_{app} + I_{noise} \tag{4.5}$$

where C_m is the membrane capacitance and V_m is the membrane potential. I_{Na} stands for the sodium current, $I_{K,DR}$ for the delayed rectifier potassium current, I_{CaL} and I_{CaN} for the calcium currents respectively through the type-L and type-N calcium channels, I_{SK} the potassium current though the SK-channels and I_{ERG} is for the potassium current through the ether-a-go-go–related gene channels. I_{NMDA} accounts for the calcium current induced by the activation of NMDAr thanks to glutamate. Finally, the current I_{noise} is added to reproduce biological noise. A summary of the source that were used to write the model is available in Table 4.1

In the appendix (Section 11.4) can be found the full description of the model with the mathematical

Current	Reference
I_{Na}, $I_{K,DR}$ and I_{leak}	[Qian et al., 2014]
I_{CaN}	[Canavier and Landry, 2006]
I_{ERG}	[Yu and Canavier, 2015]
I_{NMDA}	[Putzier et al., 2009] [Kuznetsov et al., 2006]

Table 4.1: **Sources** - Summary of the sources used by [Drion, 2015] to create the model of the dopaminergic activity

equation of each current and the dynamics of their corresponding gating variables.

4.1.3 Activation of SK channels

The model shows a distinction between the currents from the L-type calcium channels and the N-type calcium channels as both have different roles in the dynamics of the DA neuron.

- The L-type calcium channels provide a large source of calcium so their main role is to induce the burst firing of the cell. However, the concentration of calcium in the cytosol should be seen as *microdomains*, not as a homogeneous value. They do not contribute to the activation of calcium activated SK channels despite the large influx of ions they provide.
- the activation of the SK channels comes from different sources of calcium, the main one being from the N-type calcium channels. [Scuvée-Moreau et al., 2004]

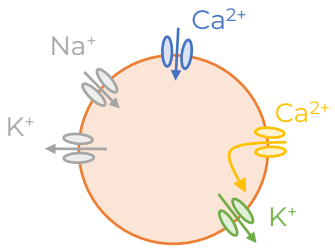

Figure 4.2: **Model description** - Representation of the currents that mediate the model of dopaminergic activity. Blue is for type-L calcium channel, yellow for type-N calcium channel and green for SK channels. Figure inspired by V. Seutin.

Actually, it is therefore assumed in this model that the SK channels are solely activated by I_{CaN} and none of the other calcium currents are included, as represented in Figure 4.2.

In the appendix is available a full description of the model. The mathematical expression of all the currents is developed with the differential equation that describes the evolution of each gating variable.

4.1.4 Modeling of ion channel blockers

In conductance-based modeling, it is actually easy to reproduce the effect of channel blockers. In fact, blocking a channel results in the suppression of the corresponding ionic current X. Mathematically, this is reproduced by setting the maximal conductance $\bar{g}_X = 0$ in equation (4.5).

In Figure 4.3 is available a summary of the different toxins and drugs that are going to be used on dopaminergic neurons during experimentation. In grey are represented the ion channels which were found to contribute to a precise modeling dopaminergic neurons but whose dynamics were not studied thanks to channel blockers.

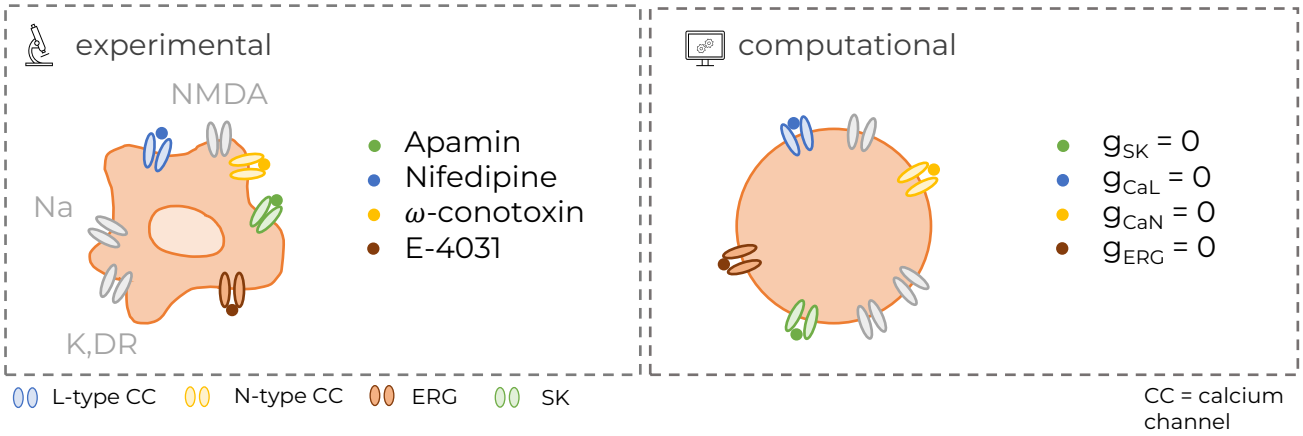

Figure 4.3: **Summary of the pharmacology** - Main channel blockers used experimentally to understand DA activity and how they are modeled computationally. Ca_L = L-type calcium channels ; Ca_N = N-type calcium channels ; SK = small-conductance potassium channels ; ERG = ether-a-go-go potassium channels.

4.2 Summary

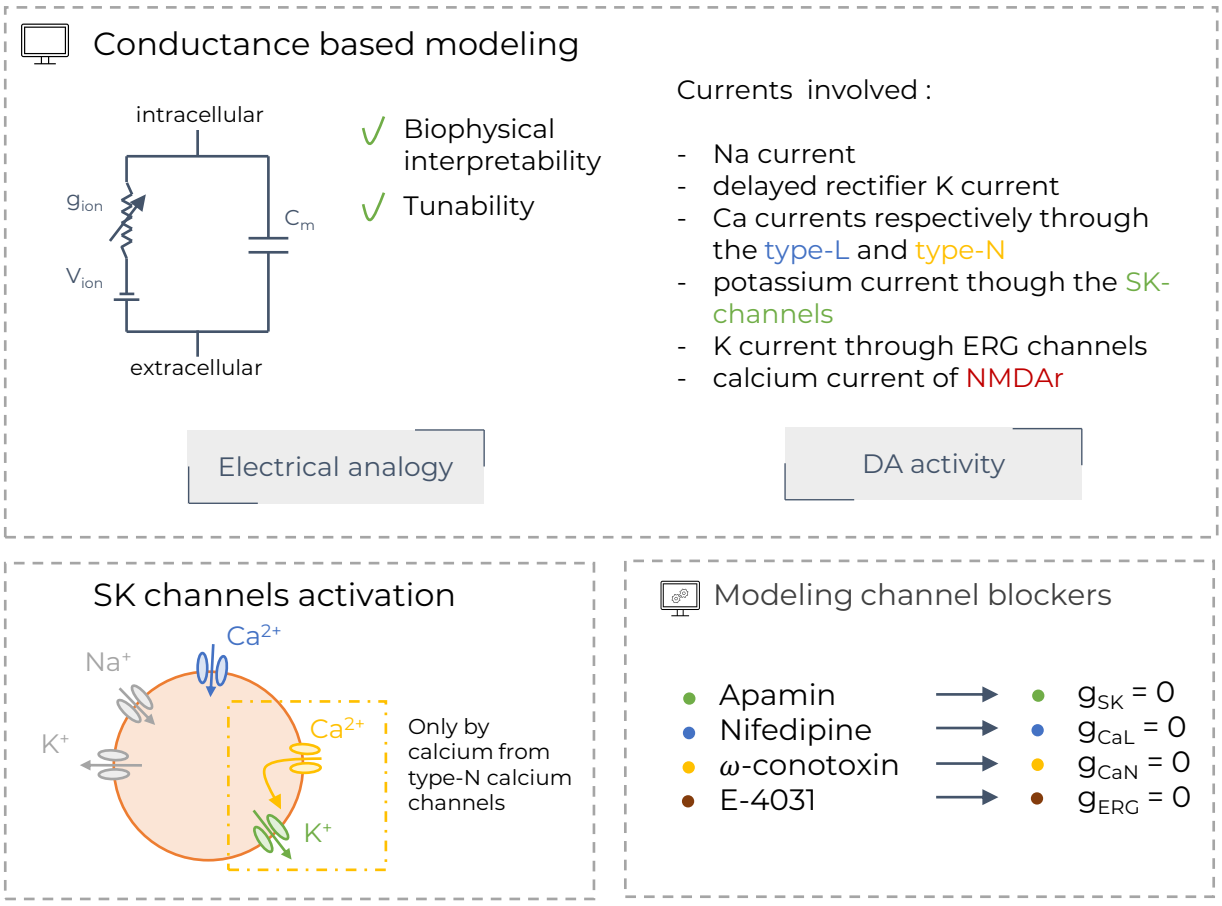
Conductance based modeling
intracellular
g_{ion}
C_m
V_{ion}
extracellular
Biophysical interpretability
Tunability
Currents involved :
- Na current
- delayed rectifier K current
- Ca currents respectively through the type-L and type-N
- potassium current though the SK-channels
- K current through ERG channels
- calcium current of NMDAr
Electrical analogy
DA activity
SK channels activation
Ca^{2+}
Na^+
K^+
Ca^{2+}
K^+
Only by calcium from type-N calcium channels
Modeling channel blockers
Apamin → $g_{SK} = 0$
Nifedipine → $g_{CaL} = 0$
ω-conotoxin → $g_{CaN} = 0$
E-4031 → $g_{ERG} = 0$

Chapter 5

Mathematical tools for dynamical analysis

The aim of this chapter is to describe the multiple tools that will be used in order to understand the dynamics of the dopaminergic model.

5.1 Dynamical analysis

The most useful tool to understand the dynamics of non-linear systems of differential equations is to represent the interplay of the states variables and to study *qualitative* dynamics.

In a system of two differential equations, its general form can be written as the following

$$\dot{V} = f(V, V_s) \tag{5.1}$$
$$\dot{V_s} = g(V, V_s) \tag{5.2}$$

where V and V_s are the state variables of the system, f and g are functions of those state variables and the dot represents the a time derivative.

5.1.1 Definitions

The system of equation (5.1)-5.2 being two dimensional allows to study the dynamics of the system using a *phase plane* on which are represented the *nullclines*, *vector fields*, *trajectories* and *fixed points*.

- The *nullclines* represent the ensemble of values where the velocity of one state variable is cancelled, i.e. $f(V, V_s) = 0$ and $g(V, V_s) = 0$.
- The *vector field* dictates the velocity $(\dot{V}, \dot{V_s})$ of each state variable of the system for every values of (V, V_s)
- The *trajectories* represent the solution of the system starting from a specific set of initial conditions $(V_0, V_{s,0})$
- *Fixed points* $(\bar{V}, \bar{V_s})$ are the equilibrium solutions of the system, which graphically corresponds to the intersection of the nullclines where the velocities of both state variables are cancelled.

- *Bifurcations* are a sudden change in the behaviour of the model is caused by a small variation of a parameter, which is subsequently called the *bifurcation parameter*.

- the *basin of attraction* is "the set of all the initial conditions in the phase space whose trajectories go to that attracting set" [Nusse et al., 1994]

For more details on the subject, refer to [Strogatz, 2015].

5.1.2 Nature of the fixed points

The stability of the fixed points $(\bar{V}, \bar{V}_s)$ can be determined by studying the linearization of the vector fields at the fixed point, i.e. the *jacobian* which is defined as

$$J_{i,j} = \frac{\partial f_i(\bar{x}_i)}{(\partial x_j)} \tag{5.3}$$

By defining $x_1 = V$, $x_2 = V_s$, $f_1 = f(V, V_s)$ and $f_2 = g(V, V_s)$, the linearized system at the fixed point is written as

$$\begin{pmatrix} \dot{V} \\ \dot{V}_s \end{pmatrix} = \begin{pmatrix} \frac{\partial f}{\partial V} & \frac{\partial f}{\partial V_s} \\ \frac{\partial g}{\partial V} & \frac{\partial g}{\partial V_s} \end{pmatrix}_{(\bar{V}, \bar{V}_s)} \begin{pmatrix} V \\ V_s \end{pmatrix} \tag{5.4}$$

By evaluating the nature of the eigen values of the jacobian matrix at such points, the dynamics of the system at the point can be analysed and the nature of the fixed points evaluated.

In fact, the eigen values λ_1 and λ_2 of the jacobian evaluated at the fixed point represent the exponent of the solution of the system around the fixed point. Several cases can be met and their interpretation are summarised in the following tables.

	$\lambda_{1,2} \in C$
$R\{\lambda_{1,2}\} > 0$	Unstable spiral
$R\{\lambda_{1,2}\} < 0$	Stable spiral
$R\{\lambda_{1,2}\} = 0$	centre

	$\lambda_{1,2} \in R$
$\lambda_{1,2} > 0$	Unstable node
$\lambda_{1,2} < 0$	Stable node
$\lambda_1 > 0$ and $\lambda_2 < 0$	Saddle node

The stability of a fixed point is solely dictated by the real part of its eigen values. The complex part, however, dictates whether the trajectory oscillates.

5.2 Model reduction

The main issue with the approach of phase plane analysis that it requires to have only two state variables that drive the model for an insightful interpretation on a plane. Conductance-based models, however biologically accurate, are usually of a much higher order.

5.2.1 Introduction

In 1961, to understand how the dynamics of the original model developed by Hodgkin and Huxley drive the generation of spikes, [FitzHugh, 1961] decided to study the model according to *time scales* and considering separately the behaviour of two subsystems. They adapted the model by considering

a *fast* subsystem that varies within *slow* one. The final expression of the model is

$$\dot{V} = f(V) - W + I \tag{5.5}$$

$$\dot{W} = a(bV - cW) \tag{5.6}$$

where V is the membrane potential and W is the adaptation variable. The dot stands for time derivative. f(V) is a polynomial of third degree, and a, b and c are constant parameters.

This reduction of the model allows to visualise the whole solution of the model on the phase plane which allows to give geometrical explanations using *phase plane analysis*.

5.2.2 Approach

The model of dopaminergic activity developed by G. Drion and studied in this work is a conductance-based model of high order. In fact, additionally to equation (4.5), each gating variable that drives the dynamics of the ionic currents is described with a differential equation as well. In their work, [FitzHugh, 1961] used qualitative resemblances to already existing models to reduce Hodgkin and Huxley's model. This is approach is difficult to apply to the model because of its complexity.

To tackle this issue, it was decided to take inspiration from [Jacquerie and Drion, 2021] who applied the method of *Dynamic input conductances* (DIC) to understand the importance of the activation time constant for type-T calcium channels in thalamocortical neurons. It was originally developed by [Drion et al., 2012] and it allows to reduce the model to a third order level of differential equations, making it more prone to a dynamical analysis.

5.2.3 Algorithm of Dynamic Input Conductances

The idea is to take the original multidimensional model and to project the gating-variables onto three time scales, *fast*, *slow* and *ultra slow* according to their contribution in each time scale. Each time scale is characterised by a corresponding variable V, V_s and V_u. In a neuron, dynamic input conductances characterise the contribution of each ion channel in the generation of a spike. For a bursting neuron, the fast variable mediates the spike initiation, the slow variable mediates the down stroke of a spike and the ultraslow variable mediates the spike adaptation and the interburst period [Drion et al., 2015].

The reduced model is described by the following expression

$$C_m \frac{dV}{dt} = \sum I_i + I_{app} \tag{5.7}$$

$$\frac{dV_s}{dt} = \frac{V - V_s}{\tau_s(V)} \tag{5.8}$$

$$\frac{dV_u}{dt} = \frac{V - V_u}{\tau_{us}(V)} \tag{5.9}$$

where the ionic currents are now expressed as

$$I_i = \bar{g}_i m_i^{p_i}(V, V_s, V_{us}) h_i^{q_i}(V, V_s, V_{us})(V - E_i) \tag{5.10}$$

Equation (5.7) represents the fast timescale while equation (5.8) (resp. 5.9) represent filtered versions

of the membrane potential whose dynamics are paced by the time constant $\tau_s(V)$ (resp. $\tau_{us}(V)$) [Jacquerie and Drion, 2021].

In equation (5.10), the inactivation and activation variables $m_i(V)$ and $h_i(V)$ are now described according to a weighted sum of their contribution in each timescale. Their expression is given by the same general form

$$X(V, V_s, V_{us}) = \underbrace{w_{fs}^X(V)X_\infty(V)}_{fast} + \underbrace{(w_{su}^X(V) - w_{fs}^X(V))X_\infty(V_s)}_{slow} + \underbrace{(1 - w_{su}^X(V))X_\infty(V_{us})}_{ultraslow} \tag{5.11}$$

where the activation (resp. inactivation) is assumed to be instantaneous in each time scale considered.

Each gating variable is projected on the different time scales according to weights, $w_{fs}^X(V)$ and $w_{su}^X(V)$, that are computed by considering regions

- The fast region which is the interval defined as [0, $\tau_f(V)$]
- The fast-slow (fs) region that is the interval defined as [τ_f(V), $\tau_s(V)$]
- The slow-ultraslow (su) region that is the interval defined as [$\tau_s(V)$, $\tau_{us}(V)$]
- The ultraslow region that is the interval [$\tau_{us}(V)$, ∞]

For a given value of voltage V, each gating variable time constant $\tau_X(V)$ is going to lie within one of the regions. For the fast (resp. ultraslow) regions, the variables are considered to be exclusively fast (resp. ultraslow). For the two other regions, the contribution in both of the time scales considered are computed by computing the logarithmic distance to the bounds of the interval. The evolution of the weights depending on which time region the time constant falls within is illustrated in Figure 5.1.

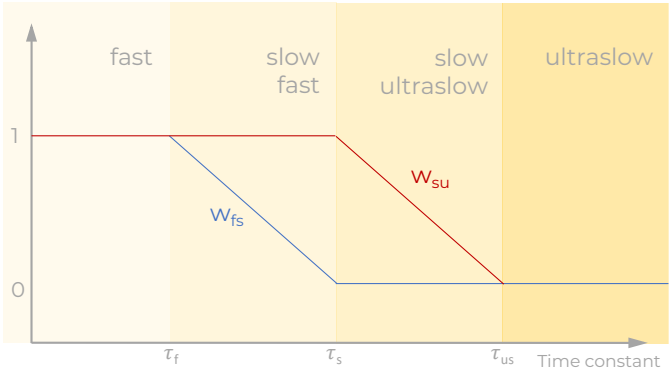

Figure 5.1: **Illustration of the algorithm** - Value of the weights w_{fs} and w_{su} depending on which region of speed the time constant falls in

For a more detailed description of the algorithm, refer to the original article [Drion et al., 2015] as well as [Jacquerie and Drion, 2021].

Thanks to this approach, this allows to reduce the complexity of the model since the gating variables that were originally described using differential equations are now only represented with weighted sums.

5.3 Summary

In this chapter, the aim is to describe the main tools that are required for dynamical analysis of the behaviour of non-linear models. Some definitions and concepts regarding phase planes are reminded (concept of *phase plane, bifurcation, vector fields, nullclines, fixed point,...*). Then the study to establish the nature of fixed points is explained.

Finally, the essence of model reduction is described as summarised in the following figure.

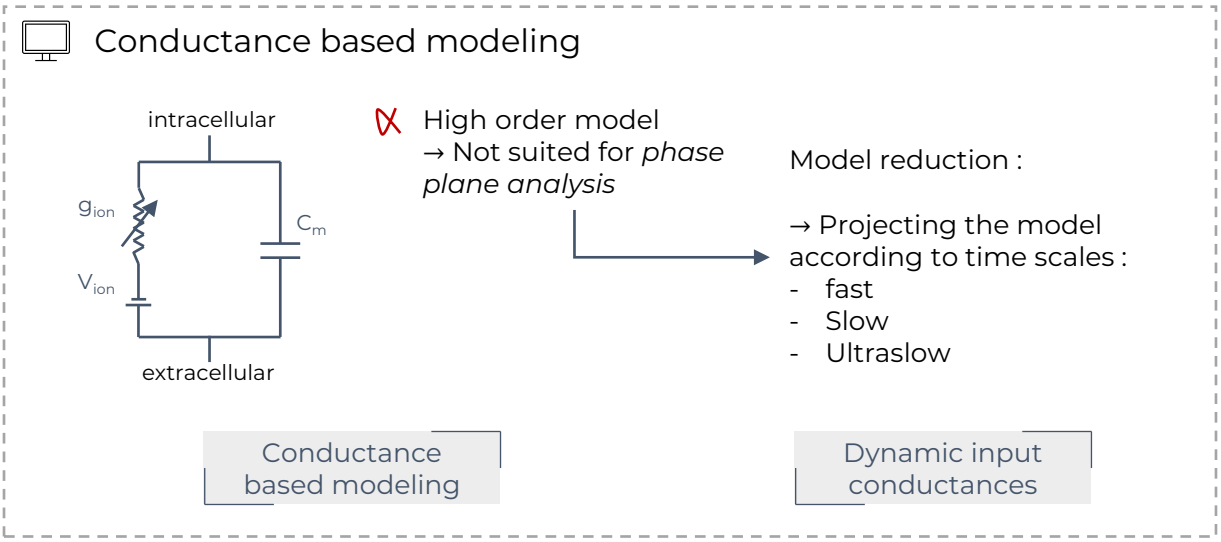

Part II

Experiments and reproduction of results

Chapter 6

Reduction of the model

This chapter aims to described the different preliminary steps that are required to develop the reduced model and use it as a tool to understand the dynamics of the actual model.

6.1 Reduction of the differential equations

To apply the DIC algorithm, one must define the boundaries of the regions, i.e. define to which values $\tau_f(V)$, $\tau_s(V)$ and $\tau_{us}(V)$ correspond. In order to visualise the regions, the time constants of the model are plotted in Figure 6.1. The full model is available in the appendix. As it can be seen, there are 5 gating variables, m_{Na}, h_{Na}, $n_{K,DR}$, m_{CaL} and m_{CaN}.

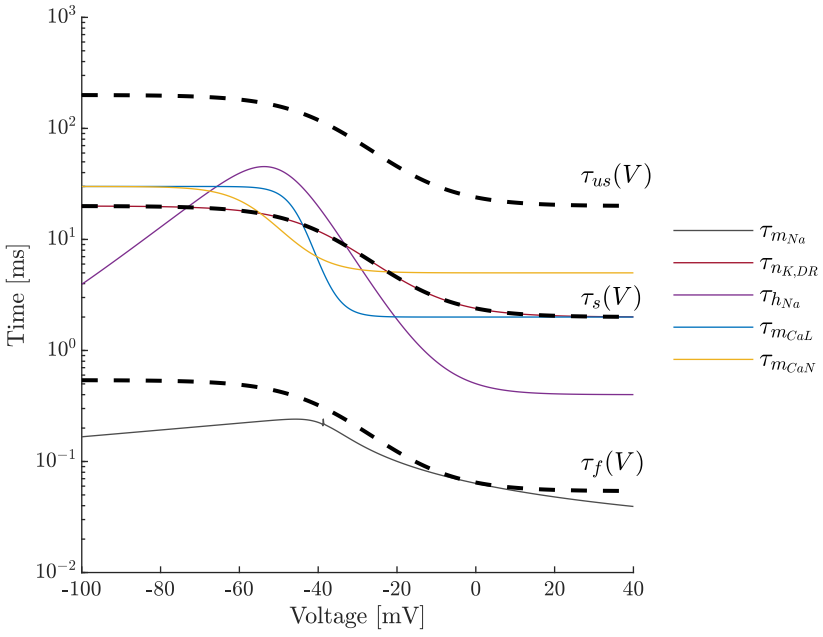

Figure 6.1: **Time constants** - Plots of the time constants of the DA model and definition of the regions for DIC algorithm

In theory, for the model of DA neurons developed in this work, the choices would be $\tau_f(V) = \tau_{m_{Na}}(V)$, $\tau_s(V) = \tau_{n_{K,DR}}(V)$ and $\tau_{us}(V) = \tau_{ERG}(V)$. However, because of the complexity of the expression of

the variation of open ERG channels, $\tau_{us} = 10\tau_s(V)$ is chosen instead. Additionally, discontinuities in the expression of $\tau_{m_{Na}}(V)$ lead to a safer choice of $\tau_f = \frac{1}{50}\tau_s(V)$.

In this work, the study is focused on the study of the switches from spiking to bursting. Those events happen in the fast-slow region. This means that the expression of $oERG$, which was not fitted for reduction because of its complexity, does not need to be altered. In fact, in such case, the variable can be considered as a parameter that influences the shape of the nullclines.

6.2 Adaptation of the parameters

Once the model has been reduced using the algorithm, it is often observed that the rhythm is lost. This is what was observed with the model. In fact, by running it with the typical parameters, the temporal traces that are obtained are available in Figure 6.2.

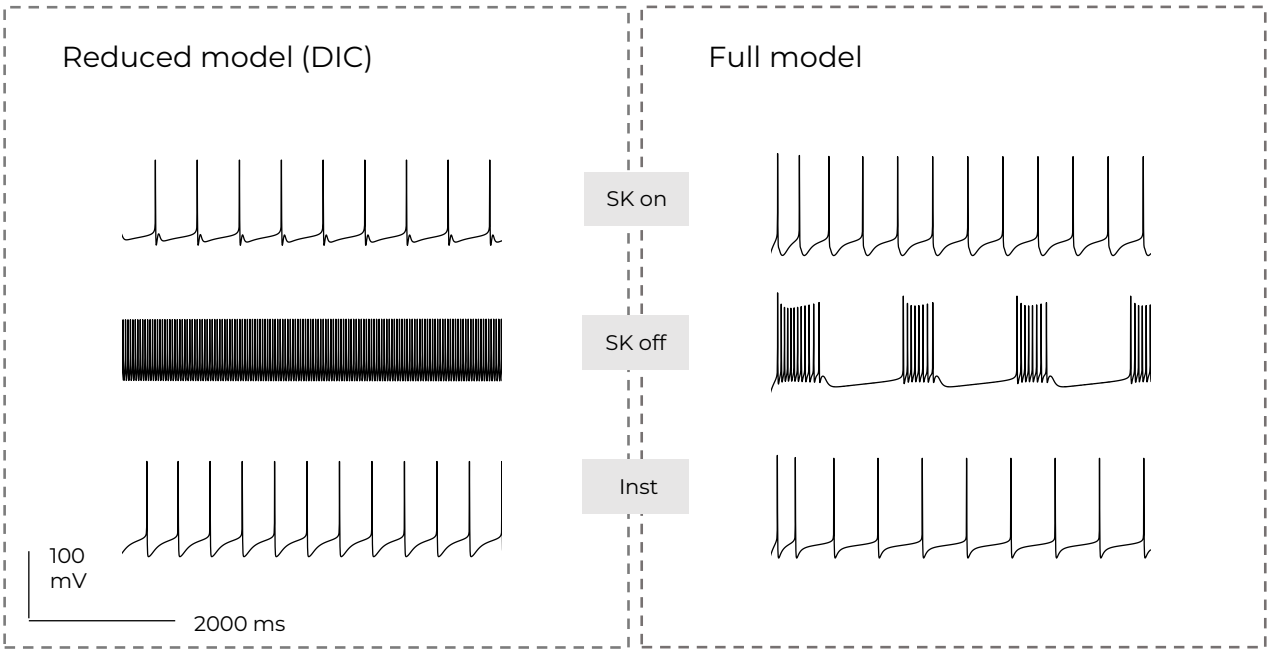

Figure 6.2: **(left)** Modelisation of the temporal traces of the reduced model without changes in the parameters value **(right)** Comparison with the unreduced model

In Figure 6.2, the model was run in three configurations. The reduced model must be able to replicate the initial model, especially in the three situations that are represented in the figure. *SK on* refers to the case where $\bar{g}_{SK} = 0$ [mS/cm²], *SK off* refers to $\bar{g}_{SK} = 0.9$ [mS/cm²] and *inst* refers to the case where calcium activation is instantaneous instead of slow (and $\bar{g}_{SK} = 0$). The model was ran for $\bar{g}_{CaL} = 0.038$ [mS/cm²] The relevance of those three different cases will be further developed in the following chapter.

It can be easily concluded from the comparison of both simulations in the three cases that the parameters require tuning to recover the rhythm.

To adapt the parameters, the first observation that was made was on the effect of $\bar{g}_{CaL}$. In fact, when the SK current is blocked, the neuron switches to a bursting pattern which is too intense compared to

the original model (see figure 6.2 in the case *SK off*). This indicates that there is too much calcium in the model so its influence must be reduced. An interplay between the sodium (which initiates the spikes) and the ERG current (which dampens the excitability) was then required to adapt the frequency of firing. Finally, by the effect of SK was added and tuned.

The list of the coefficients which are added to the initial parameters of the model are therefore listed in the following table, Table 6.1.

Parameter	**Coefficient**
g_l	1
g_{Na}	1.7
$g_{K,DR}$	1
g_{CaL}	0.6
g_{CaN}	1
g_{SK}	5
g_{ERG}	4
g_{NMDA}	3

Table 6.1: **Adaptation of the parameters** - Values of the coefficients added to the parameters of the model to recover the rythm after reduction

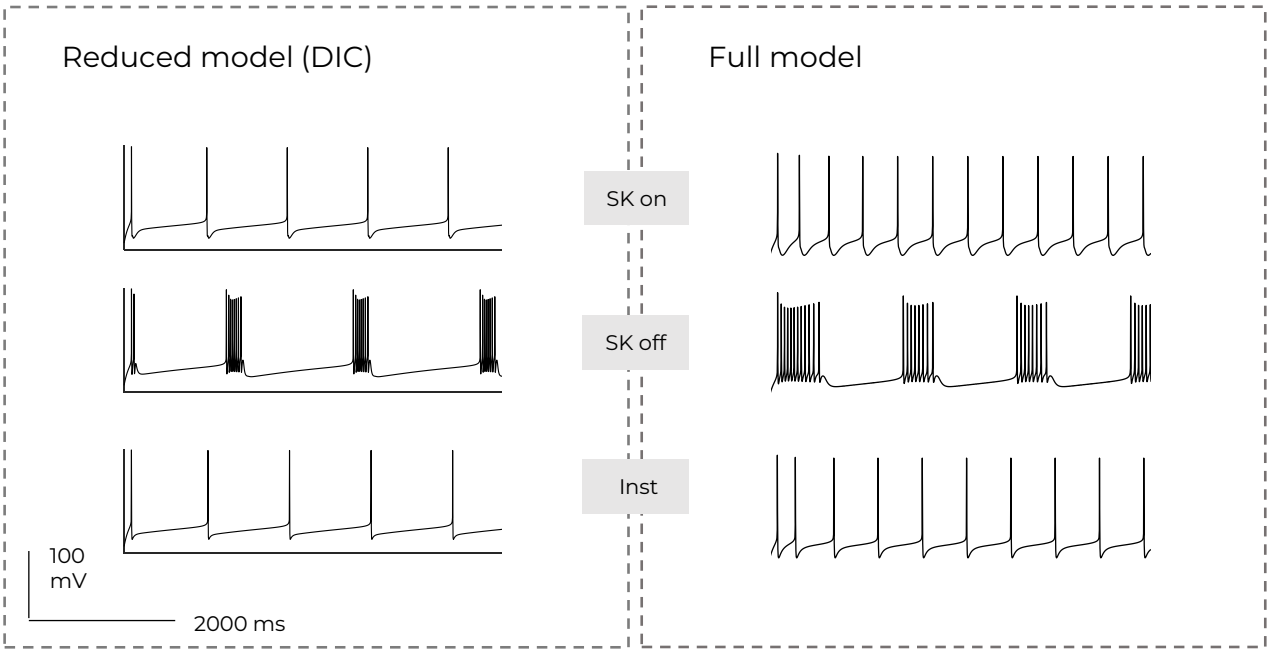

Figure 6.3: **Adapted parameters** - **(left)** Modelisation of the temporal traces of the reduced model without changes in the parameters value **(right)** Comparison with the unreduced model

As it can be seen in Figure 6.3, the model is now able to reproduce the behaviour of the original model. The dynamics appear to be slightly slower but it doesn't influence the dynamical analysis on the phase plane.

6.3 Summary

In conclusion, as it can be visualised from figure 6.3, the reduced model is able to reproduce the three types of that will be studied later on in the experiments. However, to do so, the parameters of the model must be adapted in order to recover the rhythm. The list of the added coefficients is available in Table 11.1.

Chapter 7

Dopaminergic neuron model and validation on experimental data

The aim of this chapter is to validate the model on experimental data and to study its behaviour using engineering tools. In this chapter, the following 5 experiments are performed firstly by showing experimental results, then by reproducing them using the model and finally analysing the dynamics if suited.

- *Experiment 1* : SK channel blockade is induced on the dopaminergic neuron to observe the effect on a single spike.
- *Experiment 2* : Cell-to-cell variability is uncovered by SK channel blockade.
- *Experiment 3* : Variability that is highlighted in the previous experiment is then lost by subsequently blocking L-type calcium channels.
- *Experiment 4* : Emphasis on the importance of L-type calcium channels as opposed to other type of calcium channels in this variability
- *Experiment 5* : Importance of the timescale dynamics of activation of L-type calcium channels on the behaviour of the model.

7.1 Experiment 1 - Effect of SK channel blockade

7.1.1 Experiment

In Figure 7.1, the left figure represents the experimental measurements that were obtained in vitro by [Scuvée-Moreau et al., 2004] on the spiking of DA neurons. They induced SK-channel blockade (in green) and observed that the shape of after-hyperpolarisation (period that follows a spike) is altered as it appears to bounce back faster. The neuron actually present now what is called an *after depolarisation* (ADP). SK-channels seem to dampen the excitability of the dopaminergic activity by keeping the membrane potential hyperpolarized.

7.1.2 Computational reproduction

This result was reproduced computationally by cancelling the maximal conductance $\bar{g}_{SK}$. As one can judge the results available on the right of Figure 7.1, the model is able to truthfully reproduce the

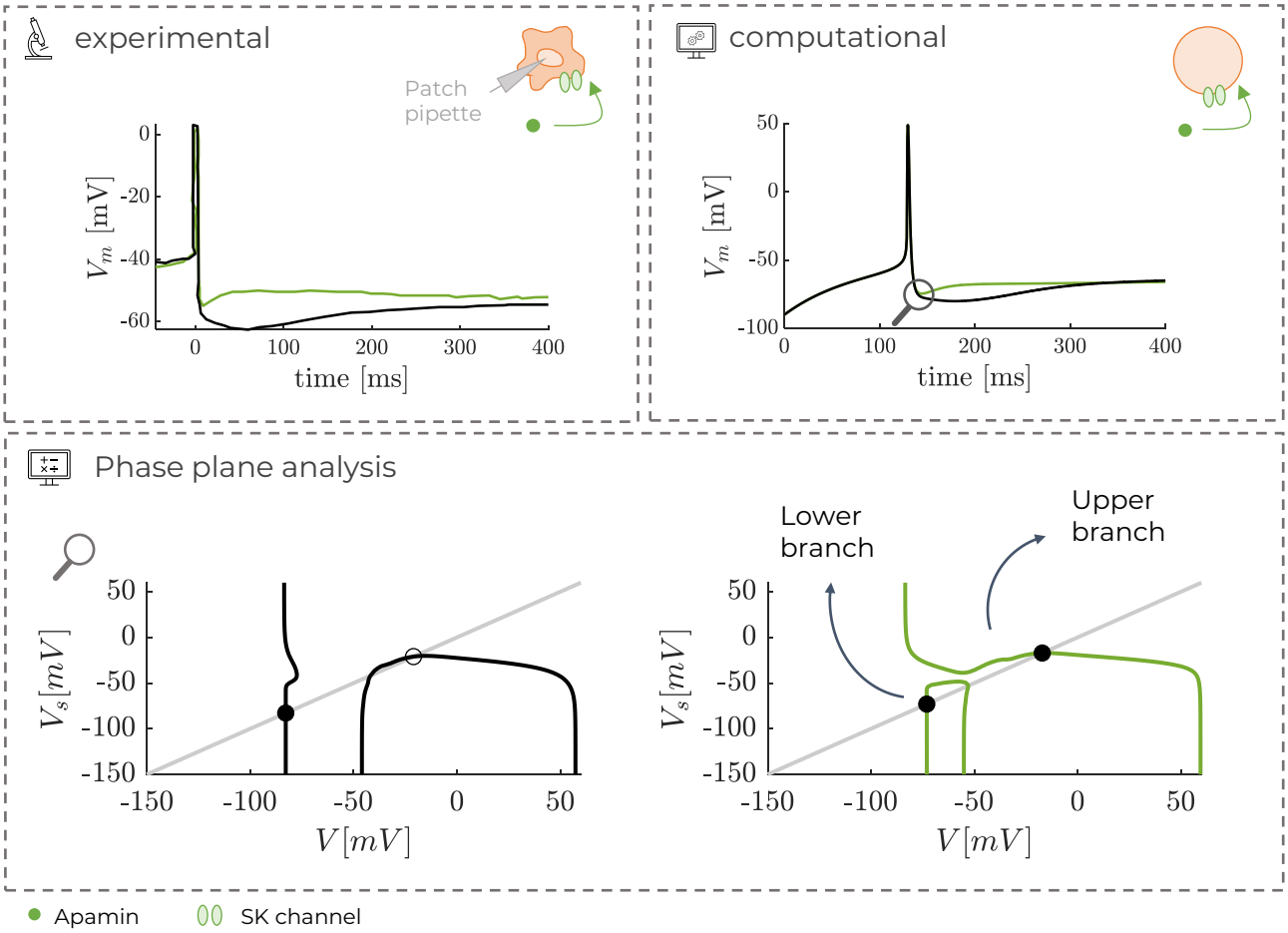

Figure 7.1: **Single spike - (left)** Experimental data from [Scuvée-Moreau et al., 2004] **(right)** Reproduction using the model. In black is a single spike under no blockade while in green is the same single spike with SK-channel blockade **(bottom)** Phase plane analysis of the both cases. Left is with SK and right is without SK.

effect of SK channels on DA activity. The membrane potential remains hyperpolarized for a longer period of time when the contribution of SK channels is included in the simulation.

7.1.3 Dynamical analysis

The nullclines of the model are computed as follows

$$\begin{aligned}\frac{dV}{dt} &= (\frac{1}{C})(-g_{Na}m_{Na}^3h_{Na}(V-V_{Na}) - g_{K,DR}n_{K,DR}^3(V-V_K) - g_{CaL}m_{CaL}^2(V-VCa) \\ &- g_{CaN}m_{CaN}(V-Ca) - g_{ERG}oERG(V-V_K) - g_l(V-V_l)) \\ &- g_{SK}\left(\frac{[Ca]_{SK}}{[Ca]_{SK}+K_D}\right)^2(V-V_K) \\ \frac{dVs}{dt} &= \frac{V-V_s}{\tau_s(V)}\end{aligned}$$

and $oERG$ and Ca_{SK} is set as parameters that vary with the ultra slow variable.

At the bottom of figure 7.1, the phase planes for both situations are plotted. As it can be seen, the phase plane has a different shape, which explains why the spiking is different.

This shape of the phase plane in the case of SK channel blockade is actually typical for a tonic firing characterised by an *after-depolarisation* (ADP).This is explained by the presence of the separation of the V-nullcline into an *upper branch* and a *lower branch*. This will be further developed in the following section.

7.2 Experiment 2 - Cell-to-cell variability

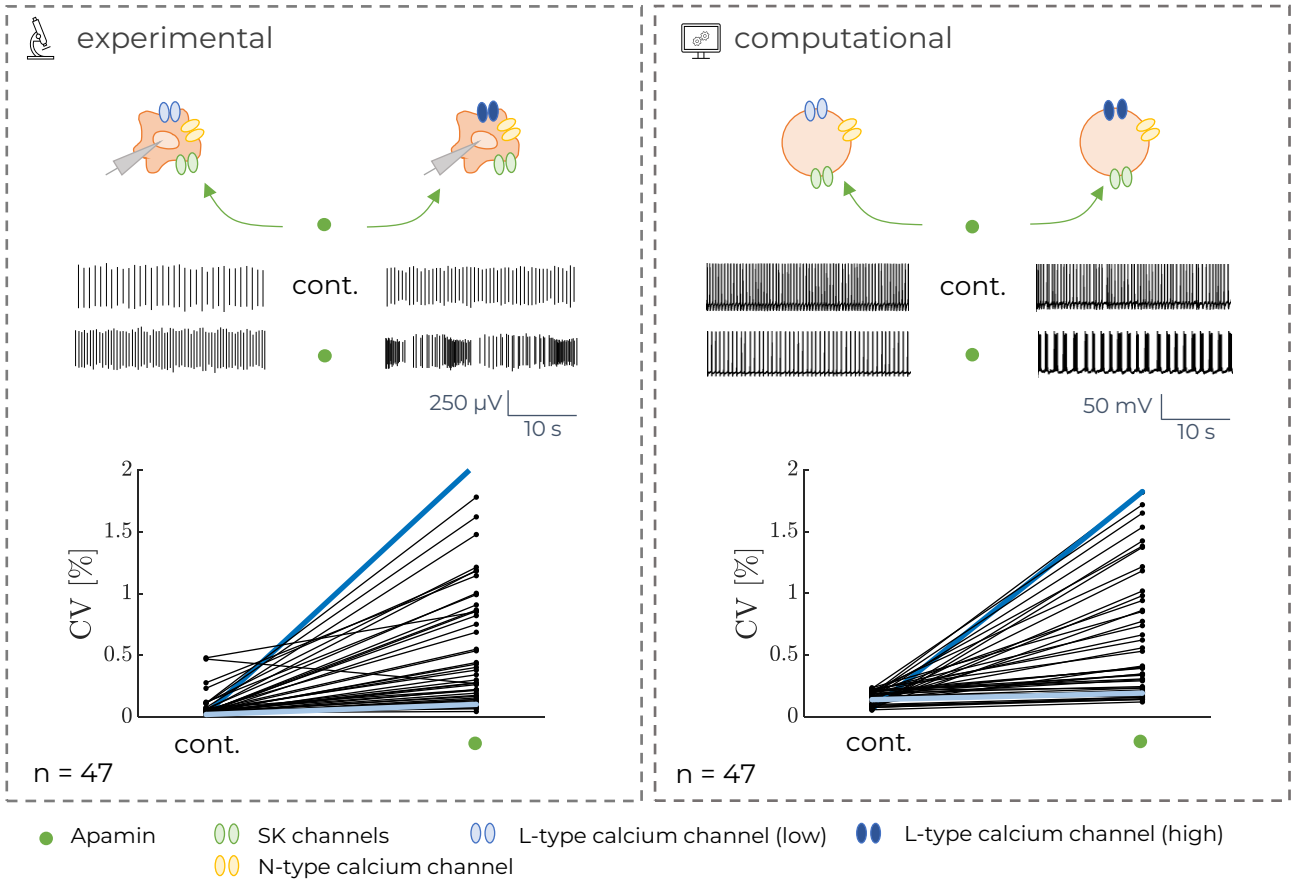

Figure 7.2: **Cell-to-cell variability - (left)** (top) Experimental results from [de Vrind et al., 2016] showing the firing pattern of two DA neurons in control conditions (cont.) and after apamin treatments (green dot) (bottom) Reproduction of results from [de Vrind et al., 2016]. Summary of the effect of apamin on the firing pattern of 47 dopaminergic neurons **(right)** Reproduction of the experimental results with the model. Light blue indicates low value of $\bar{g}_{CaL}$ and dark blue indicates higher values of $\bar{g}_{CaL}$

In results from [Scuvée-Moreau et al., 2004] , available on the left in Figure 7.2, it was shown that the heterogeneity of the mechanisms that drive the firing pattern that was highlighted in Table 3.2 can be displayed by SK channel blockade.

7.2.1 Experiment

The experimental side of Figure 7.2 shows two cases : control (cont.) and apamin 300 nM (green dot). Control is the case where the neurons fire under no alterations. The traces of two types of neurons are shown

- On the left (light blue), a neuron which fires in pacemaking in control case (top trace) and remains in pacemaking under SK channel blockade (bottom trace).
- On the right (dark blue), a neuron which fires in pacemaking in control conditions (top trace) and switches to an irregular bursting behaviour when SK channels are blocked (bottom trace).

Below, a generalised experiment was performed by [de Vrind et al., 2016]. They computed the coefficient of variation of 47 different neurons in order to characterise the firing pattern (see Equation (3.1)) and observe the heterogeneity. The low values of the variation coefficients (CV) indicate that the firing pattern in such case is consistent, indicating *pacemaking* for all neurons. The green dot represents the case where SK channel blockade is induced by apamin 300 nM. In such case, cases can be observed, either the pacemaking is lost (increase in CV), or it is sustained (low CV sustained).

The light blue and dark blue lines represent where the two neurons above would end in the experiment.

7.2.2 Computational reproduction

In order to reproduce these results, the model was simulated multiple times, each time by changing the parameters in way that reproduces *physiological variability* observed in vitro.

For each simulation, the maximal conductances for I_{CaN} and I_{CaL} were chosen randomly in a reasonable interval of values, i.e. $\bar{g}_{CaL} \in [20 - 38]\,\mu S/cm^2$ and $\bar{g}_{CaN} \in [1.5 - 2]\,\mu S/cm^2$. The traces of two types of neurons are shown

- On the left (light blue), a neuron which fires in pacemaking in control case and remains in pacemaking under SK channel blockade.
- On the right (dark blue), a neuron which fires in pacemaking in control conditions and switches to an irregular bursting behaviour when SK channels are blocked.

Similarly to the experiments, the coefficients of variability for each neuron in control conditions are computed. The low values of the CV indicate that the firing pattern is also consistent, indicating *pacemaking* for all neurons despite the variability in the parameters. To reproduce the effect of apamin, each simulation is then reproduced with the same parameters but by also choosing $\bar{g}_{SK} = 0$. Both results of either pacemaking lost or sustained are also observed when SK channels are blocked.

The light blue and dark blue lines represent where the two traces of the neurons fall on the generalised experiment. In the model, the intensity of the blue represents how large $\bar{g}_{CaL}$ is.

By inducing SK channel blockade, neurons might switch to a bursting pattern and the intensity of such burst is mediated by the value of $\bar{g}_{CaL}$. There is actually an interplay between variables in the model which is analysed in the following sections.

7.2.3 Dynamical analysis for tonic activity (low values of g_{CaL})

Under SK channel blockade, the nullclines of the model are computed as follows

$$\frac{dV}{dt} = (\frac{1}{C})(-g_{Na}m_{Na}^3 h_{Na}(V - VNa) - g_{K,DR}n_{K,DR}^3(V - VK) - g_{CaL}m_{CaL}^2(V - VCa) \\ - g_{CaN}m_{CaN}(V - VCa) - g_{ERG}oERG(V - VK) - g_l(V - Vl))$$

$$\frac{dV_s}{dt} = \frac{V - V_s}{\tau_s(V)}$$

and $oERG$ is set as a parameter that varies with the ultra slow variable. Since there is no SK, the nullclines are altered by the variations of $oERG$ and V_u (the effect of $[Ca]_{SK}$ only appears in the expression of I_{SK} which is cancelled) so it is known that it is a critical parameter in the dynamical behaviour of the model. The expression of $oERG$ is available in the appendix.

Firstly, the system is studied for a typical value of $\bar{g}_{CaL} = 0.026$ [mS/cm²] which doesn't lead to spontaneous bursting. The neuron remains in pacemaking under SK channel blockade as it can be seen in the top figure of Figure 7.3. This corresponds indeed with the case for a neuron with a low value of type-L calcium channels that was found experimentally and modeled in Figure 7.2.

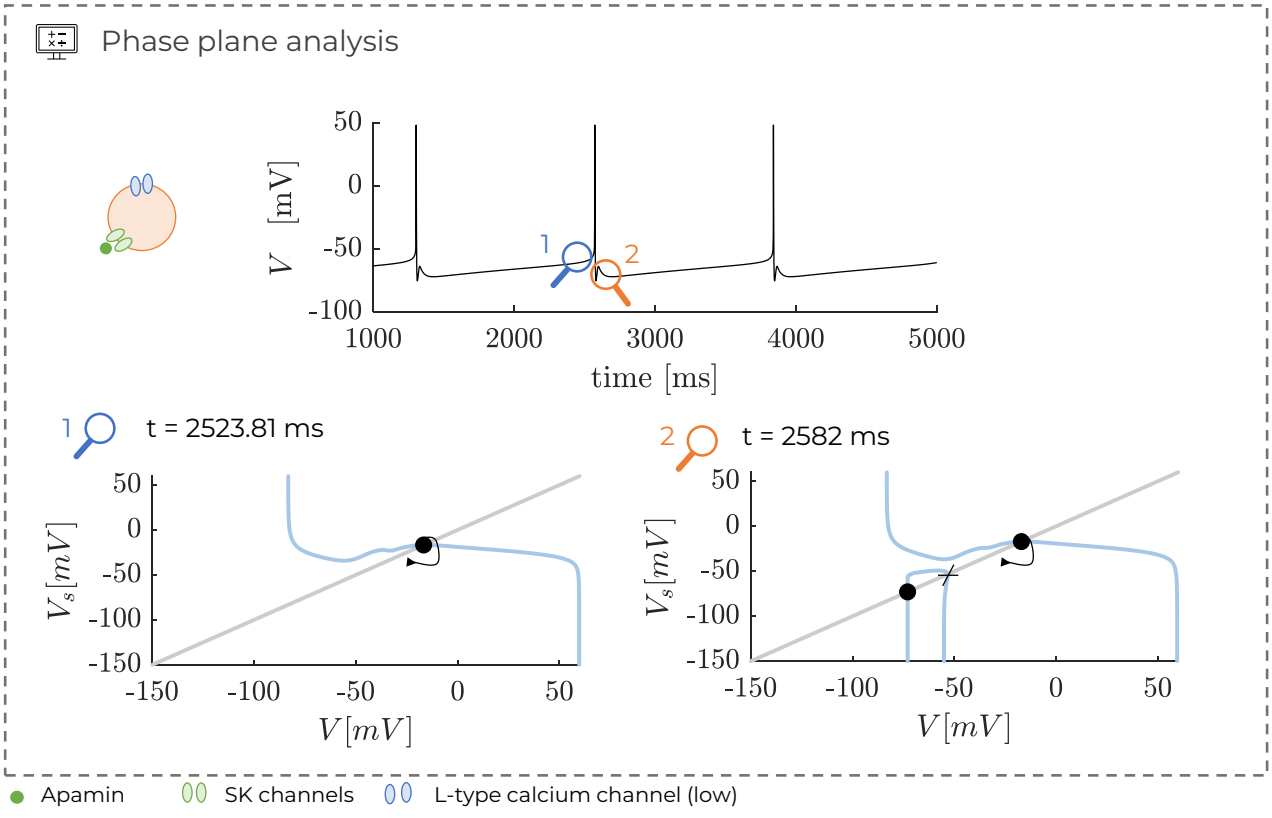

Figure 7.3: **Phase plane analysis** - Phase plane for $\bar{g}_{CaL} = 0.026$ [mS/cm²] **(top)** Trace of the reduced model **(bottom)** Comparison of the phase portraits at the two events that are highlighted on the magnifying glasses on the top figure. Full (resp. empty) dot = stable (resp. unstable) fixed point. Full (resp. empty) dot with an arrow = (resp. unstable) stable spiral. Blue = V-nullcline. Grey = V_s-nullcline.

From the visualisation of the video available in the additional files called *video_PP_noburst.mp4*, the spiking is appears to be characterised by two events which are highlighted by the two magnifying glasses on Figure 7.3

- 1^{st} event : Initiation of a spike by the disappearance of the lower branch of the V-nullcline
- 2^{d} event : The reappearance of the lower branch that leads to the end of the spike

1^{st} event The first event is the initiation of the spike is generated by the disappearance of the lower branch of the V-nullcline that was introduced in figure 7.1 (right phase plane). This leads to the phase plane that is represented on Figure 7.3 on the lower left, where there is only one fixed point at ($\bar{V}$,$\bar{V}_s$) = (-16.692, -16.692). The eigen values of the jacobian evaluated around such fixed point are

$$\lambda_1 = -0.0508 + 0.9314i \qquad \lambda_2 = -0.0508 - 0.9314i \tag{7.1}$$

Those eigen values being complex and negative lead to the fixed point being a *stable spiral*. However, this stable point is actually surrounded by a *stable limit cycle* as it can be observed that the model in the video does not converge towards the stable spiral. The coexistence of both attractive zones means that they are separated by an *unstable limit cycle*. The presence of such unstable limit cycle can be highlighted by tracing the trajectory of the solutions of the system for different initial conditions, allowing to observe the different *basins of attraction* that surround the stable spiral.

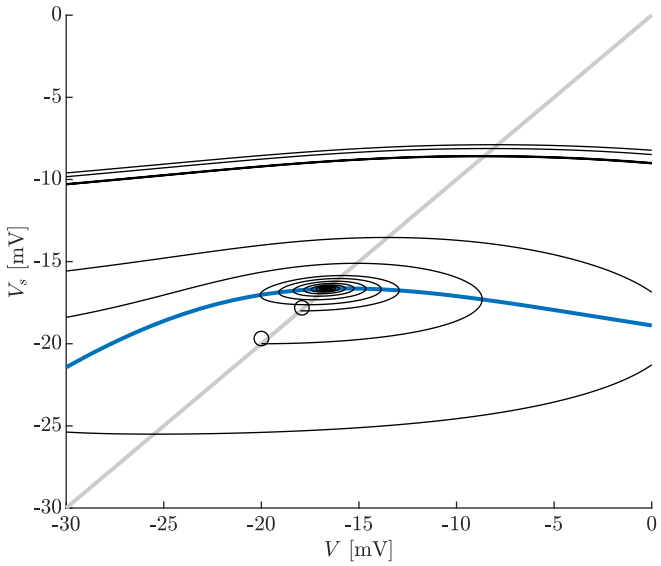

Figure 7.4: **Unstable limit cycle** - Trajectory (black lines) of the model for two different initial conditions (circles) highlighting the two basins of attraction the unstable limit cycle creates

As it can be observed in Figure 7.4, the model is simulated for $\bar{g}_{CaL} = 0.026$ and for $oERG = 0.1$ ($oERG$ must be set as a constant because the existence of such unstable limit cycle depends on its value, as it will be developed in further sections) for two different sets of initial conditions, as it is represented on the following figure by the two circles. The trajectories of both solutions are plotted and, as it can be seen, the set of initial conditions at ($\bar{V}, \bar{V}_s$)=(-20, -20) converges away from the intersection of the nullclines, to the stable limit cycle. Meanwhile, the set of initial conditions at ($\bar{V}, \bar{V}_s$)=(-18, -18) converges towards the intersection, at the stable spiral.

2^{nd} **event** The second event is the end of the spike which is characterised by the reappearance of the lower branch which leads to three fixed points. The eigen values and resulting stability of such points are summarised in the following table.

$(\bar{V}, \bar{V}_s)$	(-16.827,-16.827)	(-55.207, -55.207)	(-68.826,-68.826)
λ_1	-0.0390 + 0.9263i	0.0807	-0.0262
λ_2	-0.0390 - 0.9263i	-0.0559	-0.0515
Stability	Stable spiral	Saddle node	Stable node

Thanks to the reappearance of the lower branch, the solution tends towards the stable node at on the left of the phase plane thanks to a *homoclinic bifurcation* that includes the stable manifold, i.e. the attracting eigen vector of the saddle node. In fact, the stable manifold of the saddle node now intercepts the trajectory of the system. The model is therefore attracted towards the saddle node and then repelled towards the stable fixed point through its unstable manifold which leads to the end of the spike.

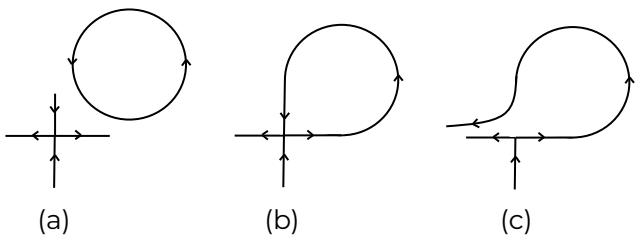

Figure 7.5: **Homoclinic bifurcation** - **(a)** Before the bifurcation **(b)** At the bifurcation, the limit cycle fuses with the saddle node **(c)** After the bifurcation. Adapted from [Drion et al., 2012]

The cycle then starts again as the lower branch starts to slowly disappear until it fully disappears, generating a spike. This whole process generates the pacemaking as the lower branch takes about 1000 ms to disappear.

7.2.4 Dynamical analysis for bursting (higher values of $\bar{g}_{CaL}$)

Now, the aim is to study the second case of Figure 7.2, where there is a bursting behaviour for larger values of $\bar{g}_{CaL}$.

To study how the burst phenomenon appears and the mechanisms that drive its behaviour, the model is studied for a typical value of $\bar{g}_{CaL} = 0.038$ [mS/cm²] which leads to spontaneous bursting as it can be seen in Figure 7.6.

Figure 7.6: **Animation** - Video (*video_PP_burst.mp4*) of the spontaneous bursting observed for $\bar{g}_{CaL} = 0.038$ [mS/cm²] and $\bar{g}_{SK} = 0$ **(top)** Time trace simulation of the model **(bottom)** Corresponding evolution of the phase plane

It can be seen in the animation Figure 7.6 that the phase plane presents three main events which are highlighted on Figure 7.7.

- 1^{st} event : The disappearance of the lower branch which leads to the initial spike
- 2^{nd} event : The reappearance of the lower branch that doesn't stop the bursting
- 3^{d} event : The reappearance of the lower branch that leads to the stop of the burst

1^{st} **event** The initiation of the spike isn't analysed as it is sensibly the same phenomenon as in Figure 7.3. Its analysis is available in the appendix.

2^{nd} **event** The second event is visible on Figure 7.7. During bursting, the lower branch of the V-nullcline appears and disappears but the trajectory remains in the basin of attraction of the stable limit cycle that was identified in the previous event. The system presents three fixed points at the time considered (t=1626 ms) summarised in the following table.

$(\bar{V}, \bar{V}_s)$	(-17.016,-17.016)	(-52.152, -52.152)	(-73.97,-73.97)
λ_1	-0.0302 + 0.9206i	0.1825	-0.0463
λ_2	-0.0302 - 0.9206i	-0.0867	-0.0509
Stability	Stable spiral	Saddle node	stable node

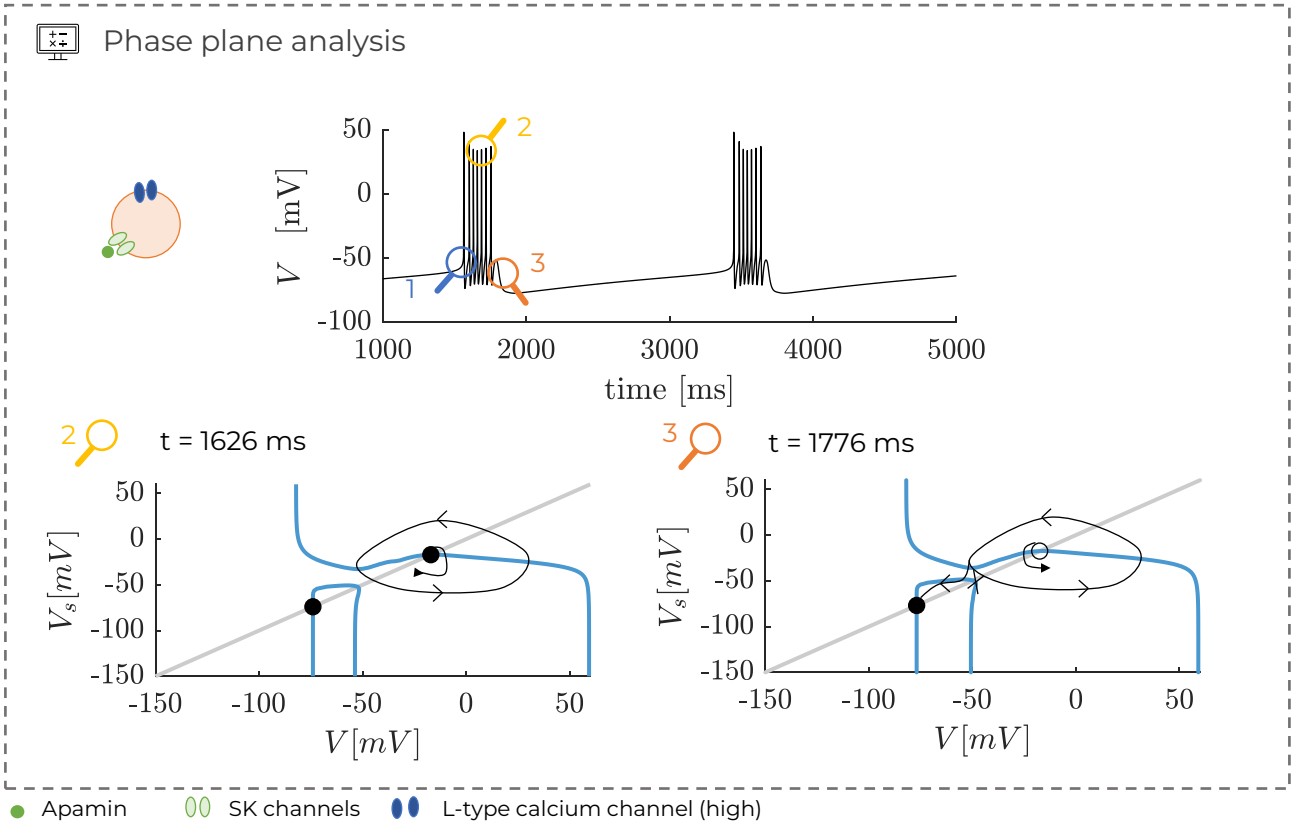

Figure 7.7: **Phase plane analysis** - Phase plane for $\bar{g}_{CaL} = 0.038$ [mS/cm²] and $\bar{g}_{SK} = O$ [mS/cm²] **(top)** Trace of the reduced model **(bottom)** Comparison of the phase portraits at the two events that are highlighted on the magnifying glasses on the top figure. Blue = V-nullcline ; Grey = V_s-nullcline ; Black = representation of the model around the time considered ; Full (resp. empty) dot = stable (resp. unstable) fixed point. Full (resp. empty) dot with an arrow = (resp. unstable) stable spiral. Blue = V-nullcline. Grey = V_s-nullcline.

The limit cycle remains stable so the system remains in its basin of attraction. There is therefore no change in the behaviour of the model, so the system oscillates and the fast spiking remains, i.e. bursting.

3^d event Finally, the last event that is observed is the end of the burst visible in Figure 7.7. As it can be seen, there is a *switch of stability* from the stable spiral that was present in the last event to an unstable spiral. In fact by computing the eigen values of the three fixed points, the following results are obtained, available in Section 7.2.4.

$(\bar{V}, \bar{V}_s)$	(-17.016,-17.016)	(-49.693, -49.693)	(-76.9,-76.9)
λ_1	0.0125 + 0.9004i	-0.1154	-0.0693
λ_2	0.0125 - 0.9004i	0.2415	-0.0509
Stability	Unstable spiral	Saddle node	stable node

Actually, this switch of stability can be explained by the presence of a *subcritical Hopf bifurcation*. The stable spiral is surrounded by a stable limit cycle. This coexistence means that the two attractive

zones are separated by an unstable limit cycle. A Hopf bifurcation is, in such case, the formation or disappearance of a limit cycle with the variations of a parameter, as it is represented in Figure 7.8. In this model, the parameter is the value of $oERG$. The increase in its value leads to the loss of stability of the stable spiral.

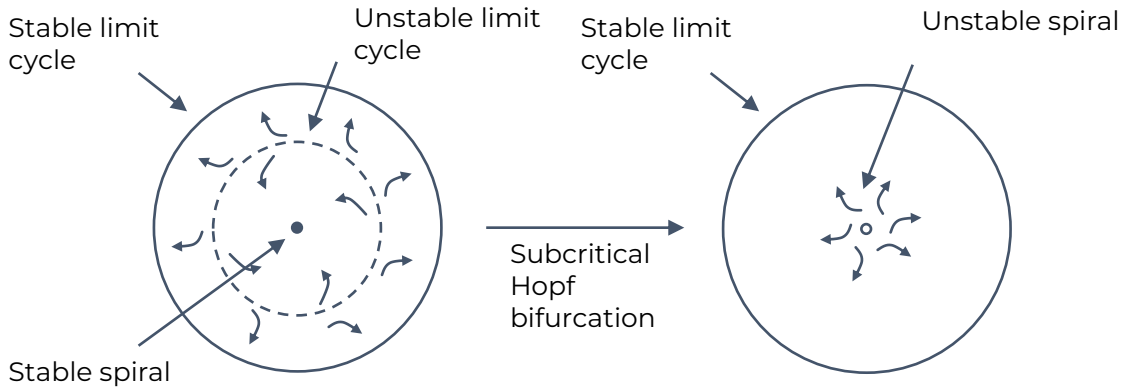

Figure 7.8: **Subcritical Hopf bifurcation** - Illustration of the disappearance of the unstable limit cycle through a subcritical hopf bifurcation. Arrows represent the appearance of the vector field.

The evolution of such limit cycle could also be shown by *a time inverse simulation*. This was however not done in this work. The principle is to effectuate a change in variable and to set t' = -t, which leads to the general form of the differential equations that run the system to become

$$\frac{dx}{dt} = \frac{dx}{dt}\frac{dt'}{dt} = -\frac{dx}{dt} \tag{7.2}$$

In terms of eigen values, this changes their signs which means that any stable limit cycle in a time inverse simulation is an unstable limit cycle in the direct simulation.

In conclusion, this switch of stability in the spiral does not influence the stability of the outer limit cycle which remains stable, it only influences the basin of attraction that are captured in the limit cycle.

7.2.5 Homoclinic bifurcation

There appears to be a bifurcation of the stability of the limit cycle according to the quantity of opened channels $oERG$ and the dynamics of the ultraslow variable. In order to understand the intuition to this, a simulation of the model with two different values of $\bar{g}_{CaL}$ that both lead to bursting are represented in the following Figure 7.9.

As it can be seen on figure Figure 7.9a, $oERG$ oscillates between a minimal value close to 0 and a maximal value which appears to increase as the burst goes on. At a certain point, for a certain value of $oERG$, the burst stops (because of the bifurcation in stability of the limit cycle as it was introduced) and $oERG$ decreases. What is observed is the vanishing of a limit cycle in a homoclinic bifurcation implying the saddle node . The same behaviour is observed on Figure 7.9b but the maximal value of oERG reached is larger. This hints that there is a positive relationship between the value of $\bar{g}_{CaL}$ and

$oERG(t)$.

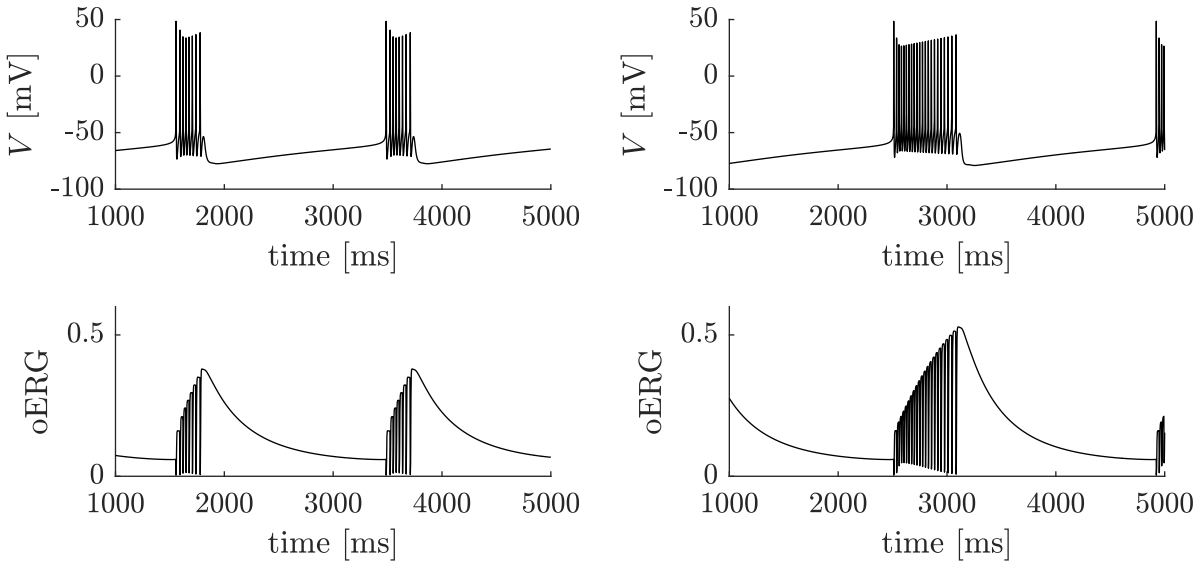

(a) $\bar{g}_{CaL} = 0.038$ [mS/cm²] (b) $\bar{g}_{CaL} = 0.05$ [mS/cm²]

Figure 7.9: **(top)** Time simulation of the reduced model for two different values of $\bar{g}_{CaL}$ leading to bursts of different duration **(bottom)** Corresponding evolution of oERG(t)

To study this relationship, a bifurcation diagram is established. The idea is to simulate the model with a fixed value of g_{CaL} and to study the behaviour of the model according to different values $oERG$ in order to determine the critical value that leads to the end of the burst.

To do so, the variable $oERG$ is turned into a fixed parameter as it is represented on figure 7.10 and its influence on the full system is studied by establishing the amplitude of the oscillations of the trajectory as represented on the middle graph. In fact, if the system oscillates then it means it is captured by the limit cycle and if it doesn't then it has reached the stable fixed point on the left. The initial values are chosen so that the trajectory will always be captured by the limit cycle, if it is stable. In fact, when the system is attracted to the stable limit cycle, it oscillates in the phase plane as represented on the figure on the left of Figure 7.10. Once the limit cycle becomes unstable, it pushes the trajectory towards the other stable variety of the system, i.e. the stable fixed point as visible on the lower right figure of Figure 7.10. In such case, the system doesn't oscillate anymore.

To compute the value of the fixed point when the system doesn't tend towards it, it is found analytically by solving the stable value of the ultraslow nullcline by solving the following equation (which comes from equalling the V_s and V_u nullclines)

$$V_u = \frac{V_s - V}{\tau_s(V)}\tau_u(V) + V \tag{7.3}$$

to obtain V_u as a function of V and V_s. Then by plugging this expression into the expression of $\dot{V}$ and $\dot{V}_s$ and solving $\dot{V}$=$\dot{V}_s$=0, ($\bar{V}$,$\bar{V}_s$) are found.

It can be observed that there exists, as expected, a value of $oERG$ which leads to the end of the oscillations. This value is marked as *critical oERG* on the figure. This value correlates with the peak

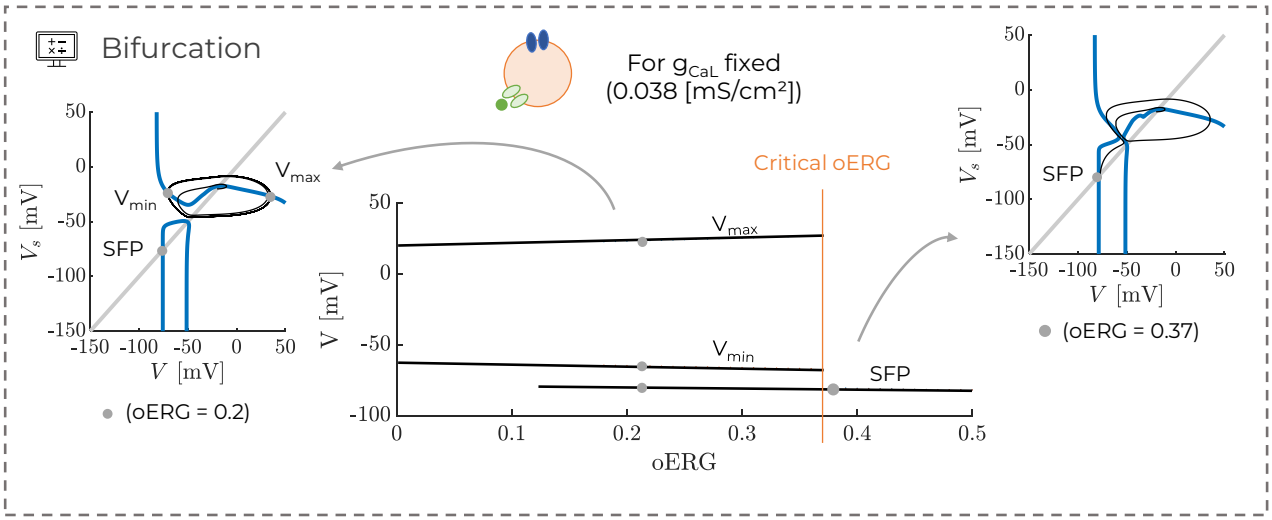

Figure 7.10: **Homoclinic bifurcation - (center)** Bifurcation diagram of the stability of (intially) stable limit cycle according to the bifurcation parameter $oERG$ **(left)** trajectory of the system for $oERG = 0.2$ on the phase plane leading equilibrium to a stable limit cycle (right) trajectory of the system on the phase plane for $oERG = 0.37$ leading to equilibrium at stable fixed point.

leading to the end of the burst that was observed in Figure 7.9a.

Now that the bifurcation diagram has been established for a single value of $\bar{g}_{CaL}$, the study is extended to multiple values of g_{CaL}, as represented below. In fact, it can be shown that the critical value of $oERG$ depends on the value of $\bar{g}_{CaL}$. To find such, the bifurcation diagram for multiple values of $\bar{g}_{CaL}$ is computed ($\bar{g}_{CaL} \in [0.01 - 0.05]$ [mS/cm²]). Figure 7.10 then summarises the critical values of $oERG$ that were found for each $\bar{g}_{CaL}$ that was computed.

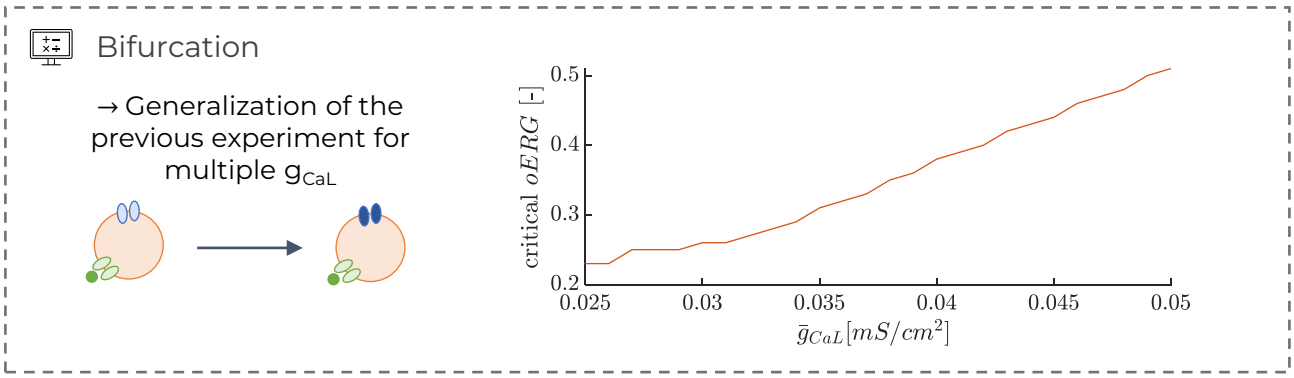

Figure 7.11: **Critical value** - Reproduction of the bifurcation diagram of the homoclinic bifurcation (see Figure 7.10) for multiple values of $\bar{g}_{CaL}$

As it can be concluded, the larger the value of $\bar{g}_{CaL}$, the more accumulation of $oERG$ is required in order to induce the end of the burst. Such end is induced by a homoclinic bifurcation which includes the fusion of the stable manifold of the saddle node that separates the stable fixed point from the limit cycle. This leads to longer bursts when $\bar{g}_{CaL}$ is larger.

7.3 Experiment 3 - L-type calcium channel blockade re-regularises dopaminergic neuron firing

In Figure 7.12, the experiment of cell-to-cell variability that was performed is extended. In fact, thanks to the second experiment, it was highlighted that SK channel blockade uncovers variability that is hidden otherwise. In this new experiment, which is represented in Figure 7.12, the aim is to show that such variability finds its essence in the L-type calcium channels.

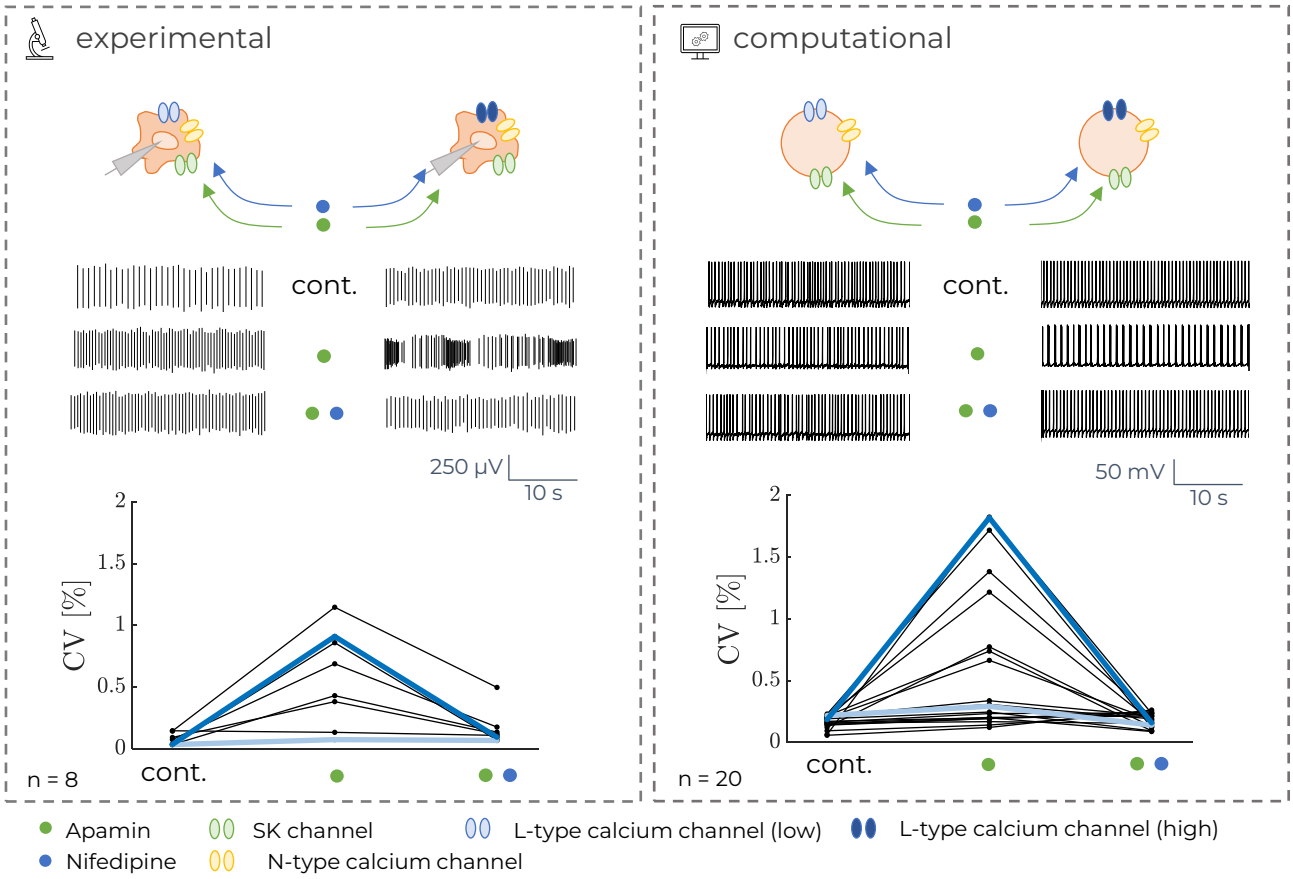

Figure 7.12: **L-type calcium channel blockade regularises dopaminergic neuron firing - (left)** Experimental results from [de Vrind et al., 2016] and [Shepard and Stump, 1999] (published and unpublished). L-type calcium channel blockade (blue dot) regularised firing pattern of DA neurons **(right)** Reproduction of the experimental results with the dopaminergic model. Light blue indicates low value of $\bar{g}_{CaL}$ and dark blue indicates higher values of $\bar{g}_{CaL}$

7.3.1 Experiment

On the left of Figure 7.12 shows, at the top, the spike times of two different neurons.

- The left neuron (light blue) shows regular pacemaking in the three conditions, i.e. control, after SK channel blockade by apamin and after SK channel blockade and L-type calcium channel blockade by nifedipine.
- The right neuron (dark blue) shows regular pacemaking in the control conditions and after

simultaneously blocking SK channels and L-type calcium channels. However, the pacemaking is lost when only SK channels are blocked.

Underneath, the results of 8 neurons are summarised by computing the coefficient of variation. As it can be seen when both L-type calcium and SK channels are blocked, the homogeneous pacemaking is recovered homogeneously.

This result indicates that the variability in the spiking pattern that is uncovered by SK channel blockade finds its source in the heterogeneity of L-type calcium channels. In fact, by homogenising L-type calcium channels thanks to their blockade, the heterogeneity of the firing is lost.

7.3.2 Computational reproduction

On the right of Figure 7.12, the experimental results are reproduced using the model as in Figure 7.2. However, here an additional L-type calcium channel blockade is induced by setting $\bar{g}_{CaL} = 0$. As it can be seen, the pacemaking is either kept (for the neuron which had initially a low value of $\bar{g}_{CaL}$, on the left) or recovered (for the neurons which has initially a high value of $\bar{g}_{CaL}$)

7.3.3 Dynamical analysis

When the L-type calcium channels are blocked, V-nullcline becomes distorted into a *hourglass shape*. This traps the trajectory to the stable fixed point on the right. It can be seen that the phase plane, in such case, resembles its shape when SK channels are activated, as it is visible on Figure 7.1.

1^{st} **event** The initiation of the spike is generated by the loss of the hourglass shape of the V-nullcline. This leads to the phase plane that is represented on Figure 7.13 on the lower left, where there is only one fixed point at ($\bar{V}$,$\bar{V}_s$) = (-17.0358, -17.0358). The eigen values of the jacobian evaluated around such fixed point are

$$\lambda_1 = -0.0044 + 0.9136i \qquad \lambda_2 = -0.0044 - 0.9136i \tag{7.4}$$

The trajectory is actually attracted to the limit cycle which is a stable spiral surrounded by the unstable and stable limit cycles, as it was proven in previous sections (Figure 7.4) and generates the oscillation around the fixed point.

2^{nd} **event** The second event is the end of the spike which is characterised by the reappearance of the hourglass shape which leads to three fixed points. The eigen values and resulting stability of such points are summarised in the following table.

$(\bar{V}, \bar{V}_s)$	(-17.121,-17.121)	(-56.104, -56.104)	(-67.215,-67.215)
λ_1	0.0033 + 0.9099i	0.0576	-0.0222
λ_2	0.0033 - 0.9099i	-0.0576	-0.0516
Stability	Stable spiral	Saddle node	stable node

The shape of the nullclines doesn't allow the bistability that was possible thanks to the lower branch shape that characterises bursting. In fact, the stability of the burst lies on this separation between the upper limit cycle and the stability of the fixed point. [Drion et al., 2012]

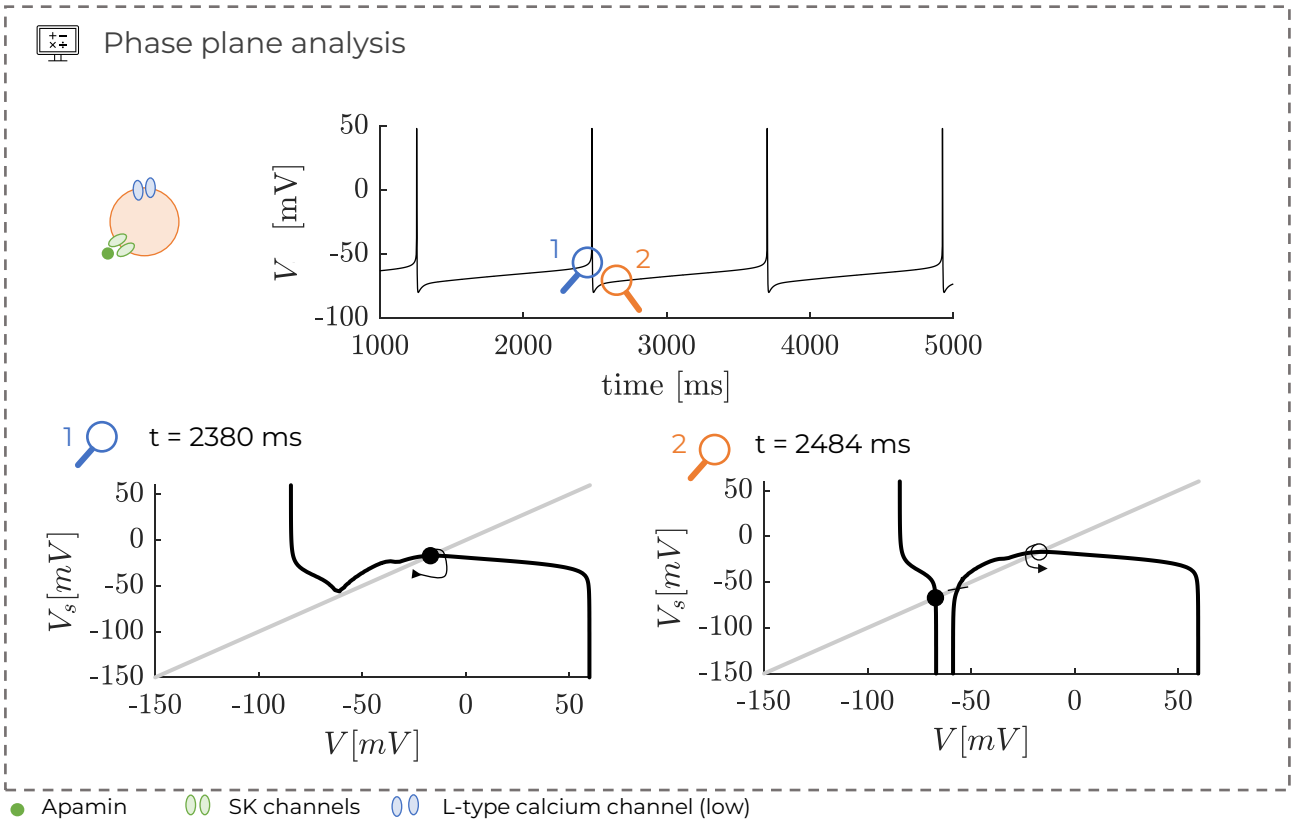

Figure 7.13: **Phase plane analysis** - Phase plane for $\bar{g}_{CaL} = 0$ [mS/cm²] **(top)** Trace of the reduced model **(bottom)** Comparison of the phase portraits at the two events that are highlighted on the magnifying glasses on the top figure. Full (resp. empty) dot = stable (resp. unstable) fixed point. Full (resp. empty) dot with an arrow = (resp. unstable) stable spiral. Blue = V-nullcline. Grey = V_s-nullcline.

7.4 Experiment 4 - No other type of calcium channel brings back pacemaking

7.4.1 Experiment

The aim of this experiment is to show that it is, in fact, the interplay with L-type calcium channels which is important, and no other types of calcium channels. To do so, in [de Vrind et al., 2016], they experimentally tested the main calcium channels and induced their blockade to observe the effect on the pacemaking. The results are summarised on the left of Figure 7.14. Each graph represents a calcium channel blockade

- in orange is T-type calcium channel blockade by TTA.
- in pink is P-type calcium channel blockade ω-agatoxin.
- in yellow is N-type calcium channel blockade by ω-conotoxin.
- in grey is R-type calcium channel blockade induced by SNX.

The overall conclusion from the experiment is that it is indeed only L-type calcium channels, which interplay with SK channels, are able to bring back pacemaking through their blockade since none of the other calcium channels were able to reproduce such result.

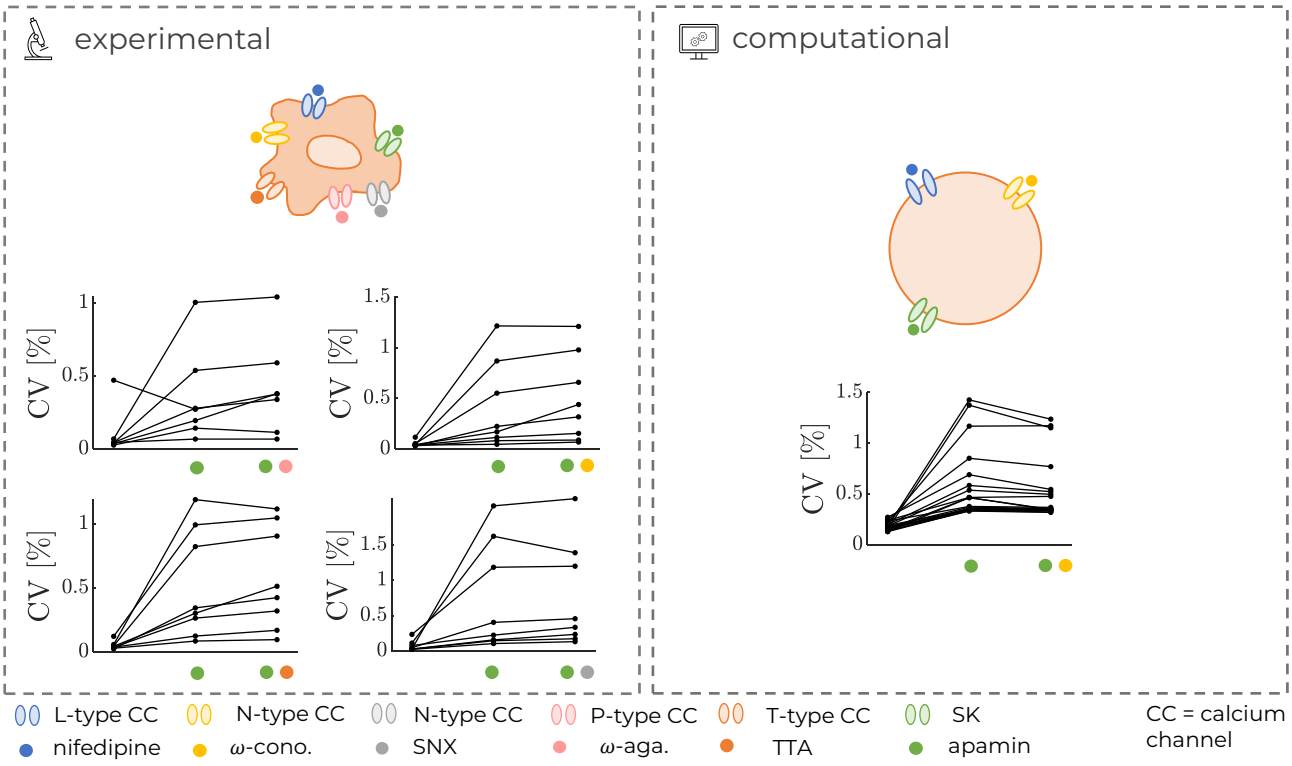

Figure 7.14: **No other type of calcium channel brings back pacemaking - (left)** Experimental results from [de Vrind et al., 2016] (unpublished). Different calcium channels blockers are tested to show that only L-type calcium channel blockade brings back pacemaking **(right)** Reproduction of experimental results from (left). N-type calcium blockade does not bring back pacemaking in the model

7.4.2 Computational reproduction

This observation was then reproduced using the model, as visible in Figure 7.14. Since it was assumed when establishing the model that SK channels are solely activated by N-type calcium channels, the only calcium currents that are included in the model are I_{CaL} and I_{CaN}. No other calcium channels are modeled so their blockade cannot be tested.

Subsequently, only N-type calcium channel blockade is tested ($\bar{g}_{CaN} = 0$) to reproduce the experiments. 8 neurons are modeled with $\bar{g}_{CaL} = [0.02 - 0.038]$ [mS/cm²]. SK channel blockade is then induced ($\bar{g}_{SK} = 0$) firstly alone (green dot) and then simultaneously with N-type calcium channel blockade (yellow dot). As it can be observed, it does not bring back pacemaking, as wanted.

7.5 Experiment 5 - Dynamics of activation

As a reminder, in conductance-based models, the dynamics of the channel activation are described with a differential equation. In the case of type-L calcium channels, the activation of the gating variable $m_{CaL}(V)$ is written as

$$\dot{m}_{CaL}(V) = \frac{m_{CaL}(V) - m_{\infty,CaL}(V)}{\tau_{m_{CaL}}(V)} \tag{7.5}$$

where V is the membrane potential, $m_{\infty,CaL}$ is the steady state value of m_{CaL} and $\tau_{m_{CaL}}$ is a voltage dependant time constant. Such equations can be interpreted as "*The variable $m_{CaL}(V)$ converges towards the steady state value $m_{\infty,CaL}(V)$ with a time constant of $\tau_{CaL}(V)$*".

The dynamics of activation of the type-L calcium channels are defined as slow [Lipscombe et al., 2004].

7.5.1 Experiment

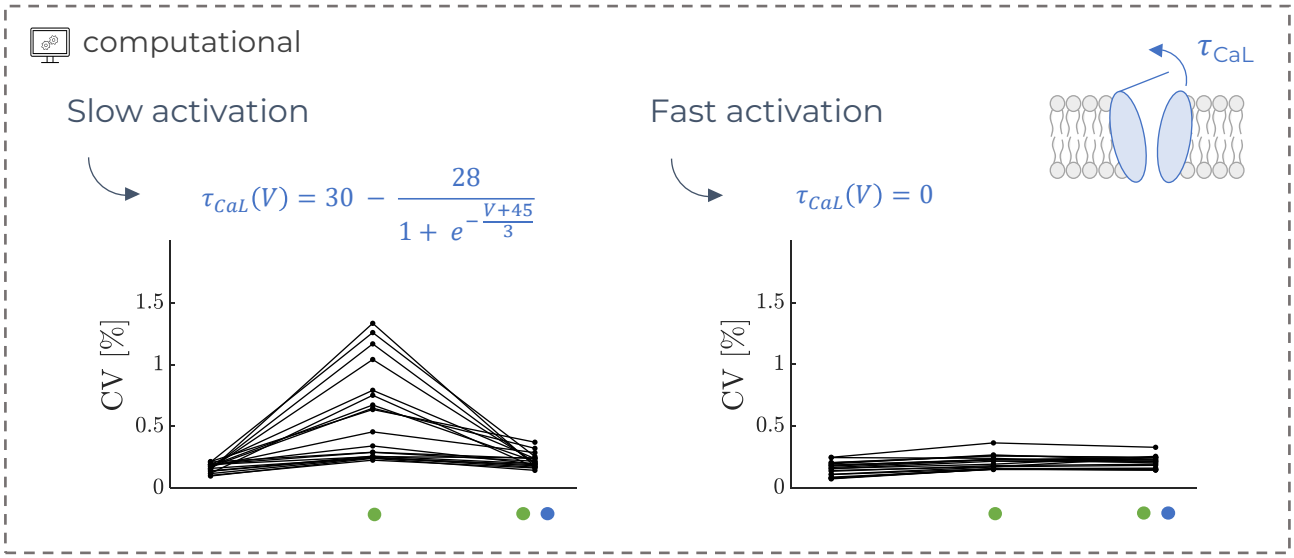

Figure 7.15: **Importance of the dynamics of type-L calcium channels** - Simulation of 20 neurons with $\bar{g}_{CaL} \in [0.02 - 0.038]$ and $\bar{g}_{CaN} \in [0.0015 - 0.002]$ [mS/cm²] with green dot $\bar{g}_{SK} = 0$ and blue dot $\bar{g}_{CaL} = 0$ **(left)** Slow dynamics. Results from previous figure provided as comparison **(right)** Fast dynamics

To show that the timescale of the dynamics is needed, in Figure 7.15, the dynamics were altered to have a fast activation instead. To simulate the instantaneous activation of L-type calcium channels, in the model, equation (7.5) was replaced by

$$m_{CaL}(V) = m_{\infty,CaL}(V) \tag{7.6}$$

which implies that $m_{CaL}(V)$ is always equal to its steady state value, meaning that the activation is instantaneous, i.e. much faster than the original dynamics.

In order obtain the Figure 7.15, the experiment that was performed in Figure 7.12 was extended. The model was first ran over 20 neurons with slow dynamics described by equation (7.5) in three cases, as visible in Figure 7.12.

- The *control* case where no channel blockade is induced.
- The $\bar{g}_{SK} = 0$ case where SK channel blockade is induced to highlight the hidden heterogeneity as it was already shown in previous experiments.
- The case $\bar{g}_{SK} = \bar{g}_{CaL} = 0$ where type-L channels are blocked to show that they are, in fact, the source of the heterogeneity visible in the previous case.

In Figure 7.15, the same experiment is performed but the dynamics of type-L calcium channels are described as instantaneous, i.e. equation (7.6). In such case, the heterogeneity of type-L calcium channels is not uncovered by SK channel blockade anymore.

7.5.2 Dynamical analysis

In order to understand how the dynamics shape the model, the reduced model is altered to reproduce a fast activation. To do so, the weights w_{fs}^{CaL} and w_{su}^{CaL} are changed and set to $w_{fs}^{CaL} = 1$ and $w_{su}^{CaL} = 1$ which leads to an instantaneous activation in the fast regime and no contribution in the slow and ultraslow timescale.

In figure 7.16 is an animation of the membrane potential simulated with $\bar{g}_{CaL} = 0.038$ [mS/cm^2] which would normally lead to bursting, as it was shown in Figure 7.2, when the activation of the type-L calcium channels is slow.

Figure 7.16: **Animation** - Video (*video_PP_CaLinst.mp4*) of the firing pattern observed for $\bar{g}_{CaL} = 0.038$ [mS/cm^2] and $\bar{g}_{SK} = 0$ and instantaneous type-L calcium activation **(top)** Time trace simulation of the model **(bottom)** Corresponding evolution of the phase plane

Here it can be observed that the neuron is in pacemaking instead because of the instantaneous activation. Two main events are observed

- 1^{st} event : Initiation of a spike
- 2^{nd} event : End of a spike

Both of the events phase planes are plotted and analysed in Figure 7.17.

1^{st} **event** The figure on the lower left of Figure 7.17 represents the first main event, which is right before a burst. As it can be seen, the shape and stability is typically the same as previously so it isn't developed.

2^{nd} **event** When the activation is instantaneous, the phase plane recovers the hourglass shape that was observed in the first experiment when SK channels are activated (see Figure 7.1). The shape and stability is the same analysis and conclusions as in figure 7.13.

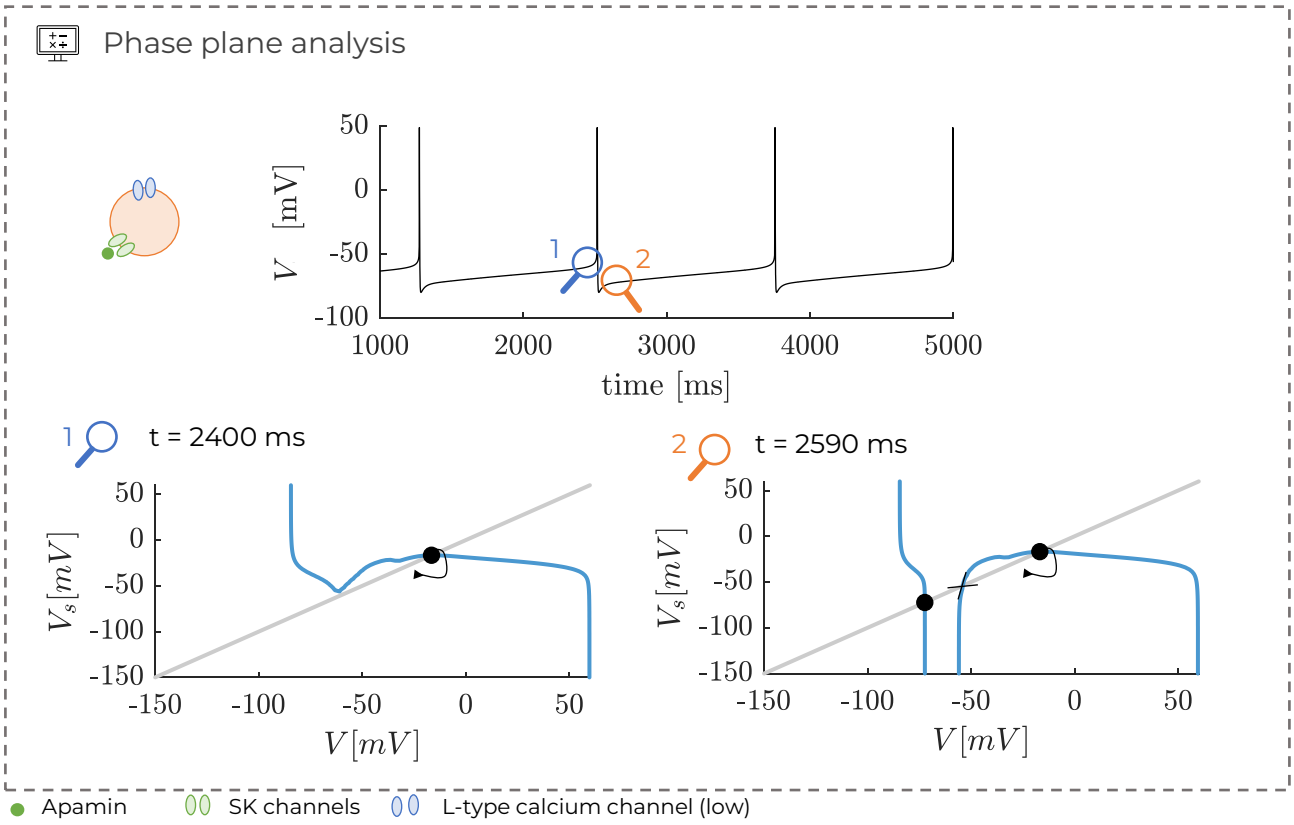

Figure 7.17: **Phase plane analysis** - Phase plane for $\bar{g}_{CaL} = 0.038$ [mS/cm²], $\bar{g}_{SK} = 0$ [mS/cm²] and instantaneous calcium activation **(top)** Trace of the reduced model **(bottom)** Comparison of the phase portraits at the two events that are highlighted on the magnifying glasses on the top figure. Full (resp. empty) dot = stable (resp. unstable) fixed point. Full (resp. empty) dot with an arrow = (resp. unstable) stable spiral. Blue = V-nullcline. Grey = V_s-nullcline.

Similar results were obtained by [Jacquerie and Drion, 2021] in thalamocortical neurons. They showed that speeding up the activation of the T-type calcium activation disrupts the ability to change the phase portrait as a response to a hyperpolarizing current.

7.6 Summary

In the following figure, Figure 7.18, is available a summary of the experiments that were performed in this chapter with the main results that are observed in terms of dynamical analysis. The different shapes of the phase plane at the end of a spike or burst are highlighted.

It can be concluded that, under SK channel blockade, the heterogeneity of the firing pattern that is observed in vitro (Figure 7.2) can be reciprocated with heterogeneous calcium channel densities (Figure 7.12) and slow dynamics of L-type calcium channels (Figure 7.15). Dynamically, SK channel blockade uncovers a separation of the V-nullcline into an upper branch and a lower branch which allows a switch to an irregular bursting pattern ; this switch is not possible otherwise because the V-nullcline has an hourglass shape (Figure 7.1). The intensity of the bursting is then mediated by the quantity of $oERG$ that needs to be accumulated to end the burst (Figure 7.11).

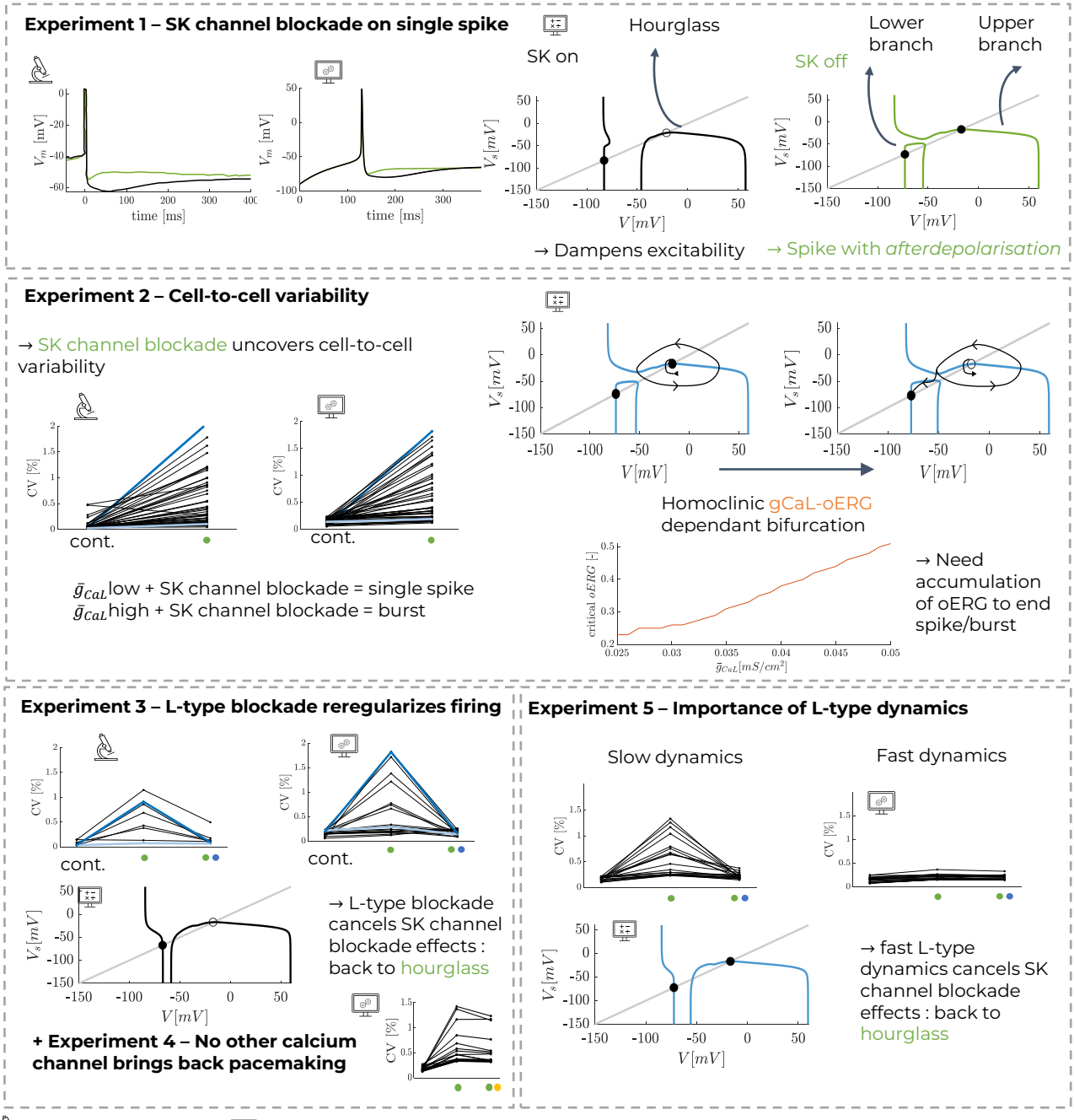

Figure 7.18: **Summary of chapter 7**

Part III

NMDA

Chapter 8

NMDA hypothesis

The idea is now to study the possible effects of NMDA on the firing of dopaminergic neurons. In fact, it was shown in [Schultz, 1997] that administration of NMDAr antagonists (which therefore block the effect of glutamate on dopaminergic neuron) decreases phasic firing without altering tonic firing. It can be concluded from this observation that the excitatory input of glutamate plays a significant role on the regulation of type of firing in dopaminergic activity [Wang et al., 2011].

The aim of this chapter is to study the effects of NMDA to the mathematical model that is studied in this work by firstly observe its impact in vitro and then by studying it on the different experiments that were reproduced in the previous chapter. Additionally, using the model, an hypothesis to introduce the concept of *quantification* of the reward will be introduced and case studies using the hypothesis will be developed.

8.1 NMDA in vitro

As it has been shown by [Johnson et al., 1992], under SK channel blockade, NMDA potentiates bursting. As a preliminary result, one must make sure that the model is able to reciprocate such behaviour.

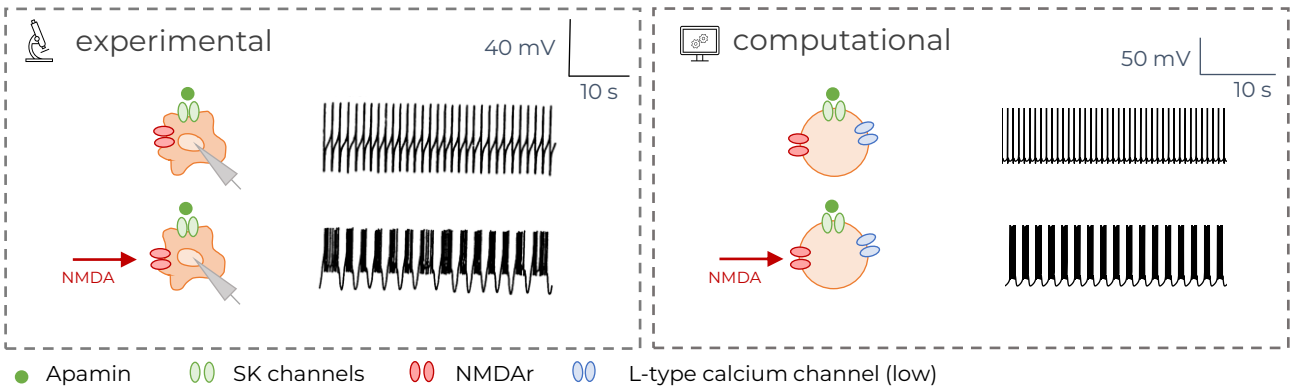

Figure 8.1: **NMDA potentiates DA bursting after SK blockade - (left)** Results from [Johnson et al., 1992] show pacemaking after SK channel blockade (green) with apamin 100 mM and switch to bursting under NMDA input and hyperpolarising current - **(right)** Reproduction of experimental results from (left) using the model. Apamin is mimicked by setting $\bar{g}_{SK} = 0$. Simulations with $\bar{g}_{CaL} = 0.026\,[mS/cm^2]$. Green = SK channels ; green dot = apamin ; Red = NMDAr

8.1.1 Experiment

In Figure 8.1, on the left is represented the experimental results that [Johnson et al., 1992] obtained in their experiment. They measured the membrane potential of a DA neuron in a solution of apamin 100 mM, leading to SK channel blockade, in two conditions : with and without NMDA (10 to 30 µM). A switch from pacemaking to bursting is observed. In the measurements, they applied an hyperpolarising current to prevent the DA neuron from being overly stimulated and enter the state of *depolarisation block* where it stops firing altogether.

8.1.2 Computational

On the right of Figure 8.1, one can see that the model is able reproduce such results. To replicate SK channel blockade, the maximal conductance $\bar{g}_{SK}$ is set to 0. The model is then tuned to reproduce a case where there is no switch to bursting in such conditions, i.e. by setting $\bar{g}_{CaL}$ low enough as it was shown in Figure 7.12. As it can be observed, the switch from pacemaking to bursting is reproducible in similar conditions. The conductance of NMDA is set to $\bar{g}_{NMDA} = 0.015\,[mS/cm^2]$ and a hyperpolarising current $I_{app} = -0.45$ [nA/cm²] is applied.

8.1.3 Dynamical analysis

In Figure 8.2 is an animation of the membrane potential simulated with $\bar{g}_{CaL} = 0.026$ [mS/cm²], $\bar{g}_{NMDA} = 0.15$ [mS/cm²] and a hyperpolarising current $I_{app} = -0.45$ [nA/cm²].

Figure 8.2: **Animation** - Video (*video_PP_burstNMDA.mp4*) of the firing pattern observed for $\bar{g}_{CaL} = 0.026$ [mS/cm²], $\bar{g}_{SK} = 0$, $\bar{g}_{NMDA} = 0.15$ [mS/cm²] and a hyperpolarising current $I_{app} = -0.45$ [nA/cm²] **(top)** Time trace simulation of the model **(bottom)** Corresponding evolution of the phase plane

As it can be seen in Figure 8.2, the bursting presents three events, as in the typical spontaneous bursting presented in the previous chapter. It can be concluded from the analysis that is performed in Figure 8.3 that the dynamics aren't much different from the typical bursting that is observed without NMDA. It is therefore not analysed in depth but the three main events visible in the video which are highlighted by the three magnifying glasses on Figure 8.3 are

- 1^{st} **event** is the initiation of the spike from the disappearance of the lower branch of the V-nullcline which attracts the trajectory towards the stable limit cycle.

- 2^{nd} **event** is the bursting that remains because not enough $oERG$ has been accumulated so the trajectory remains in the stable limit cycle that surrounds the upper fixed point.

- The 3^{d} **event** is the end of the burst through a homoclinic bifurcation because enough $oERG$ were accumulated. Here it can be noted that there is no switch in the stability of the spiral which means there is no subcritical Hopf bifurcation, in contrary to Figure 7.7. However, as it was already mentioned this bifurcation does not alter the stability of the outer stable limit cycle so the mechanism is still sensibly the same because the solutions never approaches the unstable limit cycle.

The consequence of NMDA is to have antagonist effects to $oERG$. In fact, increasing values of $oERG$ tend to bring together the two branches of the V-nullcline, leading to the homoclinic bifurcation that was developed in previous sections. On the other hand, the activation of NMDA moves the V-nullcline up the phase plane which moves apart the two branches. This allows to generate bursting for values of $\bar{g}_{CaL}$ that induced tonic firing otherwise and increase the bursting intensity.

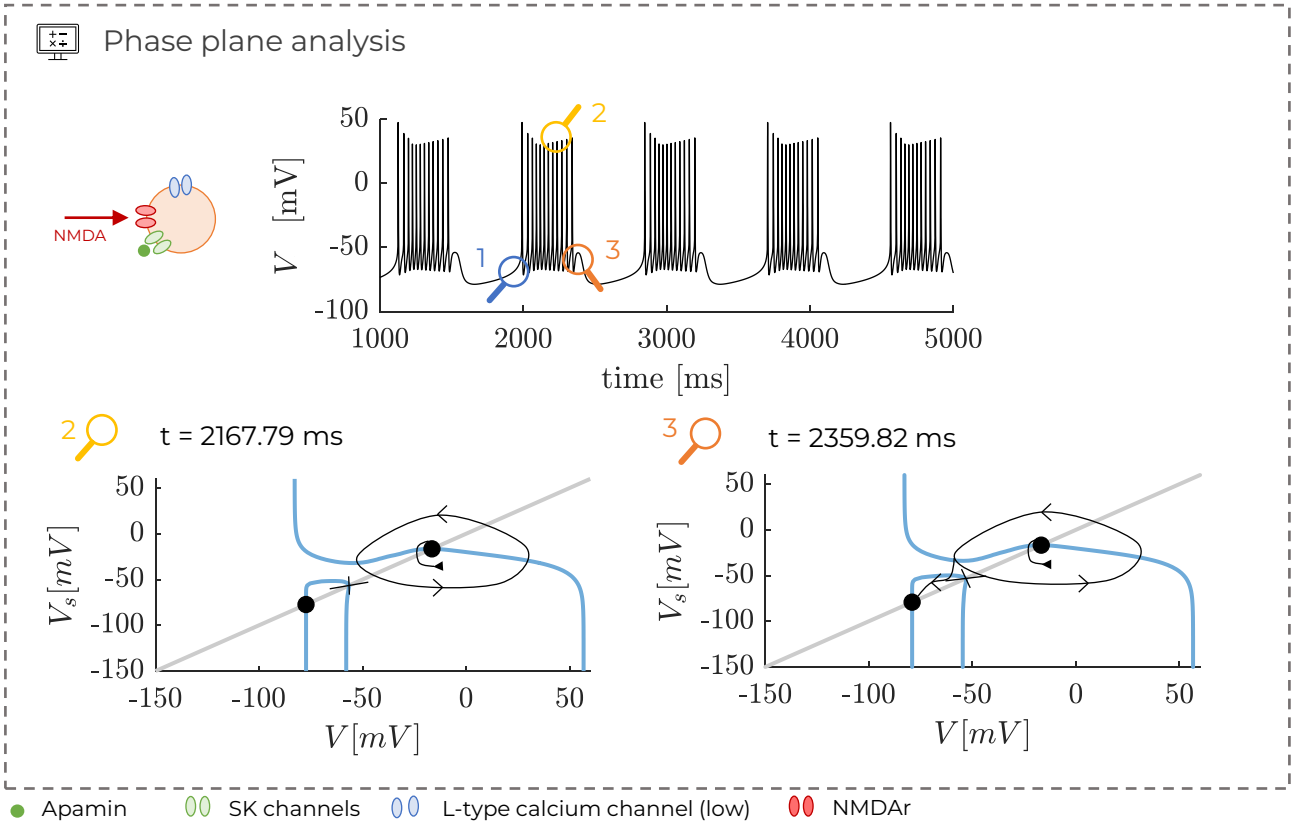

Figure 8.3: **Phase plane analysis** - Phase plane for $\bar{g}_{CaL} = 0.026$ [mS/cm^2], $\bar{g}_{SK} = 0$ [mS/cm^2], $\bar{g}_{NMDA} = 0.15$ [mS/cm^2] and $I_{app} = -0.45$ [nA/cm^2] **(top)** Trace of the reduced model **(bottom)** Comparison of the phase portraits at the two events that are highlighted on the magnifying glasses on the top figure.

8.2 Effect of NMDA on the results of previous experiments

In this section, the aim is to understand the effect of NMDA which has been shown to drive the changes in the firing pattern of dopaminergic neurons. To do so, the experiments that were performed in the previous chapter to validate the model are now reproduced with an NMDA input to observe the changes.

8.2.1 NMDA potentiates burstiness after SK channel blockade

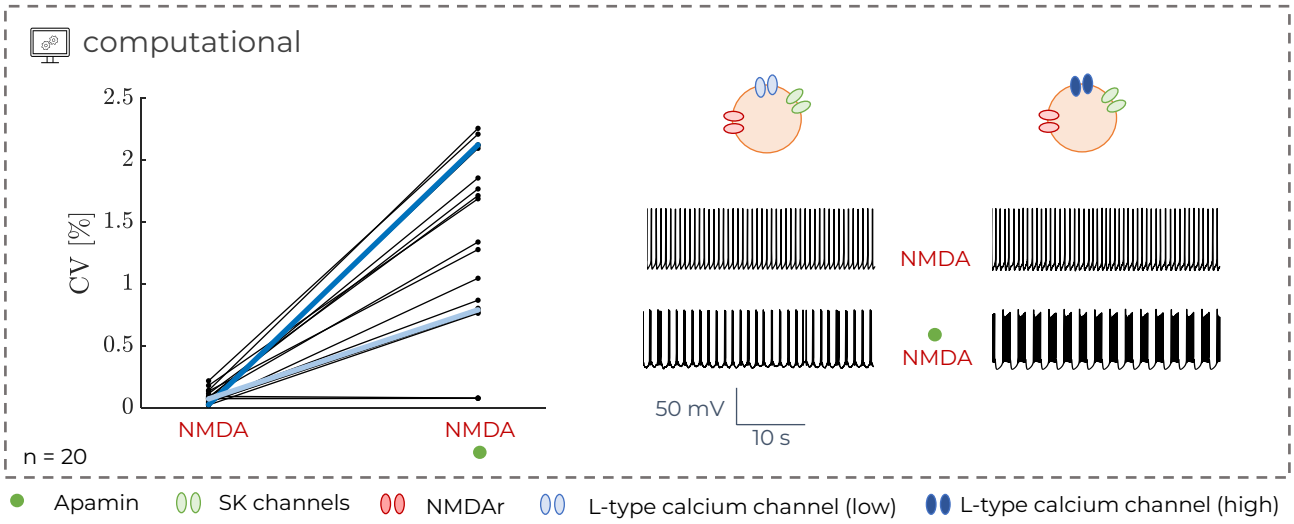

Figure 8.4: **Effect of NMDA after SK channel blockade** - Simulation of the model for 20 neurons with $\bar{g}CaL \in [0.02 - 0.038]$ [mS/cm²] under NMDA stimulation, i.e. $\bar{g}_{NMDA} = 0.15$ [mS/cm²] and $I_{app} = -0.45$ [nA/cm²] **(left)** Summary of the regularity of firing pattern without SK channel blockade and with SK channel blockade **(right)** Focus on the temporal traces of the membrane potential for a low value of $\bar{g}_{CaL} = 0.02064$ [mS/cm²] (light blue) and for a higher value of $\bar{g}_{CaL} = 0.03189$ [mS/cm²] (dark blue)

As it was shown in Figure 8.1, NMDA input on the DA neuron after SK channel blockade potentiates its burstiness. The cell-to-cell variability that is observed in vivo can be reproduced thanks to small variations in the value of $\bar{g}_{CaL}$, variations of physiological relevance as it was shown in Figure 7.12.

In Figure 8.4, the same protocol that was developed for Figure 7.12 is applied. However, this time, there is an additional input of NMDA as well as a hyperpolarising current with values are the same as the one used to create Figure 8.1.

On the left of Figure 8.4, the firing pattern coefficient of variation is computed for the 20 neurons that are simulated.

- With SK channels activated, the dopaminergic neuron CV is low for all neurons, indicating that SK channels homogenise the firing pattern despite heterogeneous properties (as it was concluded in Figure 7.12). This conclusion isn't altered for the intensity of the excitatory input that is chosen for this experiment.

- When SK channels are blocked (green dot), the CV among the different neurons becomes heterogeneous. However, here, the mean CV appears to be higher than when no NMDA is applied (approximately 1.25 as opposed to 0.75, see Figure 7.12). Additionally, less neurons remain in pacemaking.

As it can be concluded, NMDA potentiates burstiness after SK channel blockade and the intensity of such bursts depends on the value of $\bar{g}_{CaL}$.

8.2.2 Homoclinic bifurcation

As it was presented in the previous chapter, the end of the burst is mediated by a critical value of $oERG$ that is reached by the system. This value is $\bar{g}_{CaL}$-dependant. The aim now is to observe the effect of NMDA on the bifurcation diagram Figure 7.11.

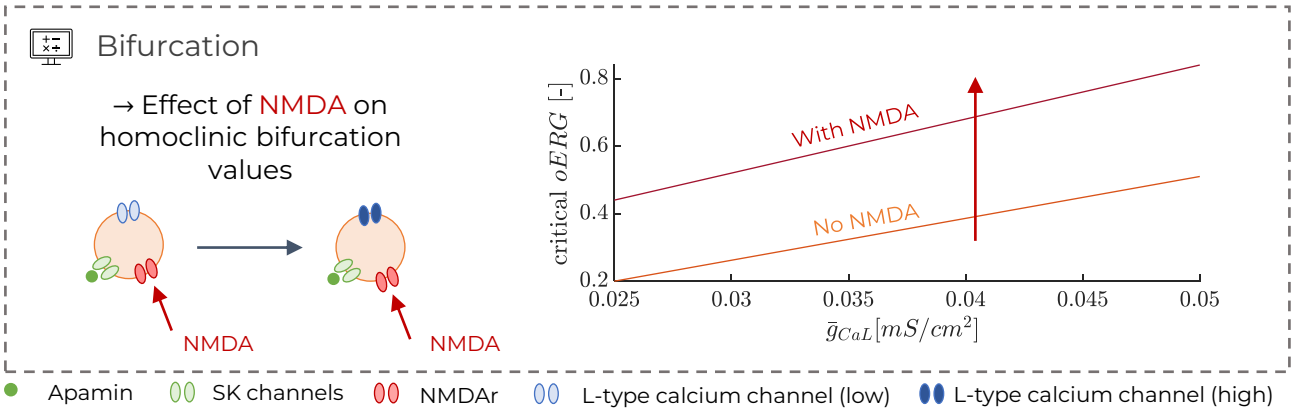

Figure 8.5: **Effect of NMDA on critical value** - Reproduction of the generalisation of figure 7.11 with an additional input of $g_{NMDA} = 0.15$ [mS/cm²] and $I_{app} = -0.45$ [nA/cm²]. Orange curve = result from Figure 7.11. Red curve = with NMDA + I_{app} input

In order to obtain Figure 8.5, the same experiment that was performed to obtain **??** and Figure 7.11 is done except this time, an additional NMDA input is added. To do so, $g_{NMDA} = 0.15$ [mS/cm²] and $I_{app} = -0.45$ [nA/cm²].

One would expect to observe a shift from the curve caused by NMDA. In fact, since it is observed to potentiate burstiness, it means that, for the same value of $\bar{g}_{CaL}$, the critical value of $oERG$ must be higher. In fact, the higher the critical value, the longer the bursting. It is the result that is obtained when computing Figure 8.5. The resulting curve is smoother than in Figure 7.11 because since the aim was to observe qualitative effect on the curve, less values of $\bar{g}_{CaL}$ were computed. For comparison purposes, the curve from Figure 7.11 (orange curve) was also smoothed down.

8.2.3 Slight variability in L-type calcium channel density affects neuron response to NMDA

In Figure 8.6 is performed a computational experiment to understand how the physiological variations shape the response to different intensities of NMDA inputs. To do so, the model was ran several times in different conditions

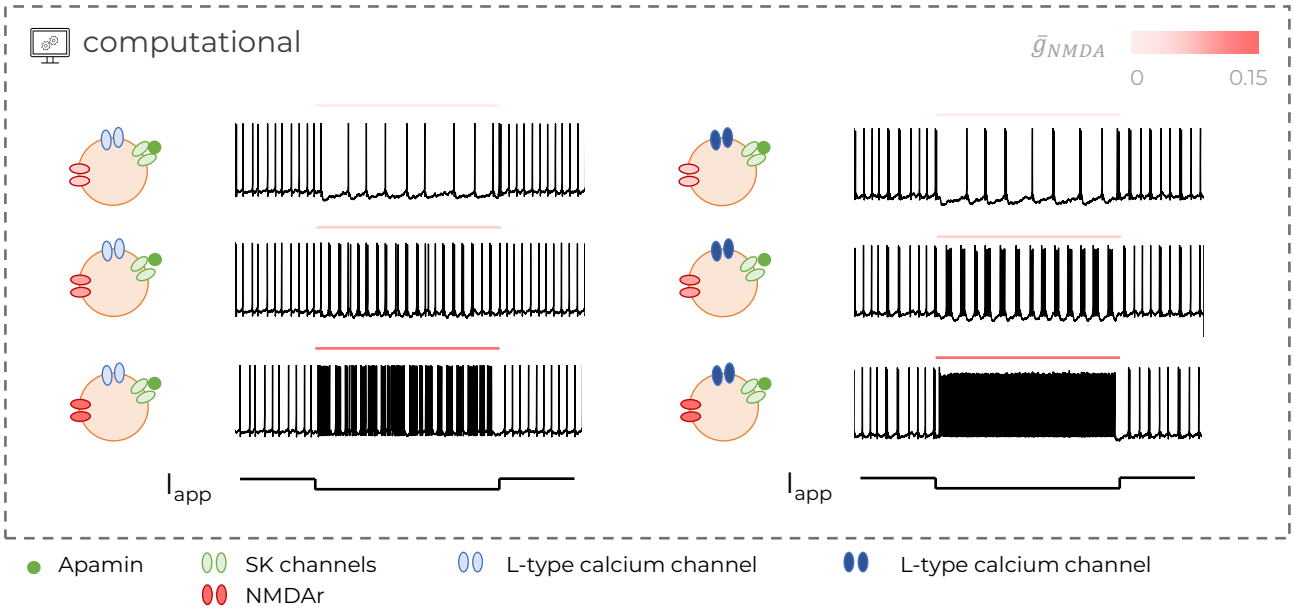

Figure 8.6: **Response to slight variability in L-type calcium channel density** - Simulations of the model for different intensities of NMDA input (top, middle and bottom) for two close but different calcium channel densities (left and right) after SK channel blockade ($\bar{g}_{SK} = 0$ [mS/cm²]) with hyperpolarising current $I_{app} = -0.45$ [nA/cm²]. **(top)** $\bar{g}_{NMDA} = 0.05$ [mS/cm²] **(middle)** $\bar{g}_{NMDA} = 0.1$ [mS/cm²] **(bottom)** $\bar{g}_{NMDA} = 0.15$ [mS/cm²] **(left)** $\bar{g}_{CaL} = 0.024$ [mS/cm²] **(right)** $\bar{g}_{CaL} = 0.03$

- On the left of the figure, the model was ran with $\bar{g}_{CaL} = 0.024\,[mS/cm^2]$ after SK channel blockade. Initially, the neuron fires freely in such conditions. Then, a hyperpolarising current of $I_{app} = 0.45$ [nA/cm²] is applied and an NMDA input is applied. Three intensities of NMDA input are applied, i.e. $\bar{g}_{NMDA} = 0.05\,[mS/cm^2]$, $\bar{g}_{NMDA} = 0.1\,[mS/cm^2]$ and $\bar{g}_{NMDA} = 0.15\,[mS/cm^2]$. Then the hyperpolarising current is removed as well as the NMDA and the neuron fires back to normal.
- On the right of the figure, the model was ran with $\bar{g}_{CaL} = 0.03\,[mS/cm^2]$ under the same conditions as on the left. .

As it can be observed, the intensity of the bursts increases with the intensity of the NMDA inputs. Additionally, a slight variability in the value of $\bar{g}_{CaL}$ induces non-negligible differences in the intensity of the bursts.

8.2.4 L-type calcium channel blockade disrupts NMDA-induced bursting

Now the aim is to see whether the L-type calcium channel blockade still regularises pacemaking.

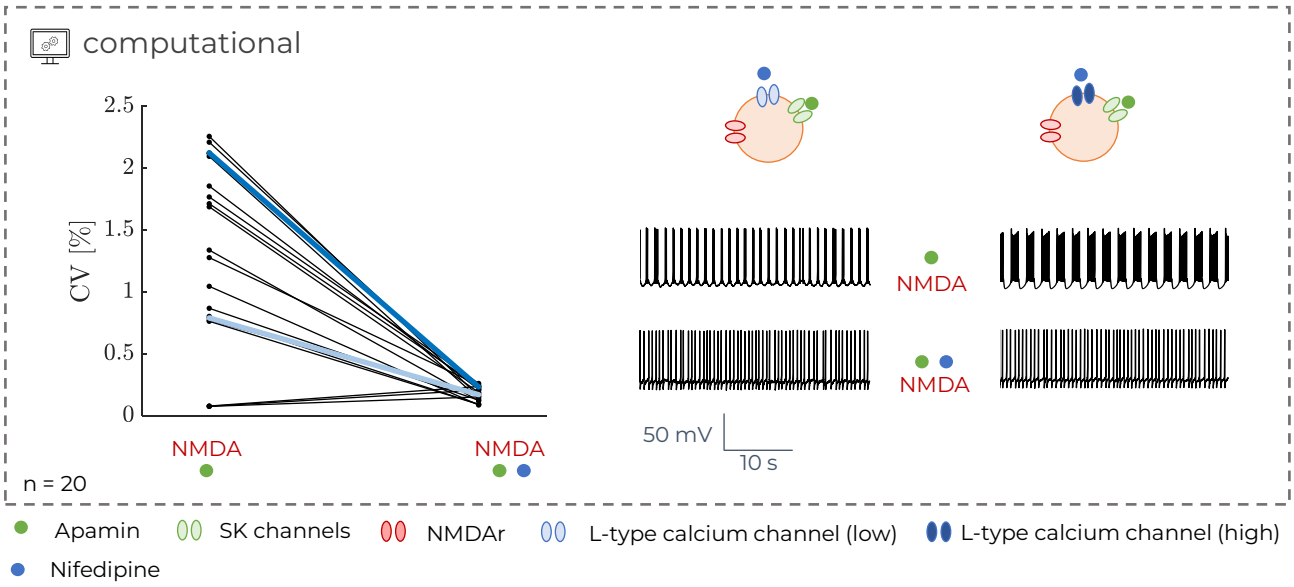

Figure 8.7: **L-type calcium channel blockade with NMDA** Simulations of 20 neurons with $\bar{g}_{CaL} \in [0.02-0.038]$ [mS/cm²] with NMDA input of $\bar{g}_{NMDA} = 0.15$ [mS/cm²] and $I_{app} = -0.45$ [nA/cm²] and SK channel blockade (green dot, $\bar{g}_{SK} = 0$ [mS/cm²]) and L-type calcium channel blockade (blue dot, $\bar{g}_{CaL} = 0$ [mS/cm²]) - **(left)** Summary of the regularity of the firing pattern with $\bar{g}_{SK} = 0$ [mS/cm²] and $\bar{g}_{CaL} = 0$ [mS/cm²] with NMDA **(right)** Focus of the temporal traces of the membrane potential for a low value of $\bar{g}_{CaL} = 0.02064$ [mS/cm²] (light blue) and for a higher value of $\bar{g}_{CaL} = 0.03189$ [mS/cm²] (dark blue) after $\bar{g}_{SK} = 0$ [mS/cm²] and $\bar{g}_{SK} = 0$ [mS/cm²] with $\bar{g}_{CaL} = 0$ [mS/cm²]

To assess it, the experiment performed in Figure 8.4 is extended. L-type channel blockade is induced by setting $\bar{g}_{CaL} = 0$ (blue dot) on all 20 neurons of the simulation. As it can be observed, the CV is brought back to low and homogeneous values, indicating homogeneous pacemaking among the simulations.

On the right are represented the membrane voltage of the two neurons from Figure 8.4 under SK channel blockade (as it was already represented before, showing different firing) and below is the same neuron when SK channels and L-type calcium channels are blocked. Both recover pacemaking.

It can be concluded that despite the NMDA input which potentiates burstiness, L-type calcium channels are still the key to the switch to a bursting pattern. NMDA only enhances the effects.

8.3 Dynamics of activation with NMDA

As it was highlighted in the previous chapter, the dynamics of L-type calcium channels plays a significant role in the firing pattern of dopaminergic neurons model. As it can be seen in Figure 8.8, this effect remains, even with the addition of NMDA that was found to potentiate burstiness in the previous section.

To obtain Figure 8.8, the same experiment that was performed for Figure 7.15 is replicated (for details

in the procedure, see section 7.5.1). Only this time, an NMDA input is added by adding $g_{NMDA} = 0.15$ [mS/cm²] together with a hyperpolarising current $I_{app} = -0.45$ [nA/cm²].

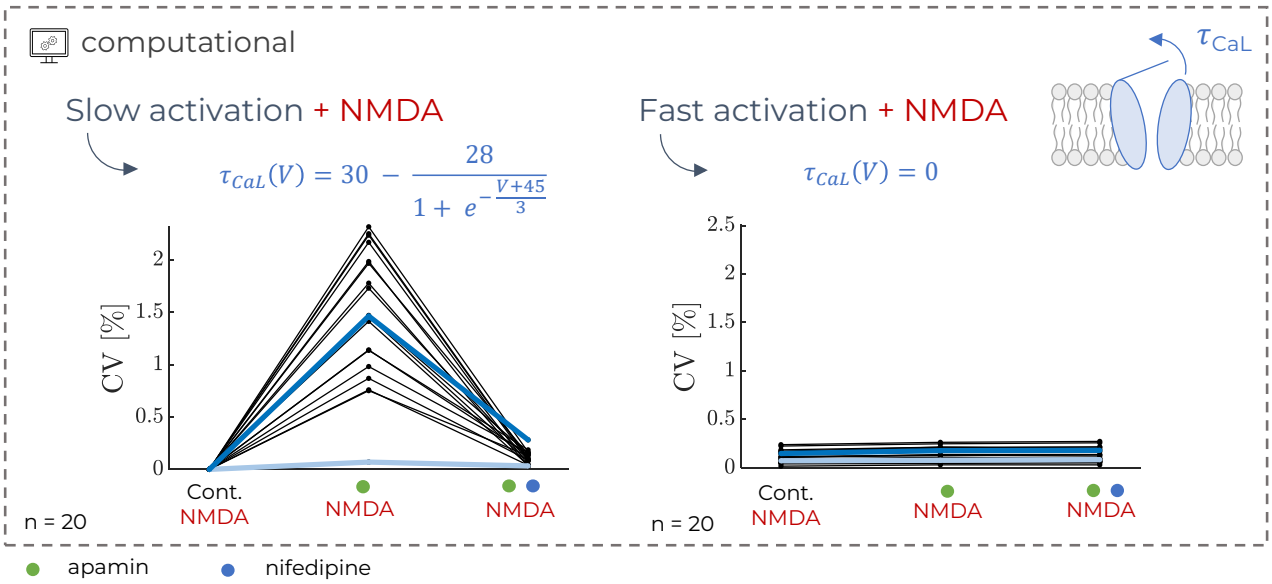

Figure 8.8: **Dynamics of L-type calcium channels with NMDA** - Simulation of 20 neurons with $\bar{g}_{CaL} \in [0.02 - 0.38]$ and $\bar{g}_{CaN} \in [0.0015 - 0.002]$ with $\bar{g}_{SK} = 0$ (green dot), $\bar{g}_{CaL} = 0$ (blue dot) and $\bar{g}_{NMDA} = 0.15 + I_{app} = -0.45$ [nA/cm²] (NMDA) **(left)** Slow dynamics. Results from previous figure provided as comparison **(right)** Fast dynamics.

In figure 8.9 is provided an animation of the firing pattern for the same case and conductance values that was presented in Figure 8.3 instead, here, the activation is defined as instantaneous.

As it can be observed, there is no bursting behaviour anymore. It is explained by the fact that there is no separation of the phase plane induced by the two branches. NMDA oscillates between activation and deactivation as it activates for each spike.

Figure 8.9: **Animation** - Video (*video_PP_CaLinstNMDA.mp4*) of the firing pattern observed for instantaneous calcium activation with $\bar{g}_{CaL} = 0.026$ [mS/cm²], $\bar{g}_{SK} = 0$, $\bar{g}_{NMDA} = 0.15$ [mS/cm²] and a current $I_{app} = -0.45$ **(top)** Time trace simulation of the model **(bottom)** Corresponding evolution of the phase plane

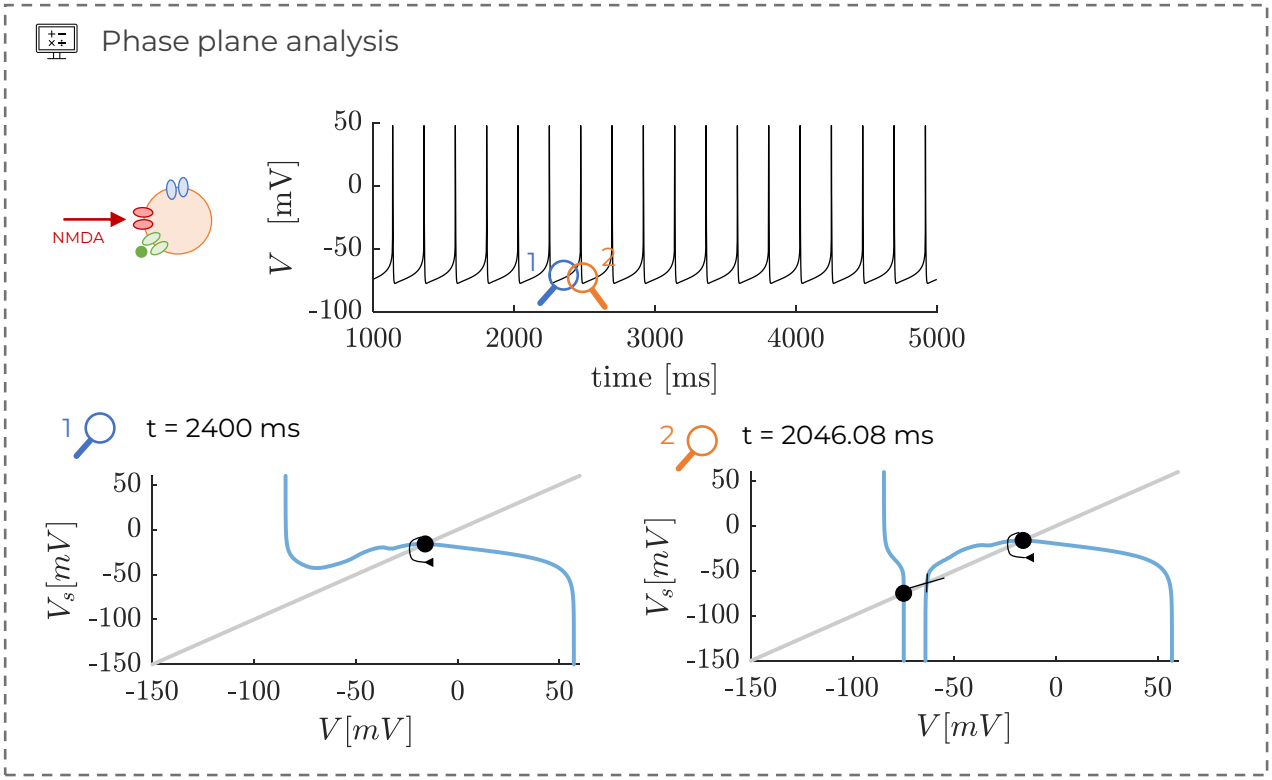

Figure 8.10: **Phase plane analysis** - Phase plane for $\bar{g}_{CaL} = 0.026$ [mS/cm²], $\bar{g}_{SK} = 0$ [mS/cm²], $\bar{g}_{NMDA} = 0.15$ [mS/cm²] and $I_{app} = -0.45$ [nA/cm²] with instantaneous type-L calcium activation **(top)** Trace of the reduced model **(bottom)** Comparison of the phase portraits at the two events that are highlighted on the magnifying glasses on the top figure.

8.4 NMDA in control conditions

Now that the effect of NMDA on the firing of dopaminergic neurons has been assessed in the conditions of different channel blockade, mainly SK channel, its effect can be assessed in *control conditions*, i.e. without any blockade. The results are summarised in Figure 8.11.

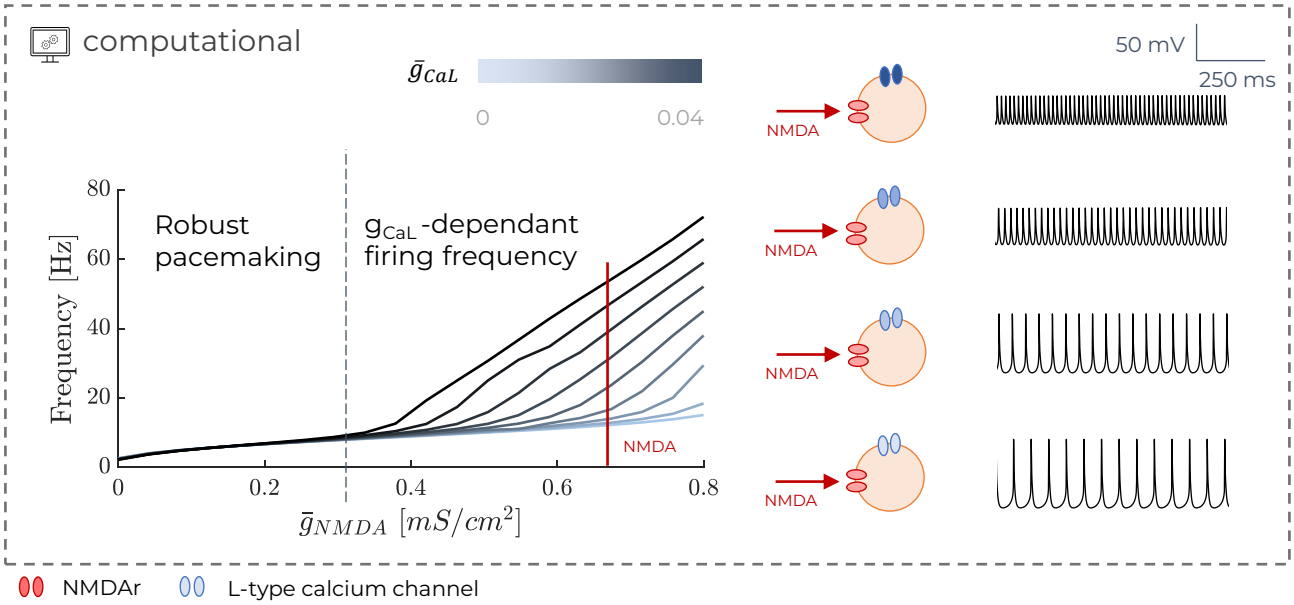

Figure 8.11: **NMDA in control conditions** - Simulations of the model without any channel blockade **(left)** Frequency of firing as a function of the NMDA input $\bar{g}_{NMDA}$ depending on the L-type calcium channel $\bar{g}_{CaL}$ **(right)** Membrane voltage for $g_{NMDA} = 0.7$ [mS/cm^2] for 4 different calcium channels (from to top bottom) $\bar{g}_{CaL} = 0.0$, $\bar{g}_{CaL} = 0.1$, $\bar{g}_{CaL} = 0.2$, $\bar{g}_{CaL} = 0.3$ [mS/cm^2]

On the left of Figure 8.11 is a graph representing the behaviour of the model in terms of frequency of firing according to the NMDA input for multiple values of $\bar{g}_{CaL}$. Two regions on the graph can be observed

- *Robust pacemaking.* Below a certain value of $\bar{g}_{NMDA}$ (marked with the dotted line), the neuron's frequency of firing does not depend on the value of the $\bar{g}_{CaL}$. This property gives a pacemaking which is robust to noise and perturbations.
- $\bar{g}_{CaL}$*-dependant firing frequency.* Above the threshold, the firing frequency will depend on its L-type calcium channel density.

On the right of Figure 8.11 is an illustration of the dependence of the firing frequency on the value of $\bar{g}_{CaL}$. The model is simulated for a fixed value $\bar{g}_{NMDA} = 0.7$ [mS/cm^2] (represented by the red line on the left graph) and four different values of four $\bar{g}_{CaL}$ (from top to bottom, $\bar{g}_{CaL} = 0.0$ [mS/cm^2], $\bar{g}_{CaL} = 0.01$ [mS/cm^2], $\bar{g}_{CaL} = 0.02$ [mS/cm^2], $\bar{g}_{CaL} = 0.03$ [mS/cm^2]). As it can be seen, the frequency of firing increases with the value of $\bar{g}_{CaL}$. This time, no hyperpolarising current is added. The amplitude of the firing decreases with the frequency.

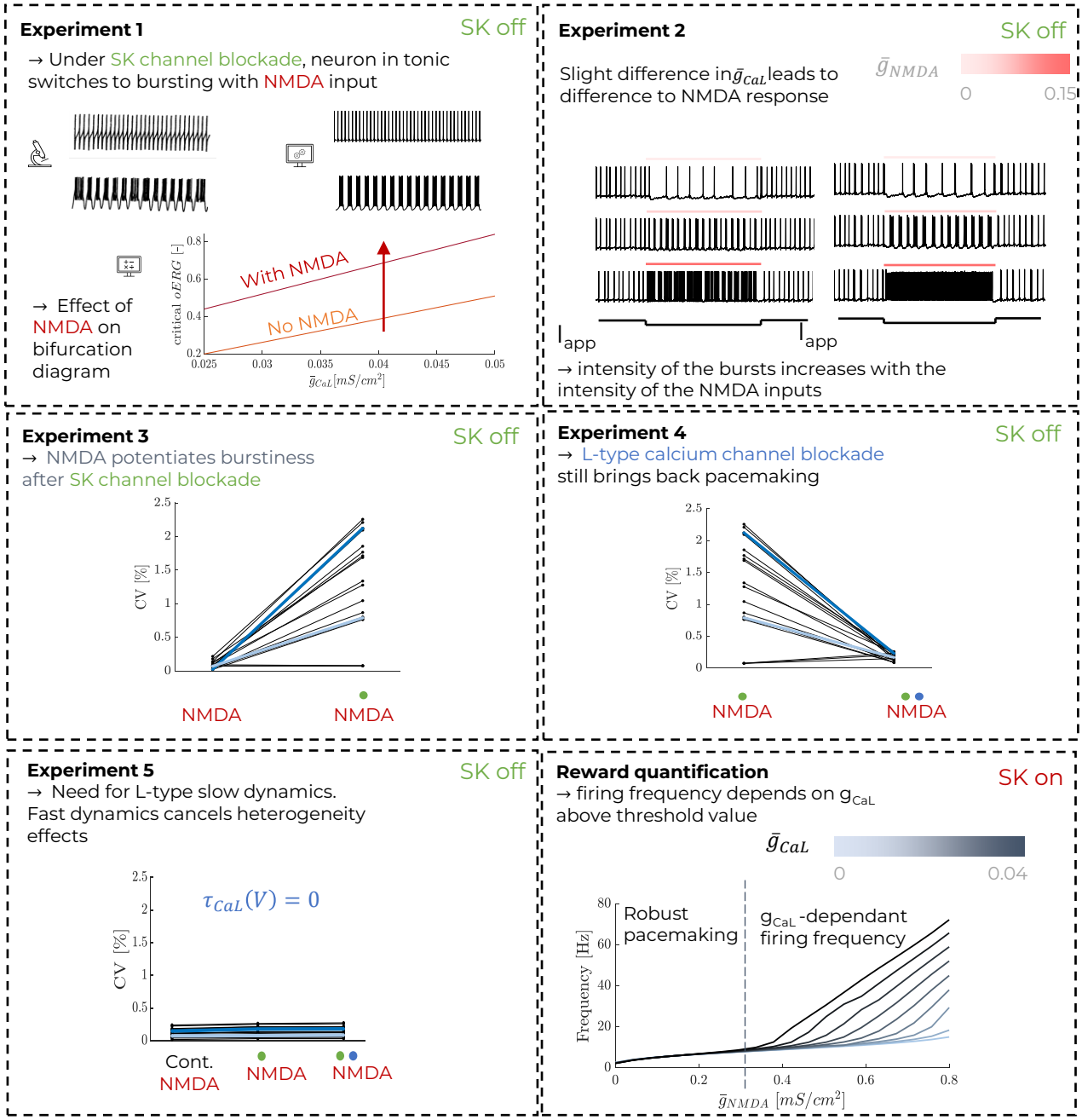

Figure 8.12: **Summary of Chapter 8**

Chapter 9

Reward

The aim of this chapter is to develop the hypothesis of a link between the firing of dopaminergic neurons in control conditions and the subsequent dopamine release as a way to quantify rewards.

9.1 Motivation

The switch from tonic to phasic firing in dopaminergic neurons is an area of interest and study in the scientific field. Several studies conclude that the mode of firing (either low frequency tonic firing or short events of high frequency phasic firing) is observed as a response to a modulating excitatory or inhibitory input [Lobb et al., 2011]. The switch from tonic to phasic firing correlates with the theory of *reward prediction errors* that was developed in [Schultz, 1997]. In fact, in [Wang et al., 1994], they observed that the application of NMDA to dopaminergic neurons in the VTA increases their firing frequency and leads to higher levels of dopamine in the NAc.

9.2 Hypothesis

In this chapter, a hypothetical situation is studied. In fact, as it was shown in Figure 8.11, the frequency of firing is dependant on the density of type-L calcium channels. It is known that those channels can be phosphorylated or not. the phosphorylation leads density of active calcium channels which can be altered or not.

9.3 Dopamine release

As it was explained before, the release of neurotransmitters in the synaptic cleft by the presynaptic neuron is triggered by its firing. In [Morozova et al., 2016b], they modified a model of release and adapted it to dopamine so that it depends on the spiking activity.

$$\frac{d[DA]}{dt} = [DA]_{max}\delta(t - t_{spike}) - \frac{v_{max}[DA]}{K_m + [DA]} \tag{9.1}$$

where [DA] is the concentration of dopamine in the synaptic cleft, the first term represents the release of dopamine with δ is the Dirac delta function which is always equal to zero except at the times of spiking, t_{spike}, which leads to the release of $[DA]_{max} = 0.1$ µM. The second term is the clearance

of dopamine in the cleft described by a Michaelis-Menten kinetics with $v_{max} = 0.004$ µM/ms and $K_m = 0.2$ µM.

By combining the model with equation (9.1), one is able to quantify the dopamine release by a small population of neurons in the VTA.

9.4 Case study 1 : Addiction

The recovery from addiction is a long process which takes time and is often impaired by triggers which can cause relapse. Those triggers are actually a *cue*. The addict sees a cue which has been associated with the addiction. It would not trigger any reaction from a standard individual who doesn't suffer from the addiction. If this situation is compared with the description of [Schultz, 1997] the addicted person is, on Figure 2.2, the (right) where there is a cue but no reward. They therefore have an *increased sensitivity* to the cue, which would be translated in terms of the model into an increased value of $\bar{g}_{CaL}$ for the population of dopaminergic neurons that code for the cue.

In [Degoulet et al., 2016], they also highlighted that L-type calcium channel blockade blocks a type of cue learning dependant on NMDAr transmission in the VTA which would correlate with the features of the model.

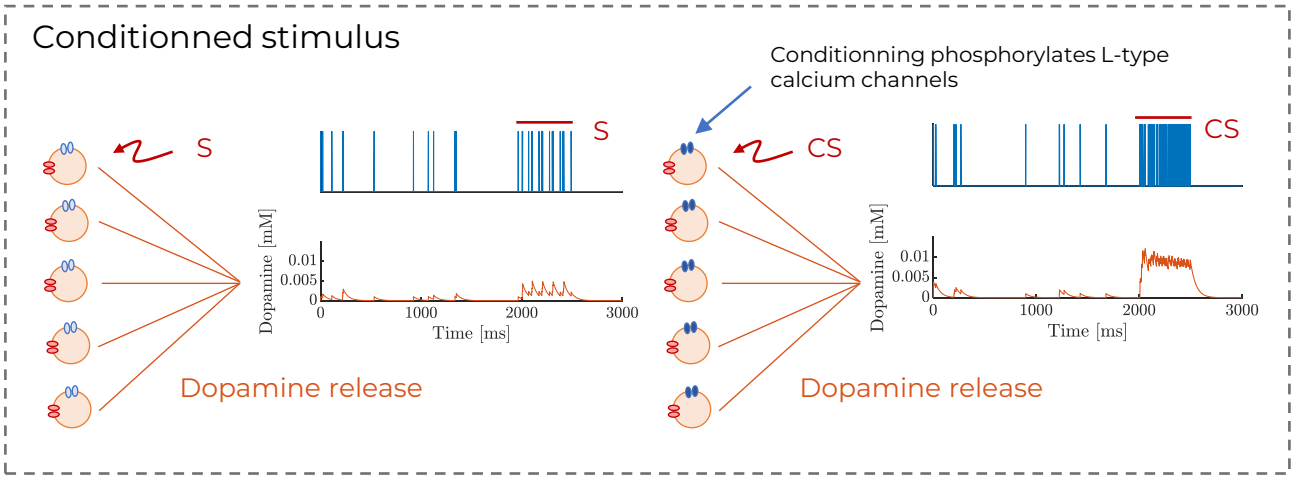

Figure 9.1: **Conditioning - (left)** Unconditioned stimulus (S) doesn't trigger significant dopamine release **(right)** Conditioned stimulus phosphorylates L-type calcium channels which lead to significant dopamine release when presented to conditoned stimulus (CS)

In Figure 9.1 is presented a small case study of a conditioned stimulus. On the left is a typical person who doesn't have an increased sensitivity to a stimulus because it hasn't been conditioned. To reciprocate this in terms of the model, the neurons population is set to $\bar{g}_{CaL} = 0.01$ [mS/cm²]. On the right, is a small population of 5 neurons which have been conditioned. This means they have an increased sensitivity to the stimulus and, in terms of the model, this is translated into an increased $\bar{g}_{CaL} = 0.04$ [mS/cm²]. For this simulation, in each situation, the 5 neurons are uncorrelated and release dopamine into the same synaptic cleft.

In both cases, the neurons fire initially under no stimulation so the dopamine levels are low. Then,

at t=2000ms, they are presented with a stimulus. In the unconditioned case (left), the increase in frequency is minimal so the dopamine release is slightly altered but not significantly. In the conditioned case, the frequency of firing increases significantly and the resulting dopamine release is visibly increased.

9.5 Case study 2 : Effects of low doses of Apamin

It has been shown that L-type calcium channels may play a role in depression. In fact, in [Li et al., 2021], they concluded that the use of hypertensive drugs are a risk factor for depression. Hypertensive drugs are actually L-type calcium channel blockers which are usually used for heart conditions as the heart also contains L-type calcium channels.

In terms of the model, this would mean that depressed individuals would have overall lower $\bar{g}_{CaL}$.

However, in [Scuvée-Moreau et al., 2004], they higlighted the fact that apamin at low doses has antidepressant effects. In the previous chapters, the value of $\bar{g}_{SK}$ was either at 0 or at 0.9 [mS/cm^2]. In this section, we now want to study the effect of SK channel partial blockade on the frequency of firing for dopaminergic neurons which present weak values of $\bar{g}_{CaL}$.

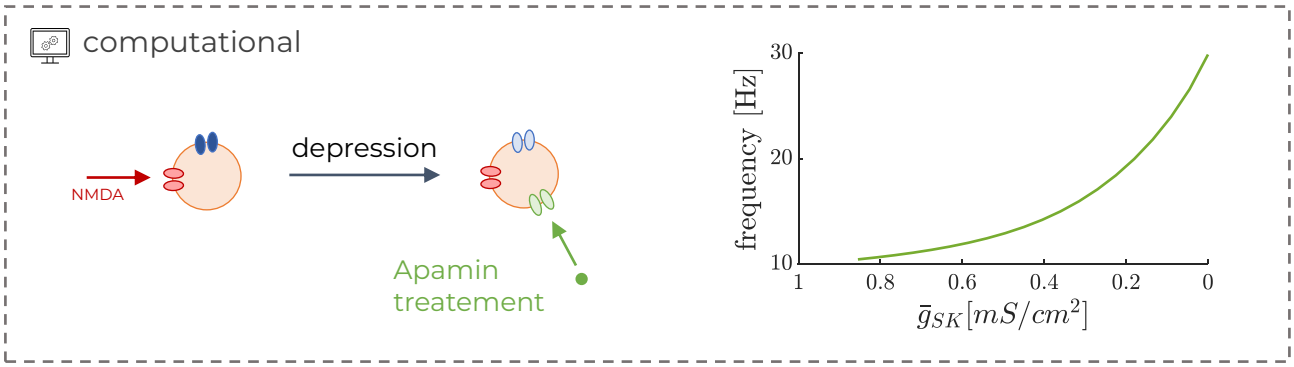

Figure 9.2: Effect of partial SK channel blockade with apamin treatement on the firing rate of "depressed" ($\bar{g}_{CaL} = 0$) dopaminergic neuron

In Figure 9.2, one can see on the left the assumed effect of depression which would cause a decrease in the $\bar{g}_{CaL}$ (represented in blue on the figure). The effect of the treatement on the firing rate is then tested on a neuron of $\bar{g}_{CaL} = 0$ [mS/cm^2]. To do so, the neuron is simulated with an NMDA input of $\bar{g}_{NMDA} = 0.5$ which would lead to significant differences in the firing rate between two neurons of different $\bar{g}_{CaL}$ values. The intensity of the blockade is increased by slowly decreasing the value of $\bar{g}_{SK}$ and observing the effect on the frequency of firing.

For $\bar{g}_{SK} = 0.9$ it corresponds to the control case that is simulated in Figure 8.11 so the firing rate is of around 10 Hz, as expected. By decreasing the value of $\bar{g}_{SK}$, the frequency of firing actually increases. This effect is expected since SK channels dampen the excitability of dopaminergic neurons.

However, it must be highlighted that in this case is simulated the extreme case of $g_{CaL} = 0$. If this value is increased then by inducing SK channel blockade, the neuron may switch to a depolarisation block. This block is caused by the fact that the neuron is overly stimulated during bursting. The value

at which depolarisation block is observed is actually $\bar{g}_{CaL}$-, $\bar{g}_{NMDA}$- and $\bar{g}_{SK}$-dependant. The higher (resp. lower) the $\bar{g}_{CaL}$ and $\bar{g}_{NMDA}$ (resp. $\bar{g}_{SK}$) the faster the depolarisation block is reached.

Part IV

Conclusion and perspectives

Chapter 10

Conclusion and perspectives

10.1 Thesis summary

The aim of this thesis was to study the model developed by G. Drion which describes the dynamics of dopaminergic neurons. The following questions were raised and have been studied

- *What is the role of dopaminergic neurons and their implications in reward?*

  The question is studied in the first chapter as it describes on a larger scale the implications of dopaminergic activity in the *reward circuitry*. Its role and implications in psychological disorders are then described.

- *What are the mechanisms underlying the behaviour of dopaminergic neurons and how can they be studied ?*

  In the second chapter, the biology of a typical neuron as well as its generalised characteristics are presented. This introduction is followed up with a description of the different firing modes that characterise dopaminergic activity is made, i.e. slow and steady tonic and high frequency phasic firing. The additional bursting observed after SK channel blockade is introduced. The different currents that have been identified to drive the changes in behaviour and their consequences on the circuitry is presented. The pharmacology required to then study the different ion currents using ion channel blockers is introduced.

- *What are the mathematical dynamics that interplay in the dynamics of dopaminergic neurons ?*

  To answer this question, the fourth chapter presents the basis of conductance-based modeling, which allows to reproduce the behaviour of neurons according to the ionic currents that are identified. This approach offers biological relevance in the interpretation of the results. The dopaminergic model is introduced. Then in the fifth chapter, an introduction on phase plane analysis and model reduction shows the motivation to such method and how it can be used to understand the dynamics of non-linear models.

- *Can the experimental results of dopaminergic neurons be reproduced ?*

  In the seventh chapter is presented experiments that were performed in the literature and their

reproduction using the model. The special case of SK channel blockade which leads to bursting is then studied on the phase plane.

- *What are the effects of afferent input on the dopaminergic neuron ?*

  In the 8th chapter, the experiments are studied in the case of an NMDA input, which is known to drive the changes in frequency of firing in the dopaminergic neuron. The effect is analysed after SK channel blockade and in control conditions (without blockade).

- *How can it be linked to reward ?*

  Finally, a hypothesis that includes the context-dependant tuning of type-L calcium channel through their phosphorylation is introduced to use the model as a way to quantify the reward. A few case studies are presented as introductory examples.

10.2 Perspectives

Firstly, it must be reminded that the current model used is initially a model of dopaminergic neurons from the SNc, not from the VTA. They do however present very similar firing patterns which is why the model was used in the work, despite differences in the ionic currents. In [Seutin, 2022], they present a hypothesis of a new ion channel which explains the similarity of the firing patterns despite the differences.

10.2.1 Modeling

In this work is presented a model of modulation of the dopaminergic activity whose variations are triggered solely by an input of glutamate that activates NMDAr. However, it is known that dopaminergic neurons receive inhibitory and excitatory synaptic inputs from several parts of the brain. The dopaminergic activity is therefore influenced by an interplay of those synaptic inputs.

In [Morozova et al., 2016b], they present a model of dopaminergic activity. This model, compared to [Drion, 2015]'s model, is less biologically accurate as does not have the ability to reproduce the experimental results that are studied in chapter 8. However, it presents a study that includes several types of synaptic input, namely NMDA, AMPA and GABA. As it was introduced before, the VTA is composed of mainly dopaminergic neurons. However, the rest of the population is actually GABAergic neurons. Those GABAergic are believed to influence locally the activity of dopaminergic neurons [Morozova et al., 2016a]

By including the contribution of GABAergic inputs, [Morozova et al., 2016a] are able to not only to have tonic and phasic firing but also cessation of the tonic firing. This behaviour would correlate with what was described in [Schultz, 1997] when a conditioned stimulus is presented without the subsequent associated reward. This result cannot be replicated with the current model.

Combining the strength of both models would offer a more accurate description of the VTA and, therefore, a better insight of the mechanisms that drive the processing of rewards.

Additionally, circuits could be modeled, instead of singe cells.

10.2.2 Model reduction and dynamical analysis

In this work, the reduction of the model was done without reducing the expression of [Ca] and $[Ca]_{SK}$ since the influence of [Ca] was always cancelled ($I_{pmax} = 0$) and the effect of Ca_{SK} was also always cancelled for dynamical analysis because the main focus of this work was on SK-channel blockade.

For further works, if the dynamics of SK channels are added to the study then a reduction of [Ca] and/or $oERG$ might be required.

Part V

Appendix

Chapter 11

Appendix

11.1 Resting potential

The value of the membrane resting potential of each ion at this equibrium can be computed thanks to Nernst's equation equation (11.1).

$$V_{nernst} = \frac{RT}{zF} ln \frac{[ion]_{in}}{[ion]_{out}} \tag{11.1}$$

where R is the gas constant, T is the temperature in Kelvin, z is the valence, F is Faraday's constant and $[ion]_{in}$ (resp. $[ion]_{out}$) represents the concentration of the ion inside (resp. outside) the membrane. In the case of the neuronal membrane, the main ions that have been identified to determine the resting potential of a neuron's membrane in physiological conditions are Na^+, K^+, Cl^- and Ca^{2+} which have respectively a nernst potential of 51 mV, -97 mV, -42 mV and 120 mV. [Sepulchre, 2008]
However, it only concerns ions which are permeable to the membrane. Therefore, Nernst's equation can be rewritten as the Goldman-Hodkin-Katz, equation (11.2).

$$V_m = \frac{RT}{zF} ln \left(\frac{\sum_{ion^+} P_{ion^+} [ion^+]_{out} + \sum_{ions^-} [ion^-]_{in}}{\sum_{ion^+} P_{ion^+} [ion^+]_{in} + \sum_{ions^-} [ion^-]_{out}} \right) \tag{11.2}$$

for which ion^+ (resp. ion^-) stands for the ions of positive (resp. negative) valence and P are the permeances of said ions.

11.2 Action potential

Description of the action potential generation as found by [Hodgkin and Huxley, 1952].

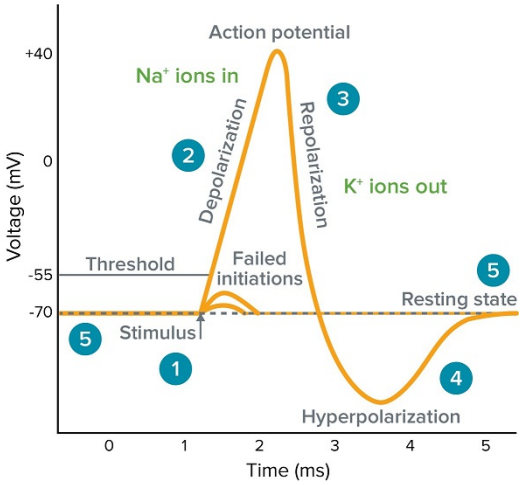

Figure 11.1: **Description of the AP** - **(1)** Too small of a stimulus leads to failed initiations of an AP **(2)** Stimulus large enough iniates AP. The membrane potential reaches a threshold that activates rapid opening of sodium channels. Sodium enters the cell which depolarizes the membrane.**(3)** Sodium channels rapidly close, potassium channels open. Potassium leaves the cell and leads to repolarization. **(4)** Potassium channels have slower dynamics which lead to a period of hyperpolarization (refractory period) as it reaches potassium's nernst potential. **(5)** Potassium channels deactivate so the potential goes back to its original resting potential. Image from https://www.moleculardevices.com/applications/patch-clamp-electrophysiology/what-action-potential

11.3 Algorithm

Algorithm 1 Determination of time-scale dependant weight factors w_{fs}^X and w_{su}^X

if $\tau_X(V) \leq \tau_f(V)$ **then**
  $w_{fs}^X(V) = 1$;
  $w_{su}^X(V) = 1$;
else if $\tau_f(V) < \tau_X(V) \leq \tau_s(V)$ **then**
  $w_{fs}^X(V) = \frac{log(\tau_s(V)) - log(\tau_X(V))}{log(\tau_s(V)) - log(\tau_f(V))}$;
  $w_{su}^X(V) = 1$
else if $\tau_s(V) < \tau_X(V) \leq \tau_{us}(V)$ **then**
  $w_{fs}^X(V) = 0$;
  $w_{su}^X(V) = \frac{log(\tau_{us}(V)) - log(\tau_X(V))}{log(\tau_{us}(V)) - log(\tau_s(V))}$;
else if $\tau_X(V) > \tau_{us}(V)$ **then**
  $w_{fs}^X(V) = 0$;
  $w_{su}^X(V) = 0$;
end if

11.4 Full model

11.4.1 Parameters

Conductance	[mS/cm²]	Potential	[mV]
g_l	0.013	V_l	-50
g_{Na}	12	V_{Na}	60
$g_{K,DR}$	1.2	V_K	-85
g_{CaL}	variable	V_{Ca}	60
g_{CaN}	variable	V_{Ca}	60
g_{SK}	0.9	V_K	-85
g_{ERG}	0.04	V_K	-85
g_{NMDA}	variable	V_{NMDA}	0

Table 11.1: **Table** of the main values of parameters. For the others, refer to the papers of the models referenced in table 4.1

11.4.2 Equations

$$\begin{aligned} C_m\frac{dV_m}{dt} = &-g_{Na}m^3h(V-V_{Na}) - g_{KDR}n^3(V-V_K) - g_{CaL}m_{CaL}^2(V-V_{Ca}) \\ &- g_{CaN}m_{CaN}(V-V_{Ca}) - g_{SK}\left(\frac{[Ca]_{SK}}{[Ca]_{SK}+K_D}\right)^2(V-V_K) - g_{ERG}oERG(V-V_K) \\ &- I_{CaPmax}\frac{Ca}{Ca+K_P} - g_l(V-V_l) - g_{NMDA}(V-V_{NMDA})\frac{1}{1+[Mg]e^{-0.008V}} \\ &+ I_{app} + I_{noise} \end{aligned} \tag{11.3}$$

$$m_{inf}(V) = \frac{1}{1+\exp-\frac{(V+30.0907)}{9.7264}} \tag{11.4}$$

$$\tau_m(V) = 0.01 + \left(\frac{-(15.6504+0.4043V)}{\exp(-19.565-0.5052V)-1.0} + 3.0212 * \exp(-7.4630\,10^{-3}V)\right)^{-1} \tag{11.5}$$

$$h_{inf}(V) = \frac{1}{1+\exp-\frac{(V+54.0289)}{-10.7665}} \tag{11.6}$$

$$\tau_h(V) = 0.4 + \frac{1}{((5.0754\,10^{-4}\exp(-6.3213e-2*V)) + 9.7529\exp(0.13442V)} \tag{11.7}$$

$$n_{inf}(V) = \frac{1}{1+\exp-\frac{(V+25)}{12}} \tag{11.8}$$

$$\tau_n(V) = 20 - \frac{18}{1+\exp\frac{-(V+55)}{6}} \tag{11.9}$$

$$mCaL_{inf}(V) = \frac{1}{1+\exp-\frac{(V+50)}{2}} \tag{11.10}$$

$$\tau_{mCaL}(V) = 30 - \frac{28}{1+\exp\frac{-(V+45)}{3}} \tag{11.11}$$

$$mCaN_{inf}(V) = \frac{1}{1 + \exp -\frac{(V+20)}{7}} \tag{11.12}$$

$$\tau_{mCaN}(V) = 30 - \frac{25}{1 + \exp \frac{-(V+55)}{6}} \tag{11.13}$$

$$I_{CaN}(V) = g_{CaN} m_{CaN} (V - V_{Ca}) \tag{11.14}$$

$$I_{CaL}(V) = g_{CaL} m_{CaL}^2 (V - V_{Ca}) \tag{11.15}$$

$$f_{SK}([Ca]) = \left(\frac{[Ca]}{[Ca] + K_D} \right)^2 \tag{11.16}$$

$$a_{oERG}(V) = 0.0036 e^{0.0759V} \tag{11.17}$$

$$b_{oERG}(V) = 1.2523\, 10^{-5} e^{-0.0671V} \tag{11.18}$$

$$a_{iERG}(V) = 0.1 e^{0.1189V} \tag{11.19}$$

$$b_{iERG}(V) = 0.003 e^{-0.0733V} \tag{11.20}$$

$$\frac{dm}{dt} = \frac{1}{\tau_m(V)} (m_{inf}(V) - m(t)) \tag{11.21}$$

$$\frac{dh}{dt} = \frac{1}{\tau_h(V)} (h_{inf}(V) - h(t)) \tag{11.22}$$

$$\frac{dn}{dt} = \frac{1}{\tau_n(V)} (n_{inf}(V) - n(t)) \tag{11.23}$$

$$\frac{dmCaL}{dt} = \frac{1}{\tau_{mCaL}(V)} (mCaL_{inf}(V) - mCaL(t)) \tag{11.24}$$

$$\frac{dmCaN}{dt} = \frac{1}{\tau_{mCaN}(V)} (mCaN_{inf}(V) - mCaN(t)) \tag{11.25}$$

$$\frac{d[Ca]_{SK}}{dt} = -k_1\, I_{CaN}(V) - k_c [Ca]_{SK} \tag{11.26}$$

$$\frac{d[Ca]}{dt} = k_2(-I_{CaN}(V) - I_{CaL}(V)) - k_{c2}[Ca] \tag{11.27}$$

$$\frac{doERG}{dt} = a_{oERG}(V)(1 - iERG - oERG) + b_{iERG}(V) iERG - oERG(a_{iERG}(V) + b_{oERG}(V)) \tag{11.28}$$

$$\frac{diERG}{dt} = a_{iERG}(V) oERG - b_{iERG}(V) iERG \tag{11.29}$$

11.5 Phase plane

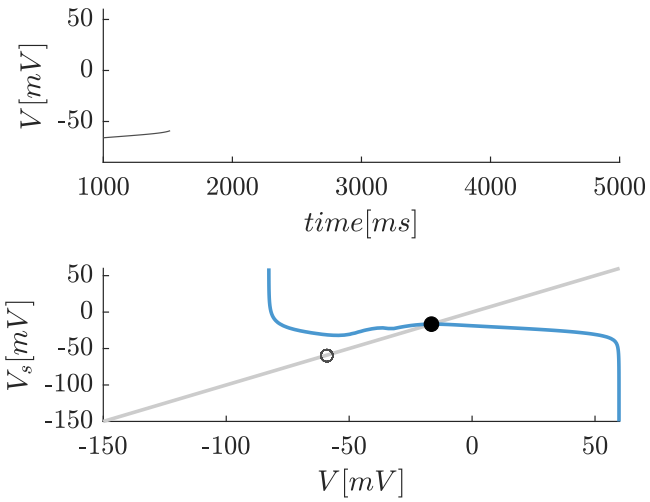

Figure 11.2: **Phase plane (top)** Vizualisation of the instant that is captured of the phase plane **(bottom)** Phase plane of the reduced model obtained at t = 1517.67 ms for $\bar{g}_{CaL} = 0.03$ [mS/cm^2] and $g_{SK} = 0$ [mS/cm^2]

Figure 11.2 represents the first main event, which is right before a burst. At such instant, the phase plane consists in only one fixed point whose coordinates are ($\bar{V}$,$\bar{V_s}$)=(-16.52,-16.52) and the eigen values of the jacobian matrix evaluated at such point are

$$\lambda_1 = -0.073 + 0.94i \qquad \lambda_2 = -0.073 - 0.94i \tag{11.30}$$

Those eigen values are complex with a negative real part which means it is a stable spiral.

Bibliography

[noa, 2022] (2022). The synapse (article) | Human biology.

[Bear et al., 2016] Bear, M. F., Connors, B. W., and Paradiso, M. A. (2016). *Neuroscience: exploring the brain*. Jones & Bartlett Learning, Philadelphia.

[Beninger and Miller, 1998] Beninger, R. J. and Miller, R. (1998). Dopamine D1-like Receptors and Reward-related Incentive Learning. *Neuroscience & Biobehavioral Reviews*, 22(2):335–345.

[Bhatia et al., 2021] Bhatia, A., Lenchner, J. R., and Saadabadi, A. (2021). *Biochemistry, Dopamine Receptors*. StatPearls Publishing. Publication Title: StatPearls [Internet].

[Bouarab et al., 2019] Bouarab, C., Thompson, B., and Polter, A. M. (2019). VTA GABA Neurons at the Interface of Stress and Reward. *Frontiers in Neural Circuits*, 13.

[Canavier and Landry, 2006] Canavier, C. C. and Landry, R. S. (2006). An increase in AMPA and a decrease in SK conductance increase burst firing by different mechanisms in a model of a dopamine neuron in vivo. *Journal of Neurophysiology*, 96(5):2549–2563.

[Chan et al., 2007] Chan, C. S., Guzman, J. N., Ilijic, E., Mercer, J. N., Rick, C., Tkatch, T., Meredith, G. E., and Surmeier, D. J. (2007). 'Rejuvenation' protects neurons in mouse models of Parkinson's disease. *Nature*, 447(7148):1081–1086.

[Chau et al., 2018] Chau, B. K. H., Jarvis, H., Law, C.-K., and Chong, T. T.-J. (2018). Dopamine and reward: a view from the prefrontal cortex. *Behavioural Pharmacology*, 29(7):569–583.

[Constantinou et al., 2016] Constantinou, M., Gonzalo Cogno, S., Elijah, D. H., Kropff, E., Gigg, J., Samengo, I., and Montemurro, M. A. (2016). Bursting Neurons in the Hippocampal Formation Encode Features of LFP Rhythms. *Frontiers in Computational Neuroscience*, 10.

[de Vrind et al., 2016] de Vrind, V., Scuvée-Moreau, J., Drion, G., Hmaied, C., Philippart, F., Engel, D., and Seutin, V. (2016). Interactions between calcium channels and SK channels in midbrain dopamine neurons and their impact on pacemaker regularity: Contrasting roles of N- and L-type channels. *European Journal of Pharmacology*, 788:274–279.

[Degoulet et al., 2016] Degoulet, M., Stelly, C. E., Ahn, K.-C., and Morikawa, H. (2016). L-type Ca2+ channel blockade with antihypertensive medication disrupts VTA synaptic plasticity and drug-associated contextual memory. *Molecular psychiatry*, 21(3):394–402.

[Drion, 2015] Drion, G. (2015). Potential functional implications of a hidden variability in SNc DA neuron excitability.

[Drion et al., 2015] Drion, G., Franci, A., Dethier, J., and Sepulchre, R. (2015). Dynamic Input Conductances Shape Neuronal Spiking. *eNeuro*, 2(1). Publisher: Society for Neuroscience Section: New Research.

[Drion et al., 2012] Drion, G., Franci, A., Seutin, V., and Sepulchre, R. (2012). A Novel Phase Portrait for Neuronal Excitability. *PLOS ONE*, 7(8):e41806. Publisher: Public Library of Science.

[Drion et al., 2011] Drion, G., Massotte, L., Sepulchre, R., and Seutin, V. (2011). How Modeling Can Reconcile Apparently Discrepant Experimental Results: The Case of Pacemaking in Dopaminergic Neurons. *PLoS computational biology*, 7:e1002050.

[Dunlop and Nemeroff, 2007] Dunlop, B. W. and Nemeroff, C. B. (2007). The Role of Dopamine in the Pathophysiology of Depression. *Archives of General Psychiatry*, 64(3):327–337.

[FitzHugh, 1961] FitzHugh, R. (1961). Impulses and Physiological States in Theoretical Models of Nerve Membrane. *Biophysical Journal*, 1(6):445–466.

[Gould et al., 2019] Gould, T. D., Zarate, C. A., and Thompson, S. M. (2019). Molecular Pharmacology and Neurobiology of Rapid-Acting Antidepressants. *Annual review of pharmacology and toxicology*, 59:213–236.

[Guzman et al., 2009] Guzman, J. N., Sánchez-Padilla, J., Chan, C. S., and Surmeier, D. J. (2009). Robust Pacemaking in Substantia Nigra Dopaminergic Neurons. *The Journal of Neuroscience*, 29(35):11011–11019.

[Hampel and Lau, 2020] Hampel, L. and Lau, T. (2020). Neurobiological Principles: Neurotransmitters. In Riederer, P., Laux, G., Mulsant, B., Le, W., and Nagatsu, T., editors, *NeuroPsychopharmacotherapy*, pages 1–21. Springer International Publishing, Cham.

[Hodgkin and Huxley, 1952] Hodgkin, A. L. and Huxley, A. F. (1952). A quantitative description of membrane current and its application to conduction and excitation in nerve. *The Journal of Physiology*, 117(4):500–544.

[Jacquerie and Drion, 2021] Jacquerie, K. and Drion, G. (2021). Robust switches in thalamic network activity require a timescale separation between sodium and T-type calcium channel activations. *PLOS Computational Biology*, 17(5):e1008997. Publisher: Public Library of Science.

[Ji et al., 2012] Ji, H., Tucker, K. R., Putzier, I., Huertas, M. A., Horn, J. P., Canavier, C. C., Levitan, E. S., and Shepard, P. D. (2012). Functional characterization of ether-à-go-go-related gene potassium channels in midbrain dopamine neurons - implications for a role in depolarization block. *The European Journal of Neuroscience*, 36(7):2906–2916.

[Johnson et al., 1992] Johnson, S. W., Seutin, V., and North, R. A. (1992). Burst firing in dopamine neurons induced by N-methyl-D-aspartate: role of electrogenic sodium pump. *Science (New York, N.Y.)*, 258(5082):665–667.

[Kauschke et al., 2019] Kauschke, C., Bahn, D., Vesker, M., and Schwarzer, G. (2019). The Role of Emotional Valence for the Processing of Facial and Verbal Stimuli—Positivity or Negativity Bias? *Frontiers in Psychology*, 10.

[Khaliq and Bean, 2010] Khaliq, Z. M. and Bean, B. P. (2010). Pacemaking in Dopaminergic Ventral Tegmental Area Neurons: Depolarizing Drive from Background and Voltage-Dependent Sodium Conductances. *The Journal of Neuroscience*, 30(21):7401–7413.

[Kirkpatrick and Bourque, 1996] Kirkpatrick, K. and Bourque, C. W. (1996). Activity dependence and functional role of the apamin-sensitive K+ current in rat supraoptic neurones in vitro. *The Journal of Physiology*, 494 (Pt 2):389–398.

[Kuznetsov et al., 2006] Kuznetsov, A. S., Kopell, N. J., and Wilson, C. J. (2006). Transient High-Frequency Firing in a Coupled-Oscillator Model of the Mesencephalic Dopaminergic Neuron. *Journal of Neurophysiology*, 95(2):932–947. Publisher: American Physiological Society.

[Leprince, 2019a] Leprince, P. (2019a). Neurones 2019.

[Leprince, 2019b] Leprince, P. (2019b). Synapse 2019.

[Li et al., 2021] Li, Y., Fan, Y., Sun, Y., Alolga, R. N., Xiao, P., and Ma, G. (2021). Antihypertensive Drug Use and the Risk of Depression: A Systematic Review and Network Meta-analysis. *Frontiers in Pharmacology*, 12.

[Lipscombe et al., 2004] Lipscombe, D., Helton, T. D., and Xu, W. (2004). L-Type Calcium Channels: The Low Down. *Journal of Neurophysiology*, 92(5):2633–2641. Publisher: American Physiological Society.

[Lobb et al., 2011] Lobb, C., Troyer, T., Wilson, C., and Paladini, C. (2011). Disinhibition Bursting of Dopaminergic Neurons. *Frontiers in Systems Neuroscience*, 5.

[Luo and Huang, 2016] Luo, S. X. and Huang, E. J. (2016). Dopaminergic Neurons and Brain Reward Pathways. *The American Journal of Pathology*, 186(3):478–488.

[MacNicol, 2017] MacNicol, B. (2017). The biology of addiction. *Canadian Journal of Anesthesia/Journal canadien d'anesthésie*, 64(2):141–148.

[Mercuri et al., 1994] Mercuri, N. B., Bonci, A., Calabresi, P., Stratta, F., Stefani, A., and Bernardi, G. (1994). Effects of dihydropyridine calcium antagonists on rat midbrain dopaminergic neurones. *British Journal of Pharmacology*, 113(3):831–838.

[Morikawa and Paladini, 2011] Morikawa, H. and Paladini, C. A. (2011). Dynamic Regulation of Midbrain Dopamine Neuron Activity: Intrinsic, Synaptic, and Plasticity Mechanisms. *Neuroscience*, 198:95–111.

[Morozova et al., 2016a] Morozova, E. O., Myroshnychenko, M., Zakharov, D., di Volo, M., Gutkin, B., Lapish, C. C., and Kuznetsov, A. (2016a). Contribution of synchronized GABAergic neurons to dopaminergic neuron firing and bursting. *Journal of Neurophysiology*, 116(4):1900–1923.

[Morozova et al., 2016b] Morozova, E. O., Zakharov, D., Gutkin, B. S., Lapish, C. C., and Kuznetsov, A. (2016b). Dopamine Neurons Change the Type of Excitability in Response to Stimuli. *PLOS Computational Biology*, 12(12):e1005233.

[Nair-Roberts et al., 2008] Nair-Roberts, R. G., Chatelain-Badie, S. D., Benson, E., White-Cooper, H., Bolam, J. P., and Ungless, M. A. (2008). Stereological estimates of dopaminergic, GABAergic and glutamatergic neurons in the ventral tegmental area, substantia nigra and retrorubral field in the rat. *Neuroscience*, 152(4):1024–1031.

[Nedergaard et al., 1993] Nedergaard, S., Flatman, J. A., and Engberg, I. (1993). Nifedipine- and omega-conotoxin-sensitive Ca2+ conductances in guinea-pig substantia nigra pars compacta neurones. *The Journal of Physiology*, 466:727–747.

[Nestler, 2015] Nestler, E. J. (2015). Role of the Brain's Reward Circuitry in Depression: Transcriptional Mechanisms. *International review of neurobiology*, 124:151–170.

[Nusse et al., 1994] Nusse, H. E., Yorke, J. A., and Kostelich, E. J. (1994). Basins of Attraction. In Nusse, H. E., Yorke, J. A., and Kostelich, E. J., editors, *Dynamics: Numerical Explorations: Accompanying Computer Program Dynamics*, Applied Mathematical Sciences, pages 269–314. Springer US, New York, NY.

[Olds and Milner, 1954] Olds, J. and Milner, P. (1954). Positive reinforcement produced by electrical stimulation of septal area and other regions of rat brain. *Journal of Comparative and Physiological Psychology*, 47(6):419–427. Place: US Publisher: American Psychological Association.

[Ortner, 2021] Ortner, N. J. (2021). Voltage-Gated Ca2+ Channels in Dopaminergic Substantia Nigra Neurons: Therapeutic Targets for Neuroprotection in Parkinson's Disease? *Frontiers in Synaptic Neuroscience*, 13:636103.

[Philippart et al., 2016] Philippart, F., Destreel, G., Merino-Sepulveda, P., Henny, P., Engel, D., and Seutin, V. (2016). Differential Somatic Ca2+ Channel Profile in Midbrain Dopaminergic Neurons. *Journal of Neuroscience*, 36(27):7234–7245.

[Puopolo et al., 2007] Puopolo, M., Raviola, E., and Bean, B. P. (2007). Roles of subthreshold calcium current and sodium current in spontaneous firing of mouse midbrain dopamine neurons. *The Journal of Neuroscience: The Official Journal of the Society for Neuroscience*, 27(3):645–656.

[Putzier et al., 2009] Putzier, I., Kullmann, P. H. M., Horn, J. P., and Levitan, E. S. (2009). Cav1.3 Channel Voltage Dependence, Not Ca2+ Selectivity, Drives Pacemaker Activity and Amplifies Bursts in Nigral Dopamine Neurons. *The Journal of Neuroscience*, 29(49):15414–15419.

[Qian et al., 2014] Qian, K., Yu, N., Tucker, K. R., Levitan, E. S., and Canavier, C. C. (2014). Mathematical analysis of depolarization block mediated by slow inactivation of fast sodium channels in midbrain dopamine neurons. *Journal of Neurophysiology*, 112(11):2779–2790. Publisher: American Physiological Society.

[Ranaldi, 2014] Ranaldi, R. (2014). Dopamine and reward seeking: the role of ventral tegmental area. *Reviews in the Neurosciences*, 25(5):621–630. Publisher: De Gruyter.

[Reneman et al., 2021] Reneman, L., Pluijm, M., Schrantee, A., and Giessen, E. (2021). Imaging of the dopamine system with focus on pharmacological MRI and neuromelanin imaging. *European Journal of Radiology*, 140:109752.

[Salgado and Kaplitt, 2015] Salgado, S. and Kaplitt, M. G. (2015). The Nucleus Accumbens: A Comprehensive Review. *Stereotactic and Functional Neurosurgery*, 93(2):75–93.

[Schultz, 1997] Schultz, W. (1997). Dopamine neurons and their role in reward mechanisms. *Current Opinion in Neurobiology*, 7(2):191–197.

[Scuvée-Moreau et al., 2004] Scuvée-Moreau, J., Boland, A., Graulich, A., Overmeire, L. V., D'hoedt, D., Graulich-Lorge, F., Thomas, E., Abras, A., Stocker, M., Liégeois, J.-F., and Seutin, V. (2004). Electrophysiological characterization of the SK channel blockers methyl-laudanosine and methyl-noscapine in cell lines and rat brain slices. *British Journal of Pharmacology*, 143(6):753–764.

[Sepulchre, 2008] Sepulchre, R. (2008). *GBIO011 - Modélisation des systèmes biologiques. Première partie [Notes de cours à l'attention des étudiants]*. ULiège - Université de Liège.

[Seutin, 2022] Seutin, V. (2022). A new hypothesis on the mechanism of pacemaking of midbrain dopaminergic neurons.

[Shepard et al., 2007] Shepard, P. D., Canavier, C. C., and Levitan, E. S. (2007). Ether-a-go-go–Related Gene Potassium Channels: What's All the Buzz About? *Schizophrenia Bulletin*, 33(6):1263–1269.

[Shepard and Stump, 1999] Shepard, P. D. and Stump, D. (1999). Nifedipine blocks apamin-induced bursting activity in nigral dopamine-containing neurons. *Brain Research*, 817(1-2):104–109.

[Strogatz, 2015] Strogatz, S. H. (2015). *Nonlinear Dynamics and Chaos: With Applications to Physics, Biology, Chemistry, and Engineering, Second Edition*. CRC Press, Boulder, CO, 2nd edition edition.

[Takemura, 1992] Takemura, M. (1992). [15] - ω-Conotoxin GVIA and Its Receptors. In Conn, P. M., editor, *Methods in Neurosciences*, volume 8 of *Neurotoxins*, pages 223–234. Academic Press.

[Tsai et al., 2009] Tsai, H.-C., Zhang, F., Adamantidis, A., Stuber, G. D., Bonci, A., de Lecea, L., and Deisseroth, K. (2009). Phasic Firing in Dopaminergic Neurons Is Sufficient for Behavioral Conditioning. *Science*, 324(5930):1080–1084. Publisher: American Association for the Advancement of Science.

[Vaughn et al., 2017] Vaughn, A., Davis, M., Sivamani, R., and Isseroff, R. (2017). A Concise Review of the Conflicting Roles of Dopamine-1 versus Dopamine-2 Receptors in Wound Healing. *Molecules*, 23:50.

[Wang et al., 2011] Wang, L. P., Li, F., Wang, D., Xie, K., Wang, D., Shen, X., and Tsien, J. Z. (2011). NMDA Receptors in Dopaminergic Neurons are Crucial for Habit Learning. *Neuron*, 72(6):1055–1066.

[Wang et al., 1994] Wang, T., O'Connor, W. T., Ungerstedt, U., and French, E. D. (1994). N-methyl-d-aspartic acid biphasically regulates the biochemical and electrophysiological response of A10 dopamine neurons in the ventral tegmental area: in vivo microdialysis and in vitro electrophysiological studies. *Brain Research*, 666(2):255–262.

[Wang et al., 2021] Wang, Y., Toyoshima, O., Kunimatsu, J., Yamada, H., and Matsumoto, M. (2021). Tonic firing mode of midbrain dopamine neurons continuously tracks reward values changing moment-by-moment. *eLife*, 10:e63166. Publisher: eLife Sciences Publications, Ltd.

[Wright et al., 2009] Wright, L., Pope, C., and Liu, J. (2009). CHAPTER 32 - The Nervous System as a Target for Chemical Warfare Agents. In Gupta, R. C., editor, *Handbook of Toxicology of Chemical Warfare Agents*, pages 463–480. Academic Press, San Diego.

[Yu and Canavier, 2015] Yu, N. and Canavier, C. C. (2015). A Mathematical Model of a Midbrain Dopamine Neuron Identifies Two Slow Variables Likely Responsible for Bursts Evoked by SK Channel Antagonists and Terminated by Depolarization Block. *Journal of Mathematical Neuroscience*, 5:5.

[Zhang et al., 2017] Zhang, H.-Y., Gao, M., Shen, H., Bi, G.-H., Yang, H.-J., Liu, Q.-R., Wu, J., Gardner, E. L., Bonci, A., and Xi, Z.-X. (2017). Expression of functional cannabinoid CB2 receptor in VTA dopamine neurons in rats. *Addiction Biology*, 22(3):752–765.

[Zweifel et al., 2009] Zweifel, L. S., Parker, J. G., Lobb, C. J., Rainwater, A., Wall, V. Z., Fadok, J. P., Darvas, M., Kim, M. J., Mizumori, S. J. Y., Paladini, C. A., Phillips, P. E. M., and Palmiter, R. D. (2009). Disruption of NMDAR-dependent burst firing by dopamine neurons provides selective assessment of phasic dopamine-dependent behavior. *Proceedings of the National Academy of Sciences*, 106(18):7281–7288. Publisher: Proceedings of the National Academy of Sciences.